INVERSE ESTIMATION OF MULTI-PARAMETERS USING BAYESIAN FRAMEWORK COMBINED WITH EVOLUTIONARY ALGORITHMS FOR HEAT TRANSFER PROBLEMS

Thesis

Submitted in partial fulfillment of the requirements for the degree of

DOCTOR OF PHILOSOPHY

by

VISHWESHWARA P S

(155046ME15F17)

DEPARTMENT OF MECHANICAL ENGINEERING

NATIONAL INSTITUTE OF TECHNOLOGY KARNATAKA,

SURATHKAL, MANGALORE - 575 025

MAY, 2020

INVERSE ESTIMATION OF MULTI-PARAMETERS USING BAYESIAN FRAMEWORK COMBINED WITH EVOLUTIONARY ALGORITHMS FOR HEAT TRANSFER PROBLEMS

Thesis

Submitted in partial fulfillment of the requirements for the degree of

DOCTOR OF PHILOSOPHY

by

VISHWESHWARA P S

(155046ME15F17)

Under the guidance of

Dr. N GNANASEKARAN

Dr. ARUN M

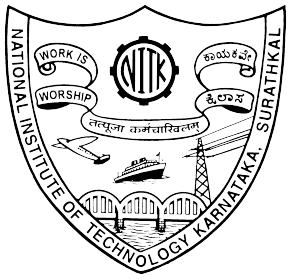

DEPARTMENT OF MECHANICAL ENGINEERING

NATIONAL INSTITUTE OF TECHNOLOGY KARNATAKA,

SURATHKAL, MANGALORE - 575 025

MAY, 2020

DECLARATION

by the Ph.D Research Scholar

I hereby *declare* that the Research Thesis entitled **"INVERSE ESTIMATION OF MULTI- PARAMETERS USING BAYESIAN FRAMEWORK COMBINED WITH EVOLUTIONARY ALGORITHMS FOR HEAT TRANSFER PROBLEMS"** which is being submitted to the **National Institute of Technology Karnataka, Surathkal** in partial fulfillment of the requirements for the award of the Degree of **Doctor of Philosophy** in **Mechanical Engineering** is a *bonafide report of the research work carried out by me*. The material contained in this Research Thesis has not been submitted to any University or Institution for the award of any degree.

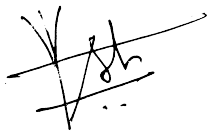

Place: NITK, Surathkal

Date: 19-05-2020

VISHWESHWARA P S

Register Number: 155046ME15F17

Department of Mechanical Engineering

NITK, Surathkal - 575 025

CERTIFICATE

This is to *certify* that the Research Thesis entitled **"INVERSE ESTIMATION OF MULTI- PARAMETERS USING BAYESIAN FRAMEWORK COMBINED WITH EVOLUTIONARY ALGORITHMS FOR HEAT TRANSFER PROBLEMS"** submitted by **VISHWESHWARA P S** (Register Number: 155046ME15F17) as the record of research work carried out by him is accepted as research thesis submission in partial fulfillment of the requirements for the award of degree of Doctor of Philosophy.

Dr. N GNANASEKARAN
Assistant Professor
Research Guide
Department of Mechanical Engineering
NITK, Surathkal - 575 025

Dr. ARUN M
Associate Professor
Research Guide
Department of Mechanical Engineering
NITK, Surathkal - 575 025

Prof. SHRIKANTHA S RAO
Professor & Head
Chairman - DRPC
Department of Mechanical Engineering
NITK, Surathkal - 575 025

ACKNOWLEDGEMENT

Guru is one who cares for the disciple without any selfish motivating factor whatsoever. His concern for the disciple is far greater than that of even parents, who in their anxiety to give their children material comfort, generally ignore the highest good. I sincerely show my gratitude to my guides **Dr. N Gnanasekaran** and **Dr. Arun M** for providing a wonderful opportunity to pursue Ph.D. The valuable time I devoted for interactions and discussions helped me to expand my vision of knowledge, understanding and interpretation beyond my thinking.

I am extremely grateful to our honourable director **Prof. Karanam Umamaheshwar Rao** for creating an attitude towards research for students. I sincerely thank our HOD, **Prof. Shrikantha S Rao** for providing all facilities needed during the time of research work. I would like to thank **Prof. Prasad Krishna** for giving valuable suggestions about my work. My special thanks to **Dr. Gangadharan K V** and **Dr. Pruthviraj U** for permitting me to utilize the facilities of Center for System Design. I am also thankful to my RPAC committee members **Dr. Rajasekaran C** and **Dr. Ramesh M R** for their counsel and recommendations during my presentation. I also thank secretary DRPC, **Dr. S kattimani** for helping in smooth conduct of the presentations. I would like to thank ex HOD **Prof. Narendranath S** for his support during my course of research. I am thankful to all the Deans, NITK for providing facilities at NITK Surathkal. I would like to thank all the teaching and non-teaching staffs, Security, Health care centre, Hostels and Physical Education and Sports Department. I express my earnest thanks to **Prof. C Balaji**, IIT Madras for his words of motivation during my research.

I feel happy to thank **Dr. Harsha Kumar, Narendran G**, **Dr. Avdhoot** and **Kiran K D** with whom I have shared most of my time in college which indeed memorable. I also thank our colleagues **Dr. Kotresh, Muthamil, Prakash, Trilok, Venakatapathy, Dr. Anil, Dr. Abdul, Thippeswamy, Nuthan, Deepak, Shankar, Vashista, Ritesh, Rudramurthy, Shashikumar, Madhu, Kishor, Dr. Arjun, Sharath, Sagar, Balaji, Bhargav** and the list goes on.

I thank Music club, Kannada Vedike of NITK for sharing a wonderful time

during my stay at NITK.

I bow down at the feet of my parents **Shri. Chandrasekhara Rao P S** and **Smt. Girija P S** for furnishing the needs to fulfill my wishes and continuously supporting to achieve them. I am thankful to my brother **Shri. Atresh P S** and sister in law **Smt. Akshatha** for motivating me during the Ph.D. I thank their daughter **Chi. Sannidhi** for spending beautiful time with me that always helped me to feel fresh after hectic schedule. I am grateful to my younger brother **Chi. Harish P S** for taking care of parents during my stay in NITK. I am much obliged to my father in law **Shri. Ramasubramanian** and mother in law **Smt. Latha Ramasubramanian** for supporting and trusting me to follow the path I was passionate about. I specially thank my wife **Smt. Nainthara R** for understanding, motivating and supporting me during my Ph.D. work. I would also like to thank my all relative, teachers and friends.

I specially thank **Smt. Poornima Bhat, Smt. Usha Bhat and family, Shri. Ramesh and family and Shri. Ganesh Rao and Smt. Sapna Ganesh Rao** for giving their care during my stay at Surathkal.

I am blessed to pursue my education in National Institute of Technology Karnataka Surathkal which gave an immense exposure towards research and way of thinking and believing.

I dedicate this Ph.D thesis to my grandparents Late **Shri. Mallari Rao P S** and Late **Smt. Janakamma Mallari Rao P S**.

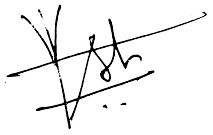

VISHWESHWARA P S

NITK, SURATHKAL - 575 025

ABSTRACT

This thesis focuses on the estimation of unknown parameters using various inverse methods for the heat transfer problems. The first class of problem elaborately discusses about the estimation of interfacial heat transfer coefficients during the solidification of casting. To accomplish this, a prevalent one dimensional transient horizontal directional solidification of Sn-5%wtPb alloy with temperature dependent thermophysical properties and latent heat is considered to be the mathematical model/forward model and numerically solved using Explicit Finite Difference Method to obtain temperature distribution from the known boundary and initial conditions. The temperatures from the forward model is validated with the literature and an absolute error of 5% from the actual measurements was observed. In order to mimic the real time experiments, the temperatures are added with σ=0.01T$_{max}$, σ=0.02T$_{max}$ and σ=0.03T$_{max}$ Gaussian white noise (simulated measurements) and compared with two different objective functions: (i) Least Squares and (ii) Bayesian Framework. Meantime, to expedite the solution of the inverse problem, the numerical model is then replaced with Artificial Neural Network (ANN), which acts as a fast forward model to estimate the unknown constants present in the correlation of interfacial heat transfer coefficient. A total of 473 data sets of inputs and corresponding outputs were used to create a trained artificial neural network which produced temperatures with an accuracy less than 0.1°C temperature difference from the exact temperature data. Genetic Algorithm (GA) was implemented as an inverse method and it was found that ANN-GA-Bayesian framework was more effective compared to ordinary least squares for noise added data with an overall average error of 2%.

Furthermore, an extended study on the advantage of Bayesian framework for the estimation of multi-parameters during Al-4.5wt%Cu alloy solidification is also discussed in detail. The main aim is to retrieve more information with less available simulated measurements. A sensitivity analysis is performed to understand the dependency of the unknown parameters like modeling error, latent heat and heat transfer coefficient parameters on the solution. It showed that the values of constants of the IHTC correlation and latent heat affect the temperature distribution in casting significantly. For

the solution of inverse estimation, the use of two different metaheuristic algorithms (i) Genetic Algorithm (GA) and (ii) Particle Swarm Optimization (PSO) is illustrated. A careful examination of the mentioned algorithms is performed to fix the algorithm parameters. The results revealed that PSO combined with Bayesian framework provides a better computational solution compared to GA-Bayesian with an overall absolute error less than 6%. Also, the study on the effect of multiple sensors revealed that using two sensor the average % error for the estimation of a ,b and latent heat was 0.247, 0.3 and 0.45 respectively and suggesting that two sensors were sufficient for the present analysis.

The second class of problem is extended to retrieve the unknown heat flux and heat transfer coefficient for a 3-D steady state conjugate fin heat transfer problem. A mild steel fin with dimensions 150x250x6 mm^3 is placed centrally on to an aluminium base of dimensions 150x250x8 mm^3 and experiments are conducted for different heat flux values of 305, 544, 853 and 1232 W/m^2 and corresponding temperature distribution along the vertical fin is recorded. Navier-Stokes equation is solved to obtain the necessary temperature distribution of the fin. Heat flux with the range between 305W/m^2 and 3300 W/m^2 and its corresponding temperature distribution of the fin is obtained using commercial software. A total of 24 Computational Fluid Dynamics (CFD) simulations are performed to create a neural network model that can surrogate the forward problem in order to expedite the computational process. The estimation of the heat flux and heat transfer coefficient using GA, PSO and PSO- Broyden Fletcher Goldfarb Shanno (BFGS) is carried out for both simulated and experimental data. A detailed comparison study on the effect of algorithm parameters on the solution is demonstrated in order to examine the performance of the algorithms. For simulated temperature measurements, all the mentioned algorithms proved to be effective but PSO-BFGS estimated the heat flux with an absolute % error of 0.86 and heat transfer coefficient with 0.105% for experimental temperatures. The results show that the PSO-BFGS method outperforms GA and PSO and is observed to be a formidable approach in the estimation of the unknown parameters.

Key words: inverse, heat transfer, evolutionary, ANN, Bayesian, hybrid.

TABLE OF CONTENTS

List of Figures

List of Tables

Nomenclature

Symbols

A area of the fin, m^2

a, b, c, d constants of the heat transfer coefficient correlation

C specific heat, (J/kgK)

c_1 cognition learning coefficient

c_2 social component

f_s fraction of solid

g gravitational constant, m^2/s

$g_{best,i}$ global best of the particles

h heat transfer coefficient, (W/m^2K)

h_a chill environmental heat transfer coefficient, (W/m^2K)

h_i interfacial heat transfer coefficient, (W/m^2K)

I current, A

k_C thermal conductivity of casting, (W/mK)

k_M thermal conductivity of chill, (W/mK)

l latent heat, (J/Kg)

ME modeling error

P power, W

$P_{best,i}$ personal best of the particles

q heat flux, W/m^2

t time, s

T_∞ ambient temperature, °C

T_C casting surface temperature, °C

T_f fusion temperature, °C

T_l liquidus temperature, °C

T_M chill surface temperature, °C

T_s solidus temperature, °C

T_{actual} target temperature data in neural network, K

T_{im} calculated temperature, °C

$T_{network}$ output temperature data from neural network, K

V voltage, V

v velocity of the particle

w inertia weight coefficient

x particle

Y_{im} measured temperature, °C

J_{Pj} scaled sensitivity coefficients

Greek

α thermal diffusivity, (m^2/s)

β coefficient of thermal expansion, K^{-1}

ϵ random variables

μ mean of Gaussian prior

μ mean

ρ density, (kg/m^3)

σ standard deviation of the Gaussian prior

σ standard deviation

ε error criterion, 10^{-5}

ϑ kinematic viscosity, m^2/s

subscripts

Al aluminum

f fusion

l liquidus

ms mild steel

p parameter

s solidus

ABBREVIATION

ANN Artificial Neural Network

BFGS Bryden Fletcher Goldfarb Shanno

CFD Computational Fluid Dynamics

GA Genetic Algorithm

IHTC interfacial heat transfer coeffiecient

PSO Particle Swarm Optimization

PPDF Posterior Probability Density Function

Other symbols

$\ddot{q}$ heat source term

P parameter

V co-variance matrix of the **P**

W co-variance matrix of the measurement errors

CHAPTER 1

INTRODUCTION

In any parameter estimation problem, it is desirable to obtain more information using one single experiment. A fine heat transfer model yields an accurate prediction of temperature distribution close to the experimental data. In order to solve numerically, it is necessary to know all input parameters that significantly affect the solution. In a heat transfer problem, solving the governing equations using the available initial and boundary conditions (cause) to obtain the temperature data (effect) is called forward problem. Contrarily, in an inverse problem the cause is determined from the available knowledge of the effect. Inverse heat transfer problems are widely used for the estimation of unknown quantities or thermophysical properties. The estimation procedure becomes challenging when the experimental design constraints are stringent and the unknown parameters are sensitive to temperature and operating conditions. Generally, the temperature distribution in the problem domain is obtained through experiments. Using these measured temperatures, the unknown parameters are estimated with the help of inverse techniques. Another way of using temperature measurements for inverse estimation is by solving forward model for an assumed unknown parameter and obtaining the corresponding temperature information at particular locations referred as exact temperature data. Addition of Gaussian noise to this exact data provides simulated measurements that mimics the experimental temperatures which is generally associated with noise.

Estimation of surface heat flux and surface temperatures becomes onerous when it is subjected to high temperatures. Locating the sensors at this position is unsuitable as it distorts the thermal field. To overcome these difficulties, inverse methods can be successfully implemented for various complicated heat transfer problems. The flowchart of the procedure of inverse estimation is represented in Figure 1.1. First, the mathematical model of a given problem is developed to obtain temperature distribution for any given value of unknown input. The temperature obtained from this model is referred as simulated temperatures (T_{im}). Y_{im} is the simulated measurements/ experi-

mental temperature data for which the estimation is performed. The input parameters of the forward model and inverse algorithm are initialized. In every iteration, the forward model is solved for a range of initialized unknown parameters. An objective function is framed that minimizes the error between the measured and the calculated temperature data from the forward model. The estimation methodology varies for the different inverse techniques and the procedure is carried out for specified iterations till the error is minimized between the measured and the calculated temperature data.

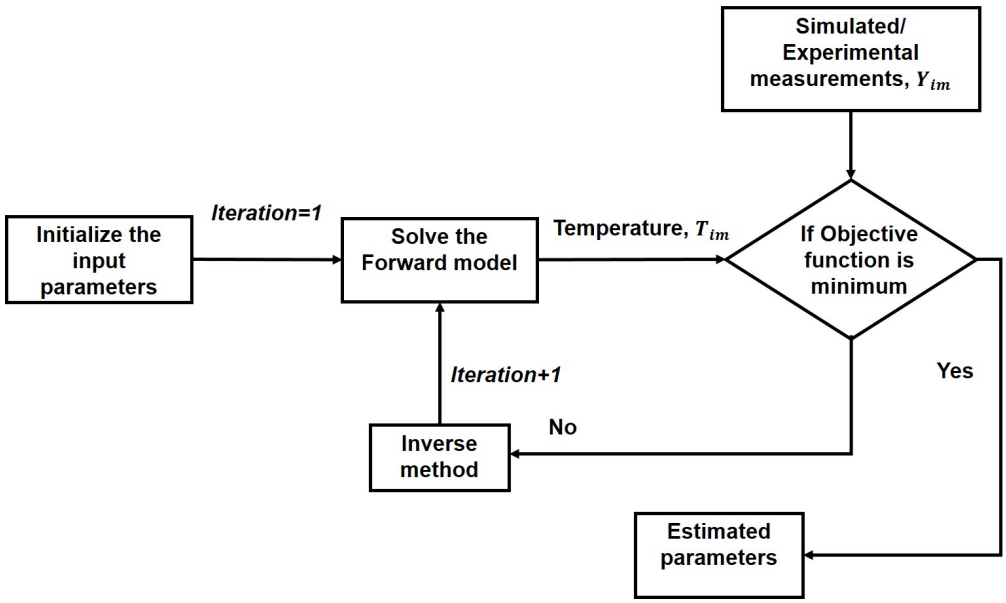

Figure 1.1 Flowchart of inverse estimation (Ozisik and Orlande 2000).

Inverse problems fall under the class of ill posed problems as the solution becomes unstable due to the errors associated with the measured temperatures thus providing vast space to explore different inverse methods (Hadamard 2003). Various deterministic and stochastic methods are used as inverse techniques for the estimation of unknown quantities. Deterministic methods use gradient information in every iteration to obtain the solution of a problem. Methods such as Levenberg-Marquardt (LM) method, steepest descent method, conjugate gradient method (CGM), Broyden Fletcher Goldfarb Shanno (BFGS) etc., belong to this category. Stochastic based methods perform random search to satisfy the objective function. Few examples are Simulated Annealing (SA), Genetic Algorithm (GA), Particle Swarm Optimization (PSO), etc. Such techniques are found to be less sensitive to modeling errors present in the measurements and serve as effec-

tive methods for the application of inverse heat transfer. The search based methods are widely used in inverse problems to improve the performance of a design by minimizing the model and experimental temperatures.

For a unique problem, the final solution using deterministic methods will be better than the stochastic methods provided the function is continuous and differentiable. Further deterministic methods converges to the solution faster than stochastic methods but sometimes tend to get trapped in local minima or maxima. Nonetheless, the convergence of the solution differs according to the type of method chosen. As discussed above, if the complexity of the problem increases then stochastic methods can effectively be used to obtain the solution. Before using these methods, an objective function is framed. For inverse heat transfer problems, the objective function with least squares that minimizes the error between the measured and calculated temperatures is used (Colaço et al. 2006; Słota 2008). Several approaches like L-Curve method, cross validation, restricted maximum likelihood, etc., are used to determine regularization parameter. Usually, the choice of regularization term varies for a class of problems in obtaining accurate inverse solutions (Sui and Cui 2008; Udayraj et al. 2015). The use of Bayesian framework eradicates the complexity of choosing regularization term and provides a solution to the inverse heat transfer problem by formulating a complete probabilistic description of the unknowns and uncertainties given temperature data. In Bayesian framework, the *a-priori* information provided as a prior distribution acts as an inherent regularization term thus curing the ill-posedness of the inverse problem.

With the advent of high performance computing facilities, it is now easy to solve complex heat transfer problems that cannot be solved analytically. Generally, solving the forward model along with the inverse methods may result into computationally costly approach. Hence, Artificial Neural network (ANN) is found to be a good replacement of the forward model that reduces the forward problem to a simple reduced model by retaining the physics of the model. ANN is a training based procedure where it approximates weight functions according to the several known inputs and outputs provided to the network. For any value specified within the trained values of input, the established network provides information about the corresponding output in very less time. Thus, ANN fulfills the objective that not only retains the full nature of the

complete model but also acts as a fast forward model in the inverse analysis. Apart from this, several approaches of hybridization of stochastic algorithm with deterministic methods can also improve the performance of the estimation. The hybrid techniques enhances the search capability of the algorithm to produce a better solution.

1.1 HEAT TRANSFER STUDY IN SOLIDIFICATION OF CASTING

Casting is one of the oldest processes used for obtaining the components required for various applications. The wide variety of casting methods are sand casting, permanent mold casting, lost-foam casting, investment casting, etc. With the use of automation, productivity and quality of products are increased and almost all components for engineering applications can be obtained to desired shape by casting process. The studies of microstructure, mechanical properties and heat transfer in casting solidification have helped the foundry industry to get high quality products. The use of computer simulations in industries also helps to understand the clarity of the solidification process. Especially, the study on solidification stage in metal casting has a direct influence on the microstructure of the cast product and hence affect the mechanical properties of the casted material. But to perform the numerical simulation, accurate information of thermal properties and boundary conditions of the numerical model is required. Moreover, the study of heat transfer phenomenon at the interface of casting and mold has become a great part of interest as it affects the evolution of microstructure of casting during solidification and the properties of the casted product. This gives a path to study the interfacial heat transfer by considering various process of solidification.

1.1.1 Air gap formation at the metal mold interface during solidification

During metal casting, when the molten metal comes in contact with the mold, it loses its heat to the mold and starts solidifying. Initially a thin solidified skin is formed at the mold metal interface and as time progresses the thickness of the solidified metal increases. Due to this, an air gap is formed between the mold and the solidified metal which creates resistance to the heat flow. The heat flux related to this air gap is called interfacial heat flux and corresponding heat transfer coefficient is called interfacial heat transfer coefficient (IHTC). The mold metal interfacial heat transfer is characterised as shown in Figure 1.2. First stage is the start of solidification, it can be assumed that a good contact between the molten metal and the mold exists. The heat transfer is mainly

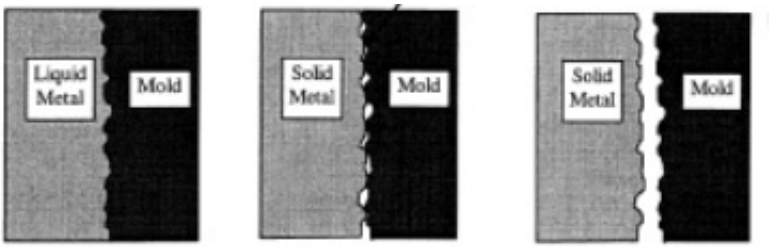

Figure 1.2 Formation of air gap at the mold metal interface during solidification of casting (Stefanescu 2015).

due to conduction from molten metal to the mold. Later, as solid skin forms, the molten metal starts shrinking from the mold wall resulting in an air gap formation (second stage). A partial contact between asperities of mold and solid metal surfaces is formed. The heat transfer through these point of contacts at the mold metal interface is assumed by conduction and through gas, conduction and radiation at the metal/mold gap. In the third stage, the thickness of solidified metal increases and the metal will move away entirely from the mold and heat transfer is only through the gap.

It is very difficult to study the interfacial heat transfer aspects in solidification because there are moving boundaries, the location of thermocouple at the interface boundaries distort the thermal field and the thermophysical properties are temperature dependent. Further, to solve the governing equations pertaining to heat transfer, more knowledge about the metallurgical as well as heat transfer aspects are needed. The IHTC values varies from several thousand W/m^{2}K with a higher value initially for liquid state and the value keeps on decreasing with solid skin and air gap formation. The heat transfer limited by conduction through the air gap is defined as

$$h_i = \frac{q}{(T_{cast} - T_{mold})} \tag{1.1}$$

where q is the interfacial heat flux in W/m^2, T_{cast} and T_{mold} are the casting and mold surface temperatures respectively in °C. The values of T_{cast} and T_{mold} cannot be measured directly as the location of thermocouples at the interface can distort the temperature field at the mold metal interface. Further, the region close to the interface will have a non-uniform surface conditions. Hence, determination of IHTC is difficult and inverse methods are widely used to find the values of IHTC.

The study of interfacial heat transfer coefficient for solidification of casting for 3-D problem becomes onerous but several researchers have attempted to obtain analytical solutions by simplifying it to one dimensional problem. However, few analytical solutions are available which are solved by assuming perfect contact between the mold and casting and neglecting the superheat. The procedure for analytical solutions from the work of Davey (1993) shows the mathematical complexity involved in solving equations for different methods of solidification. The solidification of casting problem involves the phase change hence temperature dependent thermophysical properties along with the latent heat should be considered to obtain a realistic temperature distribution. The heat transfer problem is a transient case and involves moving boundaries at the mold metal interface (Stefanescu 2015). Further, to understand the extent of errors arising due to incorrect values of the unknown parameters provided as input in simulation programs can be recognized by performing sensitivity analysis. The use of computer simulations allows one to study the processes happening inside the casting as well as mold. The sensitivity studies performed by Vasileiou et al. (2017) showed the variation of cooling curves for different input values of the IHTC during the solidification of aluminum casting. Various values of IHTC were given as an input and the corresponding temperatures are collected to understand deviation of the temperature distribution of a sensor from the actual measurements. Therefore, to obtain the accurate information at the mold metal interface, inverse methods become an effective way to estimate the values of IHTC and surface temperature during the solidification of casting. Another example which is taken up in this research is explained in next section.

1.2 PARAMETER ESTIMATION IN FIN HEAT TRANSFER

Estimation of thermophysical properties, heat flux and heat transfer coefficient is always critical in designing an efficient thermal system, for example, application like heat exchanger requires the determination of boundary condition during its operation. Fins are extensively used to enhance the heat transfer in many applications. The rate of heat transfer from a surface at temperature, T_s to the surrounding temperature T_∞ is given by the Equation (1.2)

$$Q = hA_s(T_s - T_\infty) \tag{1.2}$$

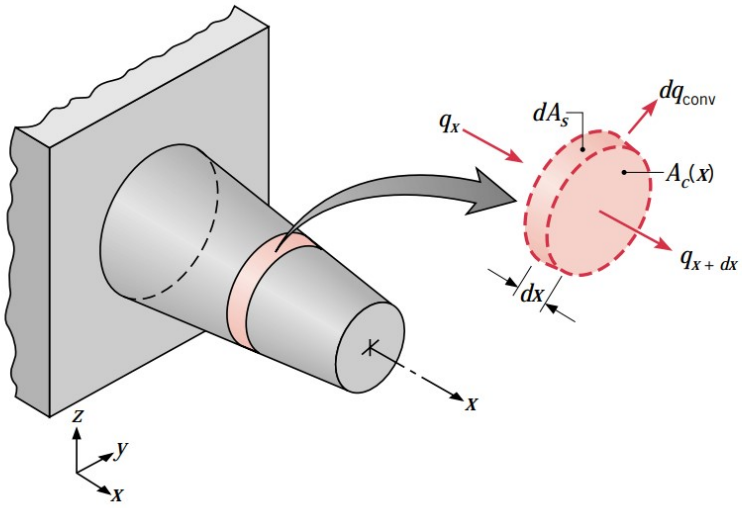

Figure 1.3 Representation of energy balance of an extended surface (Incropera et al. 2007).

Figure 1.3 shows a general representation of the extended surface. A heat flux is supplied to the base of the fin. Heat is convected from the extended surface to the ambient temperature T_∞. To obtain the temperature distribution of the fin, a steady state fin heat transfer with the constant thermophysical properties is assumed. The value of h varies for natural and forced convection. Though the value of h varies along the length of the fin due to the fluid motion, local value of h is considered for simplification. The estimation of unknown heat flux at the base is critical which cannot be measured directly by senors. Estimation of thermophysical properties, retrieval of unknown heat flux can be successfully achieved using inverse methods.

The works of Chen et al. (2007); Lee et al. (2012); Wankhade et al. (2018) involve the estimation of unknown parameters using inverse heat conduction approach. But, the mathematical model in all these works was simplified to a heat conduction equation. On contrary, to obtain more realistic information during inverse estimation, the complete or full numerical model has to be retained. There are also research work related to inverse conjugate problems but they are not adequate in literature. Especially the work of Reddy et al. (2012) and Balaji et al. (2013) assume a constant base temperature rather than a constant heat flux at the base. Hence, to keep the physics in line with the mathematical model, heat flux at the base would be more practical than

the constant base temperature. Nevertheless, solving the full model or complete model (solving Navier Stokes equation) is very expensive. With the advent of high computing facilities, it is now easy to solve the 3-D Navier Stokes equation along with the energy equation to obtain the necessary temperature distribution of the fin. Moreover, there is a paradigm shift from the deterministic models to stochastic models due to a lot of advantages with the evolutionary algorithms.

As a highlight, in this work, the 3-D CFD simulations are replaced with ANN model so as to facilitate faster computations for the proposed forward problem and a new hybrid algorithm, which is not seen in hitherto literature for heat transfer problem, is proposed for the inverse estimation. Therefore, the present work foresees a window in which the combination of evolutionary and deterministic methods is possible within the umbrella of inverse conjugate heat transfer problem to identify the heat flux and heat transfer coefficient for the measured temperature data.

1.3 DESCRIPTION OF THE PROBLEMS CONSIDERED IN THE PRESENT WORK

1. The first class of problem elaborately discusses about the estimation of interfacial heat transfer coefficients during solidification of Sn-5wt%Pb alloy casting. ANN-GA-Bayesian framework is applied to estimate the unknown parameters. Further, the estimation procedure is extended to retrieve multiple parameters associated with the solidification of Al-4.5 wt%Cu alloy using GA, PSO in conjunction with Bayesian framework.
2. The second class of problem is extended to retrieve the unknown heat flux and heat transfer coefficient for a 3-D conjugate fin heat transfer problem using GA, PSO and PSO-BFGS algorithms as inverse methods.

1.4 ORGANISATION OF THE THESIS

This thesis contains nine chapters and a brief description of the contents of each chapter is given below

Chapter 1 briefly explains the introduction to parameter estimation, methodology involved in inverse heat transfer problems.

Chapter 2 provides extensive literature review about methods used in inverse heat

transfer. The research gap observed from literature helped to configure the objectives of the present work.

Chapter 3 illustrates the procedure to solve the numerical simulations to obtain the temperature distribution in the problem domain. Also, it outlines the details of the objective functions and methodologies of Genetic Algorithm, Particle Swarm Optimization and hybrid Particle Swarm Optimization that are chosen to solve the present inverse heat transfer problems.

Chapter 4 describes the estimation of interfacial heat transfer coefficient during solidification of casting with the combination of GA-ANN-Bayesian framework.

Chapter 5 shows the capability of Bayesian framework in estimating multi-parameters during solidification of casting using GA and PSO as inverse methods.

Chapter 6 explains the application of hybrid PSO-BFGS method to retrieve the heat flux and heat transfer coefficients for a 3-D coupled conduction convection fin heat transfer problem. The comparison of hybrid PSO-BFGS along with conventional GA and PSO algorithms are also demonstrated.

Chapter 7 concludes the overall representation of research work. It explains the scope for future work.

1.5 CLOSURE

This chapter narrated the general introduction to inverse problems in parameter estimation. It explained the basic concepts of problem statement considered in this present work. This chapter also presented the details of the organisation of the thesis. The next chapter depicts the literature review, scope and objectives of the present study.

CHAPTER 2

LITERATURE SURVEY

2.1 DETERMINATION OF INTERFACIAL HEAT TRANSFER COEFFICIENT DURING SOLIDIFICATION OF CASTING

During solidification of casting, very less information at the interface boundary conditions are available. Hence, many works that were carried out to study the interfacial behaviour during casting solidification are put together in this section. The values of IHTC depend on direction of solidification, mold material and thickness, casting thickness, pressure, geometry, mold coating etc. Various methods have been proposed by several researchers but two main effective methods are: (i) air gap measurement method, where the measured air gap will be converted to appropriate interfacial heat transfer coefficients and (ii) recording the temperature data at several locations in the casting and mold which serve as information to determine the heat transfer coefficients at the interface using inverse method. Extensive research has been done in understanding the formation of air gap and studying the values of IHTC at different stages during solidification.

Beck's non-linear estimation is popularly used method to estimate the surface heat flux or heat transfer coefficients with the aid of temperature measurements available inside the feasible domain (Beck 1970). A guess value of the unknown parameter is initialized and in every iteration, the error between the measured and the calculated temperatures is minimized using least squares. The methodology considers the sensitivity coefficients for each measurement locations during the estimation procedure.

Ho and Pehlke (1985) provided an insight of effect of IHTC values on various metal mold systems by considering both analytical and experimental methods. Radiation effects at the interface on the IHTC values was not considered. Non linear transducer was used to record the movement of the metal and mold which indicates the onset of air gap from the temperature measurements. Downward and upward direction solidification were studied. In upward casting, good contact between the mold and metal

was found and further decrease in the IHTC values were due to the oxides formation on the metal. In downward direction solidification, more air gap exists; hence, more resistance to heat flow. Sensitivity analysis was also performed by considering different mold materials.

Nishida et al. (1986) observed the air gap phenomenon for flat and cylindrical castings. Displacement meters were used to measure the mold and casting movements. Finite explicit method was considered to solve the governing equations in account with radiation for cylindrical castings and approximate solution was adopted to find IHTC by knowing the temperature distribution. In flat casting, the movement of the mold was inwards in first few seconds after pouring and later moved away from casting hence higher values of IHTC were found. But in cylindrical casting, the movement of the mold was outwards.

Kulkarni and Radhakrishna (2005) used both air gap measurement technique and inverse method to estimate the IHTC during the solidification of Al-4.5wt%Cu alloy against CO_2 sand mould. The displacement gauge was used to observe the movement of the metal and mold to find the thickness of the air gap. By knowing the size of air gap and thermal conductivity of the gas mixture at the air gap, IHTC was obtained. The study concluded that the IHTC values obtained were ten times higher than the works of (Ho and Pehlke 1985; Nishida et al. 1986).

Santos et al. (2004) determined IHTC for Al-Cu and Sn Pb alloys for horizontal direction solidification with copper and steel chills. Effect of parameters such as alloy composition, position of the chills, thickness of the mold, melt super-heat on IHTC was studied. The overall heat transfer coefficient was expressed as a power law function with time, $h = at^{-m}$. Mold environment and interfacial heat transfer coefficients were calculated for different experiments. For thinner chill materials, the surface gets heated rapidly compared to thicker chills, hence higher values of IHTCs were found for thinner chills. As copper is having higher thermal conductivity, it could absorb more heat providing higher cooling rates. It was also observed that the initial super heating of the metal will influence the IHTC. As super heat temperature is increased, higher is the heat content hence the increase in fluidity of metal. The increase in alloy composition will decrease the IHTC due to the wettability of the melt with the mold.

Sahin et al. (2006) studied the effect of chill materials on IHTC by considering steel and copper chills for the solidification of Al-Si alloy. A water cooled chill system was arranged in order to ensure the unidirectional solidification. With the inverse heat conduction approach, the IHTC values determined for copper and steel chills were in the range of 19-9.5 kW/m^{2}K and 6.5-5 kW/m^{2}K respectively.

Rajaraman and Velraj (2008) compared two different methods called Beck's algorithm and control volume approach to obtain the IHTC values for aluminum and sand mold. Beck's algorithm uses information about the temperature measurements during casting to find the unknown parameters. Control volume method solves sequentially the time varying ordinary differential equations which are arrived by reducing the heat conduction partial differential equation. A deviation of 57% in the values of IHTC between the two methods was found. Though the value of the IHTC is high at the beginning, Beck's algorithm assumes low heat flux values compared to control volume approach, hence higher values of IHTC were obtained by Beck's algorithm.

Arunkumar and Kumar (2008) studied spatially varying heat flux at the metal mold interface due to mold filling. For 99.9% aluminum and cast iron mold system, a serial-IHCP algorithm was developed that has a capability of finding the multiple heat fluxes at metal mold interface.

Sun and Chao (2006) used lumped capacitance method to find the IHTC values for Sn-20wt%Pb alloy and A356 alloy cylindrical casting against green sand mold. Though the values of thermal conductivity and pouring temperatures were different for each casting, the trends of heat transfer coefficients were found to be almost similar for both castings. The validity of the lumped capacitance method was checked by finding the biot number (<0.1) . Further, the values of IHTC were given as an input to FEM solver which gave within 7% error between the measured and simulated temperatures.

Aweda and Adeyemi (2009) used the Beck's nonlinear estimation method to estimate the values of IHTC for squeeze casting of aluminium with steel mold. Thermocouples at the bottom and top positions were located in the casting by which they were able to calculate the IHTC values at two different locations. Pressure applied on the casting reduced the defects associated with shrinkage and gas porosity and resulted in higher values of IHTC compared to gravity castings. The values of IHTC were found to

be higher for pressure casting than gravity casting as the application of pressure would allow the casting surface to be in contact with the mold surface. Correlations based on numerical and experimental methods were produced with IHTC as a function of solidus, liquidus-solidus and liquidus phase temperatures.

Zhang and Li (2013) determined IHTC by using sequential function specification method with least squares for casting A356 alloy. The factors like damping factor, number of future time steps, tolerance criteria and time step of the algorithm were studied. The values of the IHTC had the range of about 900-3400 W/m^{2}K. The results showed the dependency of various inverse algorithm parameters, thus the choice of algorithm parameters was crucial for the estimation of IHTC during casting solidification.

2.2 APPLICATION OF EVOLUTIONARY ALGORITHMS FOR SOLIDIFICATION OF CASTING.

The solutions from the gradient based approaches are dependent on the initial guess, future time steps and sensitivity coefficients. Using stochastic method, the solution will not get trapped in the local minima. Apart from popularly used Beck's inverse method, nature based methods like Genetic Algorithm (GA), Particle Swarm Optimization (PSO), Artificial Neural Network (ANN) are gaining a huge scope to solve inverse problems.

Wood (1996) compared GA with sequential function specification (SFS) method as inverse methods to estimate the heat transfer coefficient during cooling of semi-infinite solid. The observations showed that the GA is immune to sensitivity coefficients and proves the robustness of the algorithm compared to the conventional sequential functional method. The results also depend on the temperature sensor locations and the future time steps considered in SFS method to obtain stable results.

Raudenskỳ et al. (1995) used GA to obtain the solution for inverse heat conduction problem where the unknown heat transfer coefficient as boundary condition was estimated by choosing both exact and noise added temperatures. The regularization term was added to the fitness function that enhanced the smoothness of the convergence of the solution. It was found that GA was computationally expensive, but it is capable of providing good results for the problems that are unstable or do not converge.

Ranjbar et al. (2010) determined IHTC values during squeeze casting process of Al-4.5wt% Cu alloy using Genetic Algorithm. A two dimensional solidification problem was solved by considering IHTC to vary with time as power law. The calculated temperatures were added with the noise to mimic the experiments and the inverse estimation was carried out for σ=0.01T_{max} temperature distribution.

Dousti et al. (2012) determined the IHTC values for Al-5wt%Si alloy against steel mold using PSO algorithm. The constants of the IHTC correlation was estimated. The work was similar to Ranjbar et al. (2010) but the application of PSO resulted in improvement in the estimation. The overall computational time for the estimation was around 8-9 hours.

Hetmaniok et al. (2013) devoted their work to estimate the boundary heat flux and heat transfer coefficients during solidification of aluminium using bio inspired algorithms. The method was tested for noisy added data up to 5% and the selection of parameters of Immune Recruitment Mechanism and Clonal Selection Algorithm were conducted. The method was also extended for continuous casting application.

Vasileiou et al. (2015) used GA for estimation of IHTC for a varying casting geometry of Brass. The estimation was directly performed for the experimental data and the temperatures from the forward model were obtained by numerical simulations performed using commercial ProCAST software. In order to achieve this, they assumed the IHTC correlation varying with temperature as stepwise, exponential as well as stepwise function with time. A good agreement between numerical and experimental results were obtained using GA.

Wang et al. (2016) determined heat transfer coefficient for a continuous casting process using PSO algorithm. The measured temperature data from the experiments were used to optimize the heat transfer coefficients of secondary cooling zone during solidification process. The study of choice of particle size showed that 20 number of particles were sufficient as selection of too many particles may lead to expensive computational cost during the estimation. The results depicted that convergence using PSO algorithm was fast and possesses strong global search ability.

Wang et al. (2018) applied hybrid artificial fish swarm algorithm (ZAFA) for the estimation of IHTC for quenching application. To increase the speed of conver-

gence, the regular artificial fish swarm algorithm was combined with the normal distribution method. The hybridization of the algorithm reduced the numerical oscillations during the IHTC estimation.

Zhang et al. (2015) modified PSO for the radiative and phase change in laser heating application. The energy and radiative equations were solved simultaneous using finite volume method to get the temperature distribution. Effective estimation of Stefan number and conduction to radiation number was accomplished for noisy temperature data.

2.3 APPLICATION OF BAYESIAN FRAMEWORK FOR THE INVERSE HEAT TRANSFER PROBLEM

The choice of objective function also decides the accuracy of the estimation. Usually, the selection of regularization term is crucial in obtaining accurate inverse solutions (Sui and Cui 2008; Harsha et al. 2018; Lugon et al. 2009). Use of Bayesian framework takes care of regularization parameter. The *a-priori* information, which is provided as a prior distribution in Bayesian framework acts as an inherent regularization term thus leading to well-posedness of the proposed inverse problem. The results from the work of Deng and Hwang give evidence that the Bayesian method delivers a best training method with the back propagation algorithm (Deng and Hwang 2006).

Reddy et al. (2012) conducted steady state natural convection experiments for discrete heat sources on vertical plate. ANN was used as a fast forward model and the experimentally measured temperature from the Liquid Crystal Thermography (LCT) was compared with calculated temperatures using Bayesian framework. Around 6000 sampling were performed using Markov Chain Monte Carlo method. The retrieved values of constants in Nusselt number correlation using Bayesian framework suggests that it can be used as an effective alternative inverse method.

Mota et al. (2010) applied Bayesian approach with Markov chain Monte Carlo (MCMC) for a one dimensional non-linear heat conduction problem to simultaneously estimate the heat flux and thermal parameters during heating of material with oxy acetylene torch. First, the method was tested for simulated measurements and later extended for the experimentally measured data. The application of MCMC to optimize the objective function resulted in clear analysis and accurate solution of the inverse method.

Yan et al. (2009) used Bayesian framework for the estimation of Robin coefficient with the help of temperatures available at the boundaries. The estimation was carried out for the simulated measurements. The results from the Bayesian framework in conjunction with Markov random field (MRF)-MCMC showed the ability in providing solutions with the uncertainties quantified.

Knupp et al. (2013) performed transient heat transfer experiments on heterogeneous plates and measured the temperatures obtained from infrared camera which were used for inverse analysis. A 1-D heat conduction problem was solved using integral transforms to obtain the solution for forward model. The spatially varying temperature and diffusivity were estimated using Bayesian MCMC method and the eigen function expansion of unknown parameters helped as data reduction technique as it allowed the estimation to perform on transformed experimental temperature field.

Orlande et al. (2014) estimated spatially varying heat flux from the available transient temperatures using MCMC method with Delayed Acceptance Metropolis-Hastings and Enhanced Approximation Error Model. The results showed the use of Approximation Error Model provided effective estimation compared to Delayed Acceptance Metropolis-Hastings as Approximation Error Model makes use of the posterior refined by the error of the reduced model that enabled for an enhancement of the accuracy of the inverse estimation.

Rojczyk et al. (2017) used Bayesian with MCMC to estimate the cancer tumor parameters for a bio heat transfer application. The sensitivity coefficients of each parameters were analysed to know their effects on the solution. A 1-D Pennes bio heat transfer equation was solved to obtain the temperature distribution in the tumor and the skin tissue. Around 200000 samples were generated using MCMC to obtain the appropriate convergence of skin thermophysical properties using temperature distribution inside the tissue.

Zeng et al. (2019) applied Approximate Bayesian Computation (ABC) to overcome the expense of computational cost of the forward simulation by reducing the number of samples selections during the parameter estimation. The methodology was tested for both linear and non linear heat transfer problems and results showed half the time less computational cost compared to the conventional estimation method.

2.4 USE OF ARTIFICIAL NEURAL NETWORK AS FAST FORWARD MODEL

Generally, gradient based methods have faster convergence compared to the evolutionary algorithms. Though the estimation procedure using evolutionary algorithms is computational costly, some research works show the blend of stochastic methods with Artificial Neural Network (ANN) as inverse method that can remarkably overcome this disadvantage (Harsha and Gnanasekaran 2018; Soeiro et al. 2004).

Zhang et al. (2010) used ANN with back propagation algorithm as inverse method and estimated IHTC for A356 alloy. Several numerical simulations were performed for a range of IHTC values and a neural network was trained between the pre assumed IHTCs and corresponding temperatures obtained from simulations. This trained network was used to compare the estimate the IHTCs from the experimental temperatures. The accuracy of the estimation was validated by giving estimated IHTCs as input and comparing it with the temperature distribution obtained from the commercial software. The maximum temperature difference was less than 5°C and the mean temperature difference less than 2°C between the calculated and experimental temperatures were observed.

Ghadimi et al. (2015) solved conjugate heat transfer problem to estimate the unknown heat flux in a braking disc using ANN and sequential method. A 3-D heat transfer problem including turbulent, unsteady and conjugate heat boundary condition was numerically solved. Several heat flux values were given as input and the corresponding temperatures obtained from numerical simulations were used to train a network. The accuracy of the results were dependent on the future time steps and the location of the sensors. It was concluded that the location of the temperature sensors should be as close to the friction interface.

Najafi and Woodbury (2015) demonstrated the use of ANN for the estimation of heat flux in one dimensional slab. An ANN was used to establish a trained neural network between the triangular heat flux and corresponding temperatures. The trained neural network was tested for both constant and temperature dependent thermophysical properties. It was illustrated that for the presumed geometry and boundary conditions, ANN took less data from future time steps to calculate the heat flux when compared to the filter form Tikhonov regularization algorithm.

Balaji and Padhi (2010) estimated the convection heat transfer coefficient and thermal conductivity for a given heat generation using Bayesian-ANN framework. The forward model was replaced by ANN which was constructed using the available temperatures obtained by solving 2-D steady state conduction through a slab for given inputs. The ANN driven MCMC improved the solution for measurements with noise than compared to ANN. By using hybrid ANN, the heat transfer coefficient was found to vary within $\pm 4\%$ and thermal conductivity 6% from the actual value respectively. The study further concludes that the results from the inverse method can be refined by training methods involved in ANN.

Lugon et al. (2009) employed Levenberg Marquardt method (LM) and Simulated Annealing (SA) as inverse methods to estimate the gas bubble interaction. The unknowns to be estimated were considered in different forms of adsorption isotherms. ANN was framed to replace the actual forward model and different variants of LM and hybrid LM-SA-ANN were considered for the estimation. Both the hybrid scheme and LM method were found to be effective and the ANN driven LM method showed less computational cost.

Vakili et al. (2017) merged GA-ANN to predict the viscosity of graphene in nanofluid. Various modification in the ANN parameters were made to check the accuracy of the trained neural network to combine with GA. Viscosity was found to be dependent on temperature and weight percentage of the added nanoparticle. The viscosity for a temperature range of 20°C-60°C was collected. The comparison of experimental and GA-ANN results showed the ANN could be a replacement of actual model thus reducing actual laboratory experimental cost.

Chanda et al. (2017) used combined GA-ANN to estimate the principal thermal conductivities of the honeycomb composite structure used in aerospace applications. Forward model was developed based on finite difference method to obtain temperature distribution and a neural network was framed between the thermal conductivities and corresponding temperatures. The trained neural network reduced the computational cost during inverse estimation using GA. Close agreements with a maximum deviation of $\pm$ 0.85°C between simulated and experimental temperatures were observed.

Yadav et al. (2019) optimised the location and number of discrete heaters for a radiating heat furnace. It was observed that the major computational cost was associated with solving the forward model. Hence an ANN was trained between six different inputs associated with the 3D radiant furnace problem and corresponding outputs were trained based on neuron independence study. The difference in the solution of conventional forward model and trained ANN was less than 4%. Genetic algorithm was used as inverse method and the GA-ANN based results were found to have less computational expense of the order of 10^3 than the conventional model.

2.5 ESTIMATION OF UNKNOWN PARAMETERS IN CONJUGATE HEAT TRANSFER PROBLEM

Huang and Tsai (2005) solved the direct problem by considering the boundary conditions, initial conditions and heat transfer coefficients as known input to obtain temperatures at particular locations for a 3-D convection fin heat transfer problem. The test cases were conducted for noisy measurements $\sigma = 0.1$ and $\sigma = 0.3$ respectively. The inverse estimation was accomplished by steepest descent method considering sensitivity and adjoint problem where the local heat transfer coefficient was estimated using temperatures reading from infrared thermography at particular locations.

Colaco and Orlande (2001) applied conjugate gradient method with adjoint problem for forced convection problem. The forward problem was concerned with the determination of flow and thermal field inside the parallel channel. Finite volume method was adopted. In the inverse problem, time dependent heat fluxes, spatially dependent heat fluxes and time and space dependent heat fluxes were estimated. It was concluded that, the inverse approach would be applicable for any forced convention problem in channel.

Farahani and Kowsary (2017) illustrated the use of inverse conjugate heat transfer problem for steady and pulsating flow. Heat transfer coefficient was estimated along with consideration of radiation and lateral heat conduction while solving 2-D governing equations for semi confined impinged slot jet. The heat flux distribution was considered instead of constant heat flux as boundary condition. Conjugate gradient method with adjoint method was used as inverse method and results depict that the geometry configuration affect the heat transfer performance in pulsating impinged jet.

For Reynolds number greater than 3000, maximum enhancement of heat transfer caused by pulsation occured for Strouhal number, *St*=0.169.

Ousegui et al. (2019) adopted conjugate gradient method with adjoint method for determining the air flow rate for PCM heat exchanger application. Numerical modeling was achieved by using COMSOL software and the inverse estimation was linked with the MATLAB. The method was demonstrated for two different flow rates. Though the inverse methodology was nonlinear in nature with conjugate heat transfer, the method showed satisfactory results with maximum relative error less than 5×10^{-3}. The parametric studies were found to be crucial in the estimation procedure.

Lugon and Silva (2011) solved heat mass transfer problem as direct model to simultaneously obtain the moisture distribution and temperatures for drying process experiments. The experimental design was based on sensitivity coefficients with respect to temperature, moisture potential. SA and LM methods were used as inverse method in conjunction with ANN to obtain quick convergence. It was observed that LM was effective for noiseless temperature data. But the use of SA resolved the problem getting trapped in local minima even for noisy temperature measurements.

Razzaghi et al. (2019) estimated spatially varying heat flux during cooling of hot plate using conjugate gradient method with adjoint method. Least squares was selected as objective function for the minimization of error between measured and calculated temperatures obtained from the solution of two dimensional convection problem. The estimation of local heat transfer coefficient was carried out for 0.01°C and 0.1°C noise added temperature data.

Mejias et al. (1999) compared Levenberg-Marquardt method (LM) and Conjugate Gradient Method (CGM) to estimate thermal conductivities of an orthogonal solids. 3-D conduction problem was solved as direct problem and the performance of the algorithms was checked for exact and $\sigma = 0.1T_{max}$ noisy measurement temperature data. The conjugation coefficients of the CGM were varied to check the accuracy of the estimation. The RMS error of estimation from LM was between 0-0.1 and the results revealed that the LM method converged quickly compared to CGM by consuming lesser CPU.

Liu (2012) studied one dimensional inverse heat conduction problem to estimate the temperature dependent heat capacity using modified GA and PSO. Suitable values of inertia weights, cognition and social component were adopted for PSO and the inverse estimation was tested for noisy temperature data. The comparison study of modified GA and PSO suggests that PSO algorithm gives more possibilities to find global minimum, thereby providing an unbiased estimation.

Azimifar and Payan (2017) modelled thin fins attached on vertical hot wall of the cavity and solved free convection problem using Finite Volume Method. The objective of the work was to optimize the characteristics of the thin fins attached to vertical wall of the cavity using PSO. It was observed that the heat transfer was decreased with attachment of three conductive fins for higher values of Rayleigh number. The results from PSO algorithm also confirmed that an array of conductive thin fins reduces heat transfer from a cavity for a higher Rayleigh number (Ra=10^7).

Tabrizi and Jaluria (2018) solved two dimensional laminar natural convection problem to estimate location and strength of the heat source on a vertical plate. The objective of their work was to obtain a connection between the heat source location and strength with respect to temperatures. A power law function between the temperatures and Grashof number was assumed and PSO was applied as inverse technique to find the best location of heat sources for a given input data.

Lee (2019) illustrated the use of Repulsive PSO algorithm for solving one dimensional heat conduction problem. The general velocity update equation of PSO was added with a product of acceleration coefficient and random velocity values that helps in preventing the algorithm getting propelled towards local minima. The estimation of constant appearing in the heat source equation from RPSO was compared with Levenberg-Marquardt method which showed that RPSO gave better estimation in spite of being computationally expensive.

Gossard and Lartigue (2013) used PSO to estimate the geometrical and thermophysical properties for 3-D partitioned enclosures by developing a simplified conjugate heat transfer model. Nusselt number correlations were used to find the convection and radiation was determined using radiosity method. The experimental and numerical temperatures were compared that showed a close agreements and the unknowns

were effectively identified using PSO for a particular thermal resistance and volumetric specific heat.

Chen et al. (2016) applied fuzzy inference to determine the unknown boundary condition for a conjugate heat transfer problem. The direct model was solved using Finite Volume Method and boundary element method to obtain the temperature distribution. For fuzzy inference, the difference between the measured and calculated temperatures was chosen and corresponding inference components were obtained. The guess value of the unknown parameters was updated using synthesizing weighted approach. The comparison of results with CGM and GA showed that fuzzy inference was less sensitive to initial guess, number of measurement points and temperature measurement noise. The average relative errors tend to fluctuate for GA and CGM compared to fuzzy inference for $\sigma = 0.1$ and $\sigma = 0.3$.

Ding and Sun (2015) determined heat source in function of time for an inverse heat conduction problem. Two test cases with (i) heat source varying smoothly and (ii) heat source varying with sharp corner with respect respect to time was considered. They developed enhanced PSO (EPSO) algorithm by introducing new way of velocity update with randomly selecting the neighborhood. The modification helped in controlling the larger and smaller values of velocity in every iterations. The estimation was carried out for simulated measurements and reasonable results were obtained using EPSO with % error of 0.02-0.4 and 0.09-3 for test (i) and (ii) respectively.

Victoire and Jeyakumar (2004) solved different economic dispatch problem by combining BFGS with PSO. The application of inverse is also found in the field of biomechanics where PSO algorithm is compared with GA, BFGS and SQP for identifying the human muscle movements.

Li et al. (2011) combined BFGS method with PSO to improve the pre mature convergence and search ability to optimize the multimodal functions. 20 number of benchmark problems were solved and various algorithms such as GA and variants of PSO. While comparing several modified PSO algorithms, few showed better results than PSO-BFGS for some functions due to the fact that the particle learning capabilities were found to be more effective in such algorithms.

Wang et al. (2014) showed that hybridization of meta-heuristic algorithms would improve the quality of the results. 51 functions were chosen to test efficiency, convergence and performance of the accelerated PSO modified with Differential Evolution (DE) mutation operator. With several combinations of PSO with DE, it was mentioned that the convergence rate could be effectively increased and as the reason of improvement was not discussed, it draws an attention to develop hybrid algorithms for the engineering applications.

Plevris and Papadrakakis (2011) proposed hybrid algorithm to optimize the structural bench mark problems. PSO was integrated with a gradient based sequential quadratic programming method (SQP) and three different variations of inertia weight parameter in PSO was chosen for the demonstration. The nonlinear weight upgradation showed better results for the optimization of the structural design based on PSO-SQP method.

Table 2.1 Summary of literature survey.

S.No	Authors	Year	Remarks
2.1 Determination of IHTC during solidification of the casting.			
1	Ho and Pehlke	1985	determined IHTC using air gap measurement method for cylindrical casting. Effect on directional solidification was also studied.
2	Nishida et al.	1986	used approximate integral method and approximate calculation method to calculate IHTC values during aluminum alloy casting. The IHTC values for cylindrical casting were found to be 2200-3200 W/m^{2}K and for Flat casting was 2900-4500 W/m^{2}K.
Continued on next page			

Table 2.1 – continued from previous page

S.No	Authors	Year	Remarks
3	Kulkarni and Radhakrishna	2005	conducted experiments for Al-4.5wt%Cu alloy against CO_2 sand mould. The IHTC values obtained from inverse method and air gap measurement technique were found to be higher compared to the studies of (Ho and Pehlke 1985; Nishida et al. 1986).
4	Santos et al.	2004	studied effects of IHTC behaviour during solidification of Sn-Pb and Al-Cu alloys with steel molds. The wide range of transient IHTC correlations were expressed from the calculations obtained from inverse non linear estimation.
5	Sahin et al.	2006	studied unidirectional solidification of Al-Si alloy and determined values IHTC for copper and steel chills which were found to be in the range of 19-9.5 kW/m^{2}Kand 6.5-5 kW/m^{2}K respectively.
6	Rajaraman and Velraj	2008	compared Beck's non linear estimation and control volume approach to determine the IHTC during for sand casting of aluminum. A deviation of 57% in the values of IHTC between the two methods was found. Though the value of the IHTC is high at the beginning, Beck's algorithm assumes low heat flux values compared to control volume approach, hence higher values of IHTC were obtained by Beck's algorithm.

Continued on next page

Table 2.1 – continued from previous page

S.No	Authors	Year	Remarks
7	Arunkumar and Kumar	2008	studied spatially varying heat flux at the metal mold interface due to mold filling. For 99.9% aluminum and cast iron mold system, a serial-IHCP algorithm was developed that has a capability of finding the multiple heat fluxes at metal mold interface.
8	Sun and Chao	2006	used lumped capacitance method to find the IHTC values for Sn20wt%Pb alloy and A356 alloy cylindrical casting against green sand mold. The validity of the lumped capacitance method was checked by finding the Biot number (<0.1).
9	Aweda and Adeyemi	2009	performed squeeze casting experiments for aluminum to estimate the IHTC values using Beck's non linear estimation. The applied pressure during squeeze casting enables the casting surface to be in contact with the mold hence higher values of IHTC was observed than the gravity die casting.
10	Zhang and Li	2013	conducted the effect of algorithm factors like damping factor, number of future time steps, tolerance criteria and time step of the algorithm on IHTC estimation where it was found to be crucial to select appropriate values of inputs while estimating IHTC during A356 alloy casting solidification.

Continued on next page

Table 2.1 – continued from previous page

S.No	Authors	Year	Remarks
11	Wood	1996	combined Sequential function method and GA for estimating heat transfer coefficient. It was observed that GA is immune to sensitivity coefficients and proves the robustness of the algorithm compared to the conventional sequential functional method.
12	Raudenskỳ et al.	1995	solved for inverse heat conduction problem and estimated unknown heat transfer coefficient using GA. GA provided an effective estimation for both exact and noise added temperatures but the procedure of estimation was found to be computationally costly.
13	Ranjbar et al.	2010	estimated the constants of the IHTC correlation for squeeze casting process of Al- 4.5wt% Cu alloy using Genetic Algorithm with a relative % error less than 1.5. The overall computational time for the estimation was around 8-9hours.
14	Dousti et al.	2012	determined the IHTC values for Al-5wt%Si alloy against steel moldusing PSO algorithm. The estimation were carried out for exact and σ=0.01T_{max} temperature measurements. The relative % error during the estimation of constants of the IHTC correlation was found between 0.01 and 2.

Continued on next page

Table 2.1 – continued from previous page

S.No	Authors	Year	Remarks
15	Hetmaniok et al.	2013	used Immune Recruitment Mechanism and Clonal Selection Algorithm for determining the boundary heat flux and heat transfer coefficients during solidification of aluminium. The performance of the methodology was tested upto 5% noise added temperature data.
16	Vasileiou et al.	2015	conducted experiments on variable casting geometry of Brass. The estimation of IHTC across various section using GA were performed by assuming the IHTC correlation varying with temperature as step-wise, exponential as well as step-wise function with time.
17	Wang et al.	2016	used PSO for estimating the IHTC for continuous casting process. Variation of number of particle size in PSO algorithm was studied and concluded that 20 number of particles were sufficient for a fast convergence and PSO showed strong global search ability.
18	Wang et al.	2018	explored the performance of hybrid artificial fish swarm algorithm (ZAFA) for the estimation of IHTC for quenching application. The speed of convergence was increased by modifying the regular artificial fish swarm algorithm with the normal distribution method.

Continued on next page

Table 2.1 – continued from previous page

S.No	Authors	Year	Remarks
19	Zhang et al.	2015	solved energy and radiative equations using finite volume method to get the temperature distribution for the radiative and phase change in laser heating application. Modified PSO algorithm was applied that provided effective estimation of Stefan number and conduction to radiation number for noisy temperature data.
2.3 Application of Bayesian framework for the inverse heat transfer problem.			
20	Reddy et al.	2012	used Bayesian-ANN approach to retrieve the values of constants in Nusselt number correlation during natural convection experiments for discrete heat sources on vertical plate.
21	Mota et al.	2010	solved one dimensional non-linear heat conduction problem to simultaneously estimate the heat flux and thermal parameters during heating of material with oxy acetylene torch. Accurate solution of the inverse method was obtained using Bayesian MCMC approach.
22	Yan et al.	2009	showed the ability of Bayesian framework in conjunction with Markov random field (MRF)-MCMC providing solutions with the uncertainties quantified using simulated measurements for inverse heat transfer problem.

Continued on next page

Table 2.1 – continued from previous page

S.No	Authors	Year	Remarks
23	Knupp et al.	2013	solved 1-D heat conduction problem was solved using integral transforms to obtain the solution for forward model. Transient heat transfer experiments were conducted and spatially varying temperature and diffusivity were estimated using Bayesian MCMC method.
24	Orlande et al.	2014	applied MCMC method with Delayed Acceptance Metropolis-Hastings and Enhanced Approximation Error Model to estimate spatially varying heat flux from the available transient temperatures.
25	Rojczyk et al.	2017	applied Bayesian MCMC for bio heat transfer application to estimate the skin thermophysical properties using temperature distribution inside the tissue.
26	Zeng et al.	2019	tested Approximate Bayesian computation (ABC) to reduce the computational time of forward model and achieved successful estimation both linear and non linear heat transfer problems.
2.4 Use of artificial neural network as fast forward model.			
27	Zhang et al.	2010	used ANN to train a network between the pre assumed IHTCs and corresponding temperatures obtained from simulations. The trained network was used to compare the estimate IHTCs from the experimental temperatures during casting solidification.

Continued on next page

Table 2.1 – continued from previous page

S.No	Authors	Year	Remarks
28	Ghadimi et al.	2015	trained a neural network input heat flux and corresponding temperatures obtained by solving 3-D conjugate heat transfer problem. The accuracy of the results were dependent on the future time steps and the location of the sensors.
29	Najafi and Woodbury	2015	used ANN to establish a trained neural network between the triangular heat flux and corresponding temperatures obtained by solving 1-D slab heat transfer problem. The trained neural network was tested for both constant and temperature dependent thermophysical properties.
30	Balaji and Padhi	2010	replaced forward model by ANN to estimate the convection heat transfer coefficient and thermal conductivity for a given heat generation using Bayesian-ANN framework for 2-D steady state conduction through a slab.
31	Lugon et al.	2019	compared Levenberg Marquardt method (LM) and Simulated Annealing (SA) algorithms in conjunction with ANN to estimate the gas bubble interaction. The results depicted that ANN driven LM method showed less computational cost.

Continued on next page

Table 2.1 – continued from previous page

S.No	Authors	Year	Remarks
32	Vakili et al.	2017	explored the performance of ANN by varying its parameters along with GA for estimating viscosity of graphene in nanofluid. The results of GA-ANN was compared with experiments which showed that the ANN could be a replacement of actual model thus reducing actual laboratory experimental cost.
33	Chanda et al.	2017	estimated the principal thermal conductivities of the honeycomb composite structure used in aerospace applications using GA-ANN approach. Close agreements with a maximum deviation of $\pm$ 0.85°C between simulated and experimental temperatures were observed.
34	Yadav et al.	2019	observed that the major computational cost was associated with solving the forward model and implemented ANN for 3D radiant furnace problem. Genetic algorithm was used as inverse method and GA-ANN based results were found to have less computational expense of the order of 10^3 than the conventional model.
2.5 Estimation of unknown parameters in conjugate heat transfer problem.			
(a) using determinstic methods.			

Continued on next page

Table 2.1 – continued from previous page

S.No	Authors	Year	Remarks
35	Huang and Tsai	2005	performed inverse analysis on 3-D convection fin heat transfer problem for noisy measurements $\sigma = 0.01$ and $\sigma = 0.03$ respectively. Inverse estimation was accomplished by steepest descent method considering sensitivity and adjoint problem where the local heat transfer coefficient was estimated.
36	Colaco and Orlande	2001	solved forced convection problem to estimate the time dependent heat fluxes, spatially dependent heat fluxes and time and space dependent heat fluxes using conjugate gradient method with adjoint problem.
37	Farahani and Kowsary	2017	illustrated the use of inverse conjugate heat transfer problem for steady and pulsating flow problem. Heat transfer coefficient was estimated with consideration of radiation and lateral heat conduction while solving 2-D governing equations for semi confined impinged slot jet using conjugate gradient method.
38	Ousegui et al.	2019	adopted conjugate gradient method with adjoint method for determining the air flow rate for PCM heat exchanger application. The inverse methodology was nonlinear in nature with conjugate heat transfer, the method showed satisfactory results with maximum relative error less than 5×10^{-3}.

Continued on next page

Table 2.1 – continued from previous page

S.No	Authors	Year	Remarks
39	Lugon and Silva	2011	employed SA and LM methods as inverse method in conjunction with ANN to obtain quick convergence for drying process experiments.
40	Razzaghi et al.	2019	determined spatially varying heat flux during cooling of hot plate using conjugate gradient method with adjoint method.
41	Mejias et al.	1999	solved 3-D conduction problem with Conjugate Gradient Method (CGM) and Levenberg Marquardt method (LM) to estimate thermal conductivities of an orthogonal solid. They concluded that the LM method converged quickly compared to CGM by consuming lesser CPU.
42	Liu	2012	performed the comparison study using GA and PSO for 1-D inverse heat conduction problem to estimate the temperature dependent heat capacity. The study suggested that PSO algorithm gives more possibilities to find global minimum, thereby providing an unbiased estimation.
43	Azimifar and Payan	2017	optimized the characteristics of the thin fins attached to vertical wall of the cavity using PSO.
44	Tabrizi and Jaluria	2018	PSO was applied as inverse technique to find the best location of heat sources. A 2-D laminar natural convection problem was solved to estimate location and strength of the heat source on a vertical plate.

Continued on next page

Table 2.1 – continued from previous page

S.No	Authors	Year	Remarks
45	Lee	2019	implemented Repulsive PSO algorithm for solving one dimensional heat conduction problem. The estimation of constant appearing in the heat source equation from RPSO was compared with Levenberg-Marquardt method which showed that RPSO gave better estimation in spite of being computationally expensive.
46	Gossard and Lartigue	2013	adopted PSO to estimate the geometrical and thermophysical properties for 3-D partitioned enclosures by developing a simplified conjugate heat transfer model.
47	Chen et al.	2016	exploited fuzzy inference to determine the unknown boundary condition for a conjugate heat transfer problem for noisy temperature data. The guess value of the unknown parameters was updated using synthesizing weighted approach. The comparison of results with CGM and GA with fuzzy showed that fuzzy inference was less sensitive to initial guess, number of measurement points and temperature measurement noise.
48	Ding and Sun	2015	developed enhanced PSO (EPSO) algorithm by introducing new way of velocity update with randomly selecting the neighborhood to determine heat source in function of time for an inverse heat conduction problem.

Continued on next page

Table 2.1 – continued from previous page

S.No	Authors	Year	Remarks
49	Victoire and Jeyakumar	2004	solved different economic dispatch problem by combining BFGS with PSO. The application of inverse is also found in the field of biomechanics where PSO algorithm is compared with GA, BFGS and SQP for identifying the human muscle movements.
50	Li et al.	2011	demonstrated the use of BFGS method with PSO for various benchmark problems where the hybrid approach improved the pre mature convergence and search ability to optimize the multimodal functions.
51	Wang et al.	2014	solved 51 functions to show the performance of several combinations of PSO with DE. The draws an attention to develop hybrid algorithms for the engineering applications.
52	Plevris and Papadrakakis	2011	integrated PSO with a gradient based sequential quadratic programming method (SQP) and three different variations of inertia weight parameter in PSO for optimization of a structural problem.

2.6 SUMMARY

The above literature review highlights: (i) the estimation of unknown parameters using various inverse methods. (ii) scope of evolutionary algorithms for inverse problems (iii) hybrid techniques along with ANN for the faster estimation of unknown parameters and (iv) application of Bayesian framework to measure the uncertainty quantification.

1. Estimation of heat flux or heat transfer coefficient for castings is very important to improve its quality and is possible only through the concept of inverse approach.

2. The gradient based methods with the least squares approach have been extensively used to determine the unknown parameters (without the quantification of

uncertainties) in the inverse estimation.

3. The solution of the inverse method is dependent on the number of sensors, location of the sensors and future time steps.

4. Regularization of the objective function is required in order to address the ill - posedness of the inverse problem when the objective function is based on least squares. But, Bayesian framework has inherent regularization of the posterior solution in the form of *a-priori*.

5. The mathematical model in most of the works is simplified to a heat conduction equation, but solving full model (considering 3-D Navier Stokes equations) of conjugate heat transfer problem provides more realistic information during inverse estimation.

6. Evolutionary algorithms are computationally expensive, but they are capable of providing good solutions for the problems that are unstable or do not converge.

7. Replacement of ANN as fast forward model provide quicker estimation and combination of ANN with evolutionary algorithm will enhance the computational efficiency during the inverse estimation.

2.7 RESEARCH GAP

1. Determination of interfacial heat transfer coefficient of metal casting is dependent on time and temperature dependent thermophysical properties; hence, the number of unknown parameters involved makes the inverse estimation more challenging.

2. The concept of modeling error associated with the temperature measurements for solidification of casting problem has not been reported in hitherto literature and uncertainties associated with the IHTC are not adequately dealt with literature.

3. Though the stochastic approach is preferred against the deterministic approach, it is found to be computationally expensive in the solution of inverse problems. Hence, model reduction can play major role that surrogates the forward model.

4. Estimation of thermal parameters in a conjugate heat transfer problem is imperative and realistic to develop an efficient thermal system.

2.8 OBJECTIVES OF THE PRESENT WORK

1. Mathematical modeling of horizontal directional solidification for different melting point alloys and inverse estimation of modeling error and heat transfer coefficient parameters using evolutionary algorithms.

2. Implementing Artificial Neural Network as a surrogate forward model to expedite the inverse process for the determination of heat transfer parameters using Bayesian framework.

3. Numerical modeling of coupled conduction and convection fin heat transfer problem to simultaneously estimate heat flux and heat transfer coefficient using hybrid inverse approach.

2.9 CLOSURE

This chapter signified the objectives of the present work framed based on research gap observed from the extensive literature study on various methods applied for inverse heat transfer problems. The next chapter explains the methodology involved in solving the present work.

CHAPTER 3

FORWARD AND INVERSE SOLUTIONS FOR SOLIDIFICATION OF CASTING AND FIN HEAT TRANSFER

3.1 INTRODUCTION

This chapter elaborates complete methodology of solving the inverse problem. It is necessary to develop an forward model that provides accurate temperature information. Forward model refers to the numerical model that provides temperature data for a corresponding assumed boundary conditions or unknown parameters. The role of artificial neural network is also portrayed that replaces the actual numerical model and provides a quicker estimation serving as fast foward model. An objective function that involves the parameters affecting the problem is framed. Finally, inverse techniques are employed to estimate the unknown parameters.

3.2 FORWARD MODEL

3.2.1 NUMERICAL SIMULATIONS

For the first class of problem, a prevalent one dimensional transient solidification heat conduction is solved representing a horizontal directional solidification of Sn-5%wtPb and Al-4.5%wtCu alloys against low carbon steel chill. During the inverse estimation, the values of IHTC and the surface temperature of the casting and chill are unknown. By solving the forward model with the available information about the IHTC correlation from literature, all the nodal temperatures in the problem domain can be obtained. Explicit Finite Difference Method (FDM) is used to discretize the governing equations. MATLAB is chosen as the computational tool.

For second class of problem, numerical simulations for 3D conjugate fin heat transfer problem is solved using ANSYS fluent. 3D vertical fin with base is provided with an external domain to facilitate the natural convection. Grid independence study is carried out to perform further case studies. Heat flux is supplied to the fin base and temperature distribution at several location, velocity contour and heat transfer coefficient are acquired as output from the numerical simulations. Based upon the residual

value, the convergence criteria for continuity equation is set as 10^{-4} and for momentum, energy equations is specified as 10^{-6}.

3.2.2 ARTIFICIAL NEURAL NETWORK

Artificial Neural Network (ANN) is a tool developed based on the biological nervous system. It creates a link between the inputs and the outputs with the help of weighted functions. The structure of the ANN includes three layers as shown in Figure 3.1. The first layer is the input layer that consists of range of input values through which data is furnished to the network. The second layer is called the hidden layer where training of the network is performed. The trained values are obtained from the output layers (Deng and Hwang 2006; Zhang et al. 2010). Initially, the input and output data are segregated

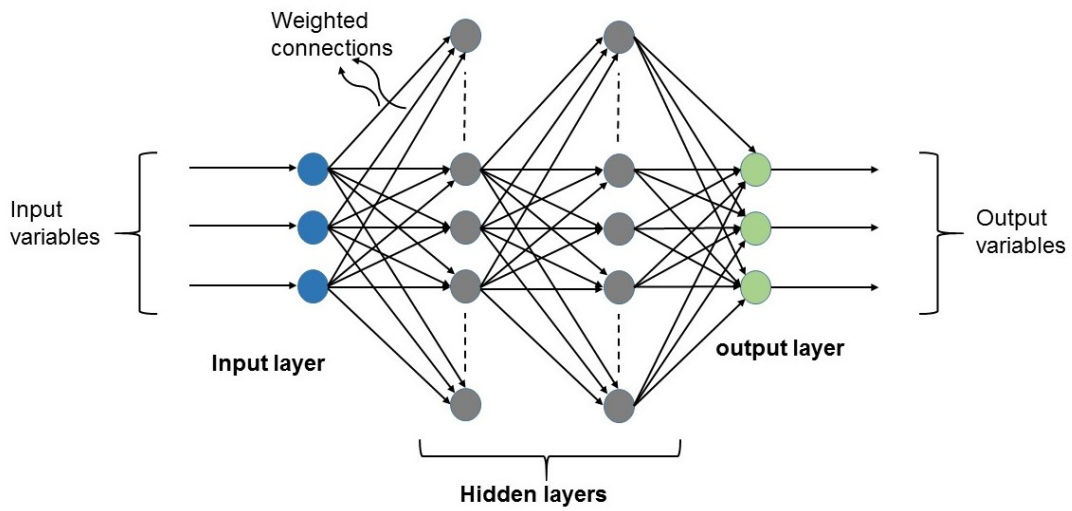

Figure 3.1 Representation of Artificial Neural Network.

as training and testing data to form a network which undergoes training until the error is reasonably less. The basic unit of the network is neuron that is interlinked by layers that carry signals which has to be processed. The weighted functions provide the strength for the signals to pass through the neurons. With the aid of certain training algorithms the weights associated with the neurons in different layer are adjusted according to the training set and the procedure is referred as training the network. The trained network represents fast forward model due to its robustness in producing the output for a given value of input.

In the present work, to obtain the solution from the forward model using numerical simulations is time consuming hence ANN is employed as a fast forward model which is created using large range of data set containing several values of unknown pare meters and corresponding temperature data obtained from numerical simulations. From the large set of data available for ANN, 70% data is chosen for training and 30% is used for testing. Neuron independence study is carried out to select the fixed number of neurons while creating the network. The selection of the neurons is based on certain parameters and is given as (Balaji and Padhi 2010),
Mean Relative Error:

$$MRE = \frac{1}{N}\sum_{i=1}^{N}\frac{|T_{actual,i} - T_{network,i}|}{T_{actual,i}} \tag{3.1}$$

Correlation Coefficient:

$$R^2 = 1 - \frac{\sum_{i=1}^{N}(T_{actual,i} - t_{network,i})^2}{\sum_{i=1}^{N} T_{actual,i}^2} \tag{3.2}$$

where, T_{actual} is the temperature data obtained from simulations, $T_{network}$ is the temperature data obtained from the network trained between known input and output. Within the range of input and output sets used to train the model, during the process of inverse estimation of unknown parameter, the ANN model will provide the output for a given input which was not a part of the training sets.

3.3 OBJECTIVE FUNCTIONS

To solve any optimization problem, an objective function has to be framed that involves the parameters affecting the problem. Least squares is commonly used objective function for the estimation of the unknowns. Choosing different type of objective function will help in smoothening of the results. In the present work, least squares method and Bayesian framework as objective function are compared.

3.3.1 LEAST SQUARES METHOD

For the purpose of demonstration, the retrieval methodology is attempted using Least squares method (LSM). The solution to the unknown parameter estimation using the least squares is achieved by minimizing the difference between the measured and the calculated temperatures obtained by the forward model (Ozisik and Orlande 2000) as

shown in Equation (3.3),

$$S = \sum_{m=1}^{M} \sum_{i=1}^{N} [Y_{im} - T_{im}]^2 \tag{3.3}$$

where Y_{im} is the i^{th} observation from the m^{th} measurement; M and N are the number of measurements and observations, respectively. T_{im} is the simulated temperature obtained from the forward model.

3.3.2 BAYESIAN FRAMEWORK

The Bayesian approach incorporates the known information regarding the unknown parameters and system uncertainties into a prior distribution model that is then combined with the likelihood to formulate the posterior probability density function (PPDF). The *a-priori* information, which is provided as a prior distribution, in Bayesian framework acts as an inherent regularization term thus leading to well-posedness of the proposed inverse problem. In addition to this, it also helps in quantification of modeling error associated with the temperature measurements. If one uses such a Bayesian framework as the objective function, there are possibilities that more information such as uncertainty of the unknown parameters can also be estimated simultaneously. According to Baye's theorem to relate measurements **Y** and the parameter **P** is given as (Wang and Zabaras 2004),

$$\pi_{posterior}(\mathbf{P}) = \pi(\mathbf{P}|\mathbf{Y}) = \frac{\pi_{prior}(\mathbf{P})\pi(\mathbf{Y}|\mathbf{P})}{\pi(\mathbf{Y})} \tag{3.4}$$

where $\pi_{posterior}(\mathbf{P})$ is the posterior probability density function (PPDF), $\pi(\mathbf{Y}|\mathbf{P})$ is likelihood function, $\pi_{prior}(\mathbf{P})$ is the prior probability density function. $\pi(\mathbf{Y})$ is the marginal probability density function of the measurements. PPDF is the probability of parameters **P** obtained for a given set of measurements **Y**.
The posterior probability is given as,

$$Posterior \propto prior \times likelihood \tag{3.5}$$

Therefore, the posterior probability density function is directly proportional to the prior probability times likelihood function. **P** in the Equation (3.4) is the unknown parameter to be estimated and **Y** is the temperature vector. Assuming the temperature data to be additive, uncorrelated, Gaussian, with zero mean and constant standard deviation, the

likelihood can be written as Equation (3.6) (Mota et al. 2010),

$$\pi(\mathbf{Y}|\mathbf{P}) = (2\pi)^{-\frac{M}{2}}|\mathbf{W}|^{-\frac{1}{2}}\exp\{-\frac{1}{2}[\mathbf{Y}-\mathbf{T}(\mathbf{P})]^T \mathbf{W}^{-1}[\mathbf{Y}-\mathbf{T}(\mathbf{P})]\} \tag{3.6}$$

Where M-number of measurements, **W**-co-variance matrix of the measurement errors. The Gaussian prior is assumed to be normal distribution with mean μ_p standard deviation σ_p is expressed as

$$\pi(\mathbf{P}) = (2\pi)^{-\frac{N}{2}}|\mathbf{V}|^{-\frac{1}{2}}\exp[-\frac{1}{2}(\mathbf{P}-\mu_p)^T\mathbf{V}^{-1}(\mathbf{P}-\mu_p)] \tag{3.7}$$

where μ_p is the known mean, **V** is the co-variance matrix **P**. Therefore, the posterior probability density function becomes,

$$\begin{aligned}\pi(\mathbf{P}|\mathbf{Y}) = (2\pi)^{-\frac{M}{2}}|\mathbf{W}|^{-\frac{1}{2}}\exp\{-\frac{1}{2}[\mathbf{Y}-\mathbf{T}(\mathbf{P})]^T\mathbf{W}^{-1}[\mathbf{Y}-\mathbf{T}(\mathbf{P})]\} \\ \times (2\pi)^{-\frac{N}{2}}|\mathbf{V}|^{-\frac{1}{2}}\exp[-\frac{1}{2}(\mathbf{P}-\mu_p)^T\mathbf{V}^{-1}(\mathbf{P}-\mu_p)]\end{aligned} \tag{3.8}$$

The above equation can be written in terms of -$lnPPDF$ as,

$$-lnPPDF = \sum_{m=1}^{M}\sum_{i=1}^{N}\frac{[\mathbf{Y}_{im}-\mathbf{T}_{im}(\mathbf{P})]^2}{2\sigma^2} + \frac{[\mathbf{P}-\mu_p]^2}{2\sigma_p^2} \tag{3.9}$$

where $\mathbf{Y}_{im}$ is the i^{th} observation from the m^{th} measurement, M and N are the number of measurements and observations, respectively. $\mathbf{T}_{im}$**(P)** is the simulated temperature obtained from the forward model solution.

3.4 INVERSE METHODS

This section explains various algorithms used as inverse techniques to estimate the unknown parameters. Stochastic methods are adopted as they have a great tendency to provide the solution through exploration over a large range of population. Genetic Algorithm, Particle Swarm Optimization and Hybrid Particle Swarm Optimization algorithms are discussed.

3.4.1 GENETIC ALGORITHM

Genetic algorithm (GA), developed by Goldberg and Holland, is recognised to be one of the robust optimization algorithms (Goldberg and Holland 1988). GA can be exploited for various applications in optimization problems. The technique works on the

evolution concept where the best candidate will always survive and becomes the successor to carry through the next generation where the worst individuals are ignored from the population in each generation. The primary steps in GA are population initialization, evaluation of the fitness function, selection, crossover, mutation and off spring generation. Initially, a set of population, generally called as chromosomes is randomly initialized. Each chromosome is encoded by bit strings referred as genes. The fitness function values are calculated for the chromosomes and ranking is performed on the basis of type of problem (to maximize or minimize). According to this, the chromosome having best fitness value is retained for next iteration. The selected set of chromosomes produce new off springs by the process called crossover where the chromosomes are randomly swapped at random cross over sites to generate new offspring. This new set of chromosomes has a great tendency to produce good performance in retrieving the solution. In order to prevent the solution getting trapped in local minima/maxima, the process of mutation is carried out. Thus the newborn population is used to find the fitness function and the process continues until the stopping criterion is reached.

3.4.2 PARTICAL SWARM OPTIMIZATION

Kennedy and Eberhart developed Particle Swarm Optimization (PSO), a widely used technique developed based on the swarm of birds moving in search of food (Eberhart and Kennedy 1995). Each individual swarm particle in the group communicates their experience of search in its proximity in space which provides a learning experience among them that results in finding its destination. PSO algorithm consists of three basic steps: initializing the random position and velocities of the swarm particles, secondly, calculating the fitness values for each particle in the swarm and finally, updating the velocities of the particles. PSO is very easy to implement with fundamental steps like random initialization of the particles and velocities, calculation of fitness function and updating the position and velocity of the particles in each iteration. For k^{th} iteration, the velocity v_i^k of the particle x_i^k and its position are updated as Equations (3.10) and (3.11) respectively.

$$v_i^{k+1} = w.v_i^k + c_1.r_1.(P_{best,i} - x_i^k) + c_2.r_2.(g_{best,i} - x_i^k) \tag{3.10}$$

$$x_i^{k+1} = x_i^k + v_i^{k+1} \tag{3.11}$$

The term particle best, P_{best} is the personal best fitness value of the particles. The overall best position of the swarm particles is termed as global best, g_{best}. w is inertia weight coefficient that influences the searching capabilities of particles and is chosen between 0 and 1, c_1 and c_2 are cognition learning coefficient and social component that drives the particles towards the local and global best positions. r_1 and r_2 are random vectors whose value lie between 0 and 1.

3.4.3 PSO-BFGS ALGORITHM

The procedure for BFGS is explained as below (Rao 2009; Nocedal and Wright 2006; Li et al. 2012),

Step 1: Set the value of initial point x^0 and convergence criterion ε>0.

Step 2: Initialize a Hessian matrix H^0=I_n, calculate the gradient d^0=$\nabla J x^0$.

Hessian matrix H^{k+1} of the Lagrangian function is evaluated in each iteration replacing the previous Hessian matrix H^k. The search direction y^k is given by

Step 3:

$$y^k = -H^k d^k \tag{3.12}$$

Step 4: Set the values

$$d^{k+1} = \nabla J(x^{k+1}) \tag{3.13}$$

$$x^{k+1} = x^k + \gamma_k y^k \tag{3.14}$$

The value γ_k can be computed by the Equation. (3.15)

$$J(x^k + \gamma_k y^k) = min J(x^k + \gamma y^k) \quad for \quad \gamma \geq 0 \tag{3.15}$$

Step 5: If $\| d^{k+1} \| \leq \varepsilon$, calculation is stopped and the output is the solution. Else go to Step6.

Step 6: Set g^k= d^{k+1} - d^k and β^k= x^{k+1} - x^k, evaluate H^{k+1} which is given by Equation. (3.16)

$$H^{k+1} = H^k + (1 + \frac{g^k H^k g^{kT}}{\beta^{kT} g^k}) \frac{\beta^k \beta^{kT}}{\beta^{kT} g^k} - \frac{\beta^k g^{kT} H^k + H^k g^k \beta^{kT}}{\beta^{kT} g^k} \tag{3.16}$$

Step 7: Set the value *k* to next iteration *k+1* and go to step 3.

For PSO-BFGS method, after finding the global best for the current iteration using PSO (Victoire and Jeyakumar 2004).

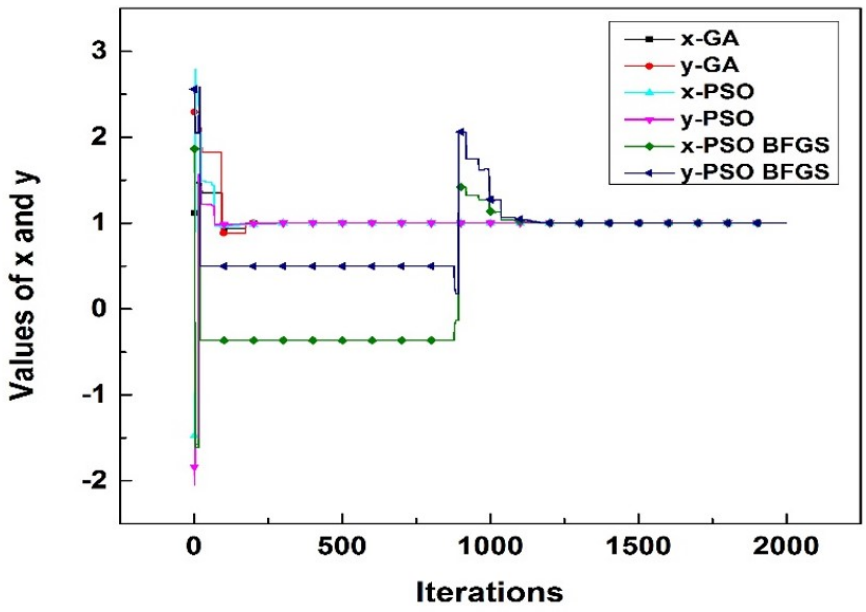

Figure 3.2 Minimum values of Rosenbrock banana function.

Step 8: Evaluate the fitness function and update the inertia weight and count *t*.

Step 9: Identify the g_{best}^t, If $g_{best}^t < g_{best}^{t-1}$, solve the inverse problem with BFGS algorithm using the present global best g_{best}^t.

Step 9: Replace the g_{best}^t value with the final solution obtained using BFGS method, else

Step 10: otherwise go to step 8.

Step 11: Change the velocities and positions.

Step 12: Iteration continued till the stopping criterion is reached.

3.5 BENCHMARK PROBLEM

A benchmark problem is solved using the above mentioned algorithms to provide a firm establishment of the accuracy of these algorithms. The bench mark problem used is Rosenbrock's banana function, which is given by (Rosenbrock 1960),

$$f(x) = 100(y - x^2)^2 + (1 - x)^2 \tag{3.17}$$

The range of (x,y) is chosen between -5 and 10. The minimum of the banana function lies at (1,1). Figure 3.2 shows the evaluation of Rosenbrock function using GA, PSO

and PSO-BFGS and it is evident that the in-house code was able to predict the values of and accurately.

3.6 CLOSURE

This chapter has put up the information of the forward model used in the present work along with the details of ANN fast forward model. The details of the least squares and Bayesian framework as objective functions were also discussed. The steps involved in various evolutionary and hybrid algorithms chosen to solve the inverse problem associated with the present work was illustrated.

CHAPTER 4

SIMULTANEOUS ESTIMATION OF UNKNOWN PARAMETERS FOR THE ESTIMATION OF INTERFACIAL HEAT TRANSFER COEFFICIENT DURING SOLIDIFICATION OF Sn–5wt%Pb ALLOY

4.1 INTRODUCTION

The present chapter focuses on model reduction in which the prevalent one-dimensional transient heat conduction equation for a horizontal solidification of Sn–5wt%Pb alloy is replaced with Artificial Neural Network (ANN) in order to estimate the unknown constants present in the interfacial heat transfer coefficient correlation. As a novel approach, ANN-driven forward model is synergistically combined with Bayesian framework and Genetic algorithm (GA) to simultaneously estimate the unknown parameters and modelling error for noise added temperature data. The hallmark of this work is to reduce the computational time of both the forward and the inverse methods and to simultaneously estimate the unknown parameters using *a-priori* engineering knowledge.

4.2 FORWARD MODEL

A mold cavity of length 110mm with 60mm low carbon steel chill is considered for solving horizontal solidification of Sn-5wt%Pb alloy casting as shown in the Figure 4.1. The main purpose of the design was to ensure a unidirectional solidification. The heat transfer exists mainly between the casting and chill with the provision of sufficient insulation around the mold cavity. The insulation prevents the heat loss through the wall surroundings and the steel chill initiates the solidification in the horizontal direction. The effects of flow of the molten metal inside the mold are neglected. As the area of the air gap at the mold metal interface is very small, the heat transfer at the casting-chill interface is assumed to happen only by conduction and the effects of convection and radiation are neglected. Two temperature sensors T_1 and T_2, one placed inside the mold cavity at a distance of 20 mm and other 3mm in the steel chill respectively from mold metal interface to measure the temperatures (Santos et al. 2004). The domain is

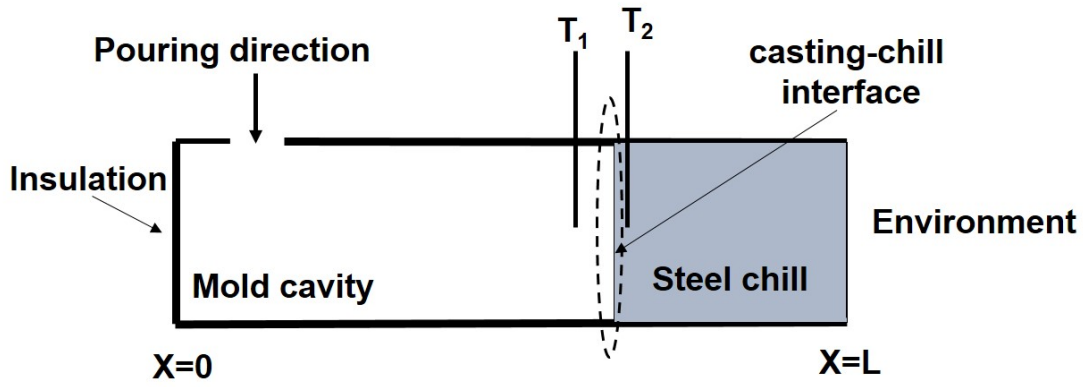

Figure 4.1 Schematic representation of the cast mold system.

discretized as shown in the Figure 4.2. The cast surface node T_C and chill surface node T_M at the mold metal interface are represented by subscripts i_g and i_{g+1} respectively.

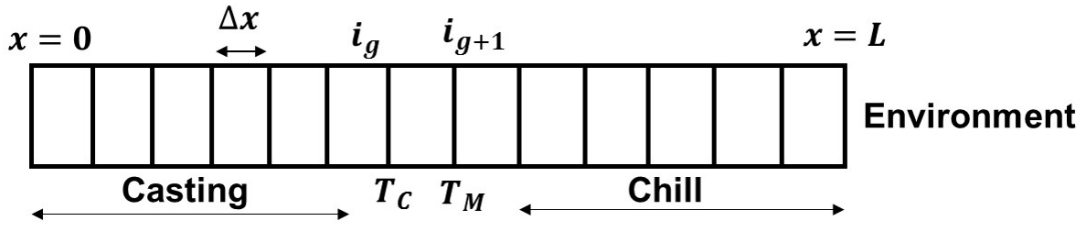

Figure 4.2 Discretization of the mold and metal interface.

The average interfacial heat transfer coefficient h_i in W/(m^{2}K) at the casting-chill interface interface is given by,

$$h_i = \frac{q}{T_C - T_M} \tag{4.1}$$

where q is the average heat flux across the casting-chill interface in W/m^2 and T_C is casting surface temperature, T_M is chill surface temperature (°C). It is presumed that heat flux released by casting is equal to the heat flux gained by the chill.

4.2.1 Governing equation for heat transfer in the chill

The unsteady one dimensional heat conduction equation is given as follows,

$$k\frac{\partial}{\partial x}(\frac{\partial T}{\partial x}) = \rho C\frac{\partial T}{\partial t} \tag{4.2}$$

where T is the temperature in °C, t is the time in seconds, α is the thermal diffusivity in m^2/s.

$$\alpha = \frac{k}{\rho C_p} \tag{4.3}$$

Where k is the thermal conductivity, W/(mK), ρ is the density, kg/m^3 and C_p is the specific heat capacity, J/(kgK).

4.2.2 Governing equation for casting

One dimensional transient heat conduction for casting solidification process is given as,

$$\frac{\partial}{\partial x}(k\frac{\partial T}{\partial x}) + \ddot{q} = \rho C\frac{\partial T}{\partial t} \tag{4.4}$$

where k is the thermal conductivity (W/(mK)), ρ is the density (kg/m^3), C is the specific heat capacity (J/(kgK)), $\ddot{q}$ is the heat source term which is included to account latent heat, $\ddot{q}$=ρl $\frac{\partial f_s(x,t)}{\partial t}$, where *l* is the latent heat of the casting. The term f_s is solid fraction of casting and its value varies between 0 and 1. A linear form of f_s defined in Equation (4.5) in the freezing zone $T_s \leq T \leq T_l$ was assumed (Voller and Swaminathan 1991).

$$f_s = \frac{T_l - T}{T_l - T_s} \tag{4.5}$$

where T_s is the solidus temperature, T_l is the liquidus temperature of the casting material. The term f_s is expressed as a parameter dependent on temperature, f_s=$f_s(T)$, then, $\frac{\partial f_s(x,t)}{\partial t}$=$\frac{\partial T(x,t)}{\partial t}$ $\frac{df_s(T)}{dT}$ and substituting back in to Equation (4.4), the final form of the governing equation by considering substitute thermal capacity method can be written as Equation (4.7) (Majchrzak et al. 2008)

$$\frac{\partial}{\partial x}(k\frac{\partial T}{\partial x}) = \rho C\frac{\partial T}{\partial t} - \rho l\frac{\partial T}{\partial t}\frac{df_s}{dT} \tag{4.6}$$

Hence,

$$\frac{\partial}{\partial x}(k\frac{\partial T}{\partial x}) = \rho C'\frac{\partial T}{\partial t} \tag{4.7}$$

where

$$C' = C - l\frac{df_s(T)}{dT} \tag{4.8}$$

4.2.3 Boundary conditions

At $x = 0$, $\frac{\partial T}{\partial x}|_{x=0} = 0$

At $x = i_g$ (casting surface), $-k_C \frac{\partial T}{\partial x}|_{x=i_g} = h_i(T_C - T_M)$

At $x = i_{g+1}$ (chill surface), $-k_M \frac{\partial T}{\partial x}|_{x=i_{g+1}} = h_i(T_C - T_M)$

At $x = L$ (chill environment), $-k_M \frac{\partial T}{\partial x}|_{x=L} = h_a(T_M - T_\infty)$

Initial condition, at $t = 0$, $T = T_i$

where k_M is the thermal conductivity of chill, W/(mK), k_C is the thermal conductivity of casting, W/(mK), h_i is the interfacial heat transfer coefficient W/(m^{2}K), h_a is the chill-environment heat transfer coefficient W/(m^{2}K), T_i is the initial temperature of the cast and chill (°C), T_∞ is the ambient temperature (°C).

Table 4.1 Thermophysical properties of the Sn-5wt%Pb alloy and low carbon steel materials (Santos et al. 2004).

Properties	k_s	k_l	C_s	C_l	ρ_s	ρ_l	T_l	T_s	T_f	K_p	l
Sn-5wt%Pb	64	33	221	259	7720	7380	216	183	232	0.0656	57120
Low carbon steel	46		7860		527						

Table 4.1[1] reports the thermo-physical properties of the materials. The initial temperatures of casting and chill were assumed as 256°C and 27°C respectively. The IHTC (h_i) is assumed to vary with time as power law shown in Equation (4.9) ,

$$h_i = at^{-b} \tag{4.9}$$

The values of h_i and h_a are assumed based on available literature data (Santos et al. 2004) as mentioned in Equation (4.10),

$$h_i = 18000t^{-0.47} \quad and \quad h_a = 5.7t^{0.15} \tag{4.10}$$

The solution of the direct problem (forward model) is obtained by solving the governing equations subjected to the known initial and boundary conditions using Explicit Finite Difference Method that provides the temperature distribution inside the casting and mold. The discretized form of the governing equation with the applied boundary

[1]SI units: T-°C, ρ-kg/m^3, C-J/(kgK), k-W/(mK), l-J/kg,suffix l-liquidus, s-solidus,f-fusion

conditions is given below (Kulkarni and Radhakrishna 2005),
For the internal nodes in casting from T_C to i_{g-1},

$$T_m^{p+1} = T_m^p (1 - 2f_0) + f_0 \left(T_{m+1}^p + T_{m-1}^p\right) \tag{4.11}$$

For the node i_g (casting surface),

$$\rho C \left(\frac{\Delta x}{2}\right) \left(\frac{T_m^{p+1} - T_m^p}{\Delta t}\right) = -k_c \left(\frac{T_m^p - T_{m-1}^p}{\Delta t}\right) - h_i \left(T_{ig}^p - T_{m+1}^p\right) \tag{4.12}$$

Upon simplification,

$$T_{ig}^{p+1} = 2f_0 T_{ig-1}^p + \left(1 - 2f_0 - \left(\frac{2h_i \Delta t}{\rho C \Delta x}\right)\right) T_{ig}^p + \left(\frac{2h_i \Delta t}{\rho C \Delta x}\right) T_{ig+1}^p \tag{4.13}$$

For the node i_{g+1}, (chill surface node),

$$T_{ig+1}^{p+1} = \left(\frac{2h_i \Delta t}{\rho C \Delta x}\right) T_{ig}^p + \left(1 - 2f_0 - \left(\frac{2h_i \Delta t}{\rho C \Delta x}\right)\right) T_{ig+1}^p + 2f_0 T_{ig+2}^p \tag{4.14}$$

The value of the grid size Δx= 1mm and the time step size is chosen to be 2ms. By solving the Equations (4.2)-(4.7) along with the boundary conditions, the exact temperatures are obtained. These exact temperatures are added with Gaussian white noise of $\sigma = 0.01T_{max}$, $\sigma = 0.02T_{max}$ and $\sigma = 0.03T_{max}$ as shown in Equation (4.15), as the experimental temperatures are usually subjected to errors. In order to mimic real time experiments, the simulated measurements are represented as,

$$Y_{iM} = T_{exact}(t_i, Sensor_M) + \epsilon\sigma \tag{4.15}$$

Where M is the number of sensors, σ is the standard deviation of the temperature measurements and ϵ is the random numbers varying between -2.576 to 2.576 for normally distributed errors with zero mean and 99% confidence bounds. The term $\epsilon\ \sigma$ represents the temperature measurement error (Dousti et al. 2012). The noisy data is now considered as simulated measurements Y_{iM}, which in turn used to solve the inverse problem.

4.3 NEURAL NETWORK

Neural network is an artificial intelligence tool developed based on the biological nervous system provides a relationship between the inputs and outputs with the help of weighted functions. Figure 4.3 shows insight of layers associated in ANN. ANN con-

sists of input, hidden and output layers. Initially, the input and output data are segregated as training and testing data to form a network which undergoes training until the error is reasonably less. The basic unit of the network is neuron that is interlinked by

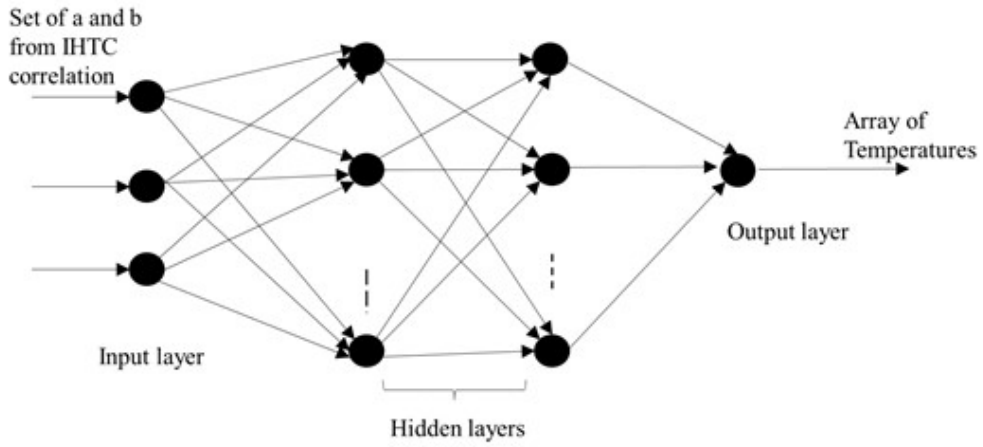

Figure 4.3 Representation of ANN trained for the present work.

layers that carry signals which has to be processed. The weighted functions provide the strength for the signals to pass through the neurons. The trained network developed provides an output for a given input and hence helps in fast computation. In other words, the trained network provides the temperature distribution for any set of input parameters specified within the range. In the present work, following steps were conducted to create a neural network.

1. Training the network: Input layers consists of set of assumed range of constants of the h_i correlation as given in Equation (4.9) and the output layers consists of corresponding temperature array at the given location from the available training data.
2. Building the network: Two hidden layers are created and the learning process is directed by Feed forward back propagation algorithm. Feed forward back propagation neural network changes the weights in such a way that output vector produces the result which is closer to the target data.
3. Training the network: From Equation (4.9), *a* and *b* are the unknown parameters, within the specified range of *a*=[1000 30000] and *b*=[0.3 0.6]. 473 data sets of numerical simulations were performed to generate neural network and the temperature measurements of the sensor at the location 20mm inside the casting for

150s is used for developing trained network. The trained network was able to produce temperatures with an accuracy less than 0.1 °C temperature difference from the exact temperature data. 70% of data is used for training and 30% of data is used for testing. 50 number of neurons are selected to produce a good fit between the output and the target data as shown in the Figure 4.4.

4. Testing the network: The trained network is referred to as fast forward model due to its robustness in producing the temperature data for any values of *a* and *b* within the specified range. A random value from the testing data is chosen to check the accuracy of the trained neural network. The output of ANN is fed in to the objective function to estimate the unknown parameters by inverse method.

4.4 INVERSE ESTIMATION

Inverse estimation is carried out using Genetic Algorithm (GA) as an inverse method. A detailed procedure of the GA is explained in the chapter 3.4.1. Here, ANN is used as fast forward model that will be employed to solve the objective functions for a defined range of populations assigned during the process of iterations. For the purpose of demonstration, the retrieval methodology is attempted using Least Squares method. But, eventually it has been identified that the methodology fails to obtain proper results when the temperature data contains more noise which will be discussed in the later section. The solution to the unknown parameter estimation using the least squares is achieved by minimizing the difference between the measured and the calculated temperatures obtained by the fast forward model (Ozisik and Orlande 2000) as shown in Equation (4.16),

$$S(h_i) = \sum_{m=1}^{M} \sum_{i=1}^{N} [Y_{im} - T_{im}(h_i)]^2 \tag{4.16}$$

The Bayesian framework is a combination of Likelihood function, which is based on the mathematical model and the prior information about the parameter to be estimated. The *-lnPPDF* from the Bayesian framework is given as (Mota et al. 2010; Wang and Zabaras 2004),

$$-lnPPDF = \sum_{m=1}^{M} \sum_{i=1}^{N} \frac{[Y_{im} - T_{im}(h_i)]^2}{2(ME * T_{max})^2} + \frac{(a - \mu_a)^2}{2\sigma_a^2} + \frac{(b - \mu_b)^2}{2\sigma_b^2} + \frac{(ME - \mu_{ME})^2}{2\sigma_{ME}^2} \tag{4.17}$$

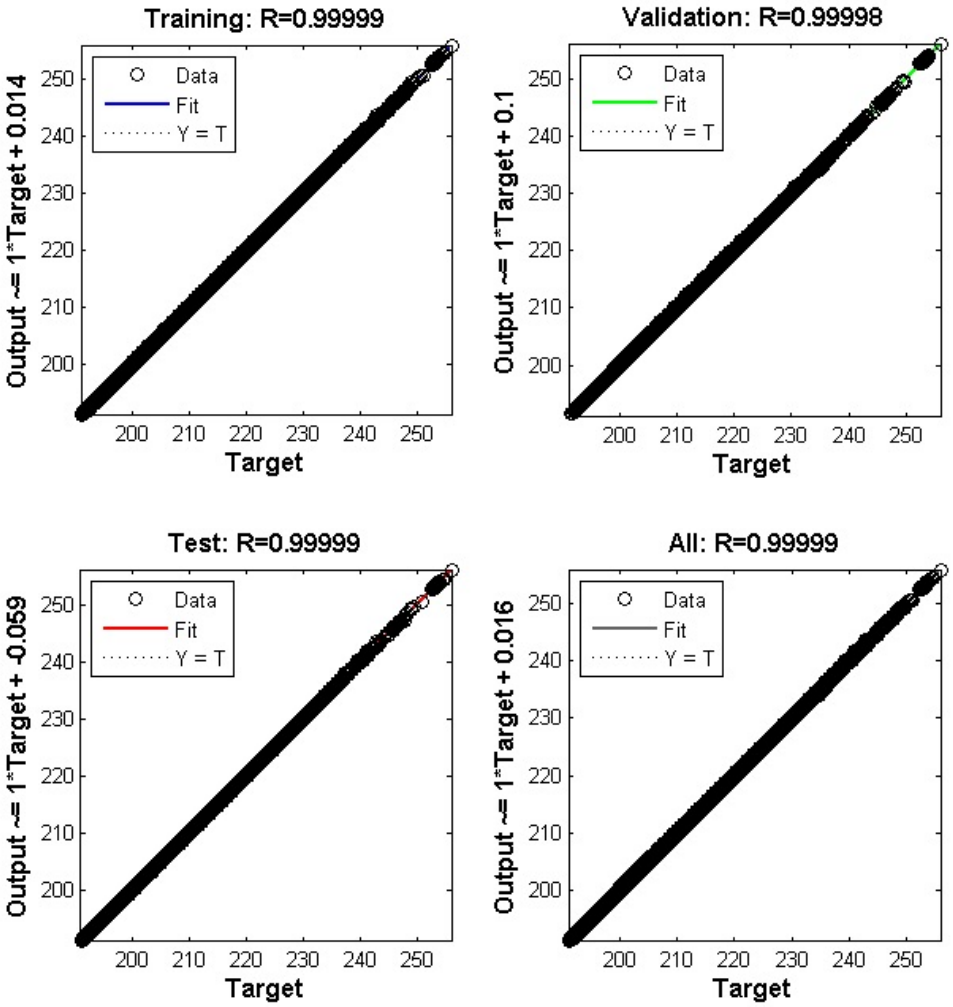

Figure 4.4 Regression plot between the output and Target data. (a) Training (b) Validation (c) Testing (d) Overall.

where h_i is the unknown parameter, Y_{im} is the i^{th} observation from the m^{th} measurement, *M* and *N* are the number of measurements and observations, respectively. $T_{im}(h_i)$ is the calculated temperature obtained from the fast forward solution, *a* and *b* are the range of values generated by GA, *ME* is the modeling error associated with the temperature measurement, μ_a=18000, μ_b=0.47, σ_a and σ_b are taken as $0.01\mu_a$ and $0.01\mu_b$ respectively.

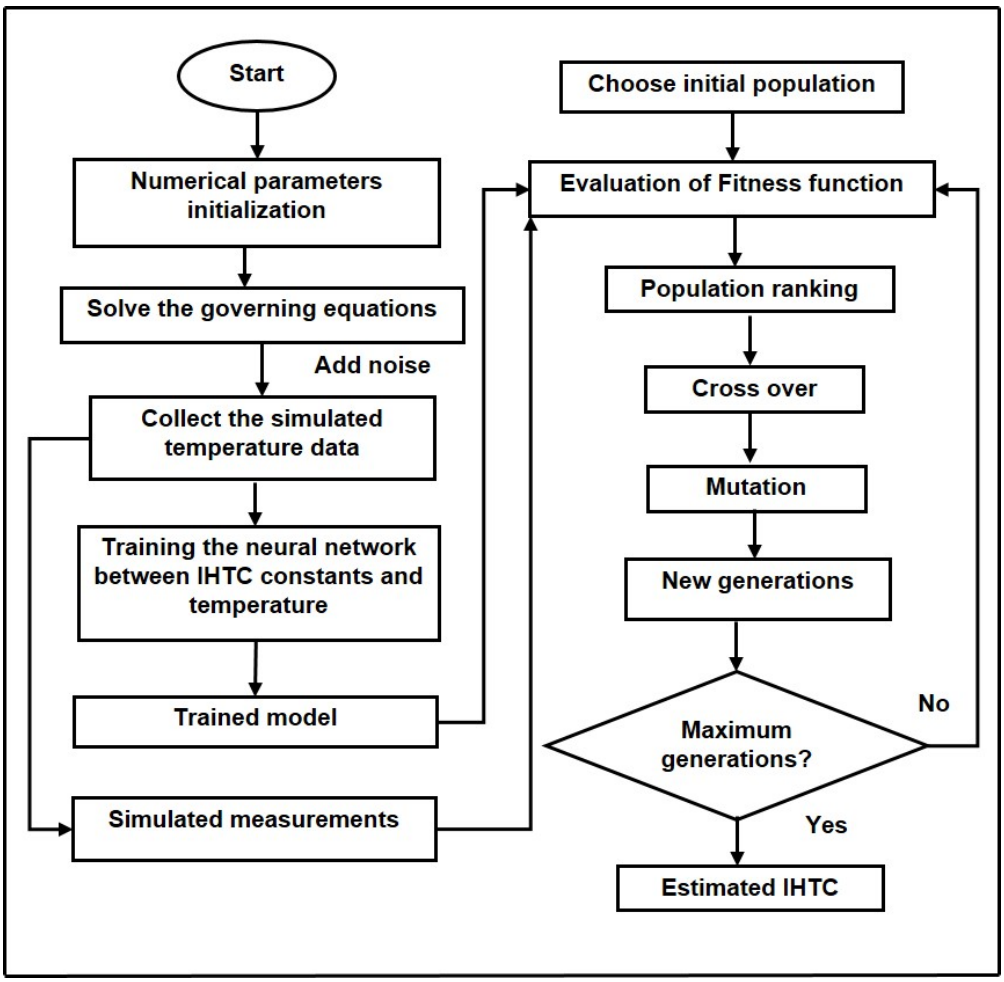

Figure 4.5 Overview of the present work.

Figure 4.5 shows the overview of the present work. In the beginning, Genetic Algorithm parameters and a range of population of the values of a and b are initialized. For every value of population, the temperatures are calculated using ANN. The error between the calculated and simulated measurements are minimized using the objective/fitness function. The fitness values are then ranked using the GA procedure and the process of crossover and mutation are performed to obtain a new set of population to proceed the iterations. The process of estimation is carried out for a specified iterations and the values of a and b for which the fitness values are minimum is the estimated values.

4.5 RESULTS AND DISCUSSION

Figure 4.6 shows the transient IHTC (h_i) and chill-environment heat transfer coefficient values (h_a) variation of pre assumed values from Equation (4.10).

Using these pre assumed values, the forward model is solved and the temperature distribution inside the casting and chill is obtained as shown in Figure 4.7. The h_i possess higher values during the initial stages of the solidification due to the good contact between the molten metal and chill surface at the interface. When the molten metal comes in contact with the chill, it loses its heat to the chill which increases the chill temperature. A thin solidified skin is first formed at the interface which acts as a resistance for the incoming molten metal. As time progresses, an air gap is formed hence the values of h_i decrease. The temperature distribution at the sensor location 20mm inside the mold cavity from the casting chill interface is used for the inverse analysis is validated as shown in the Figure 4.8.

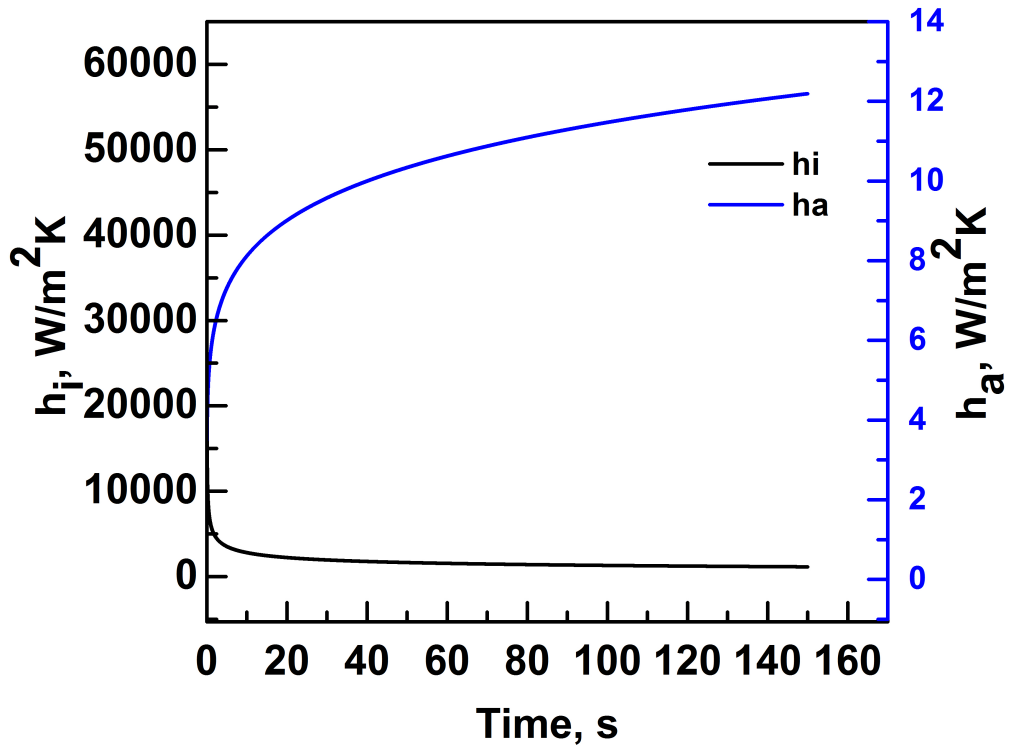

Figure 4.6 IHTC (h_i) and chill-environment heat transfer coefficient (h_a) used to solve the forward problem.

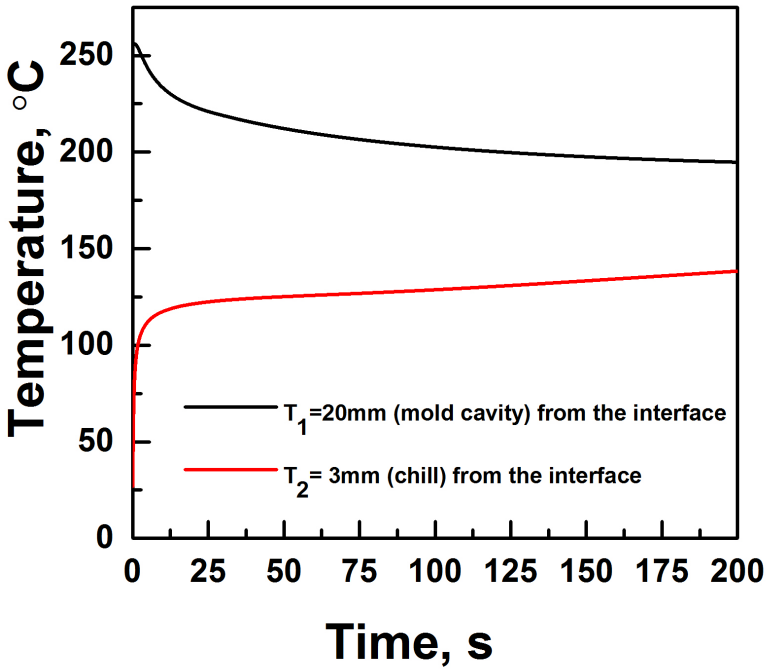

Figure 4.7 Temperature distributions at the location T_1 and T_2 from the casting chill interface.

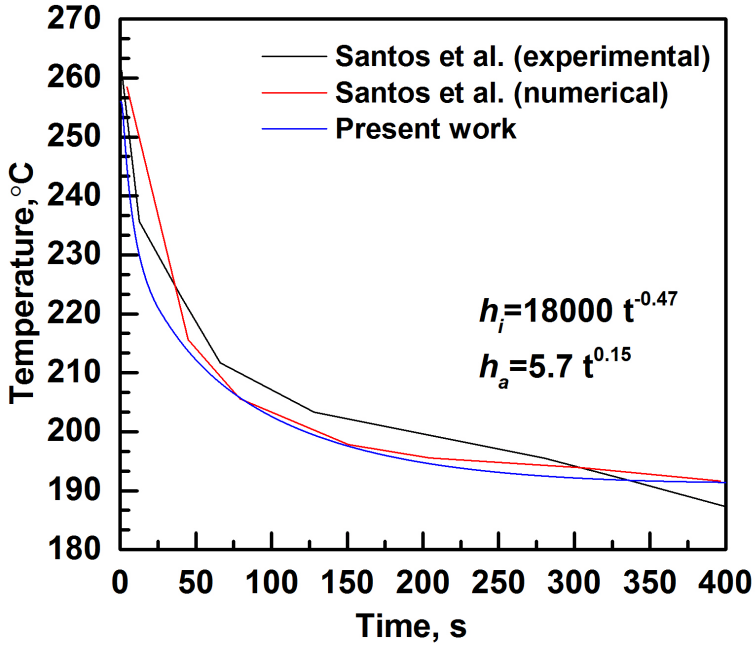

Figure 4.8 Validation of the forward model (Santos et al. 2004).

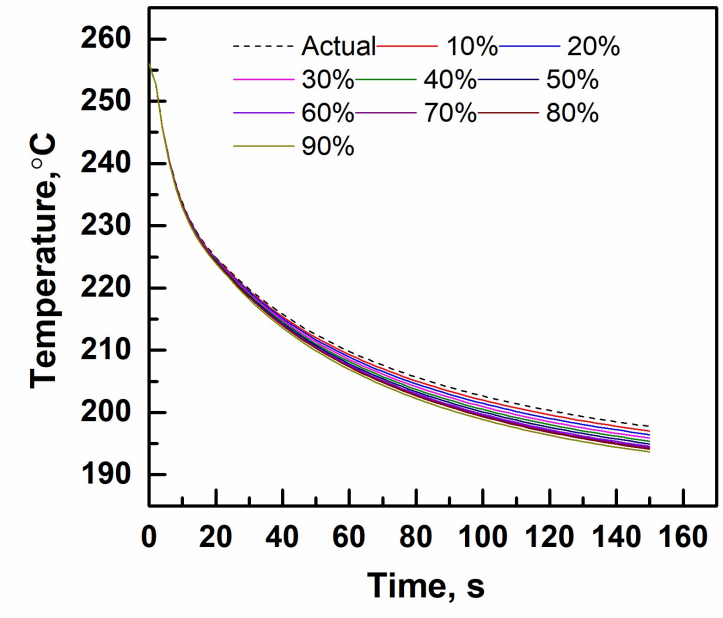

(a)

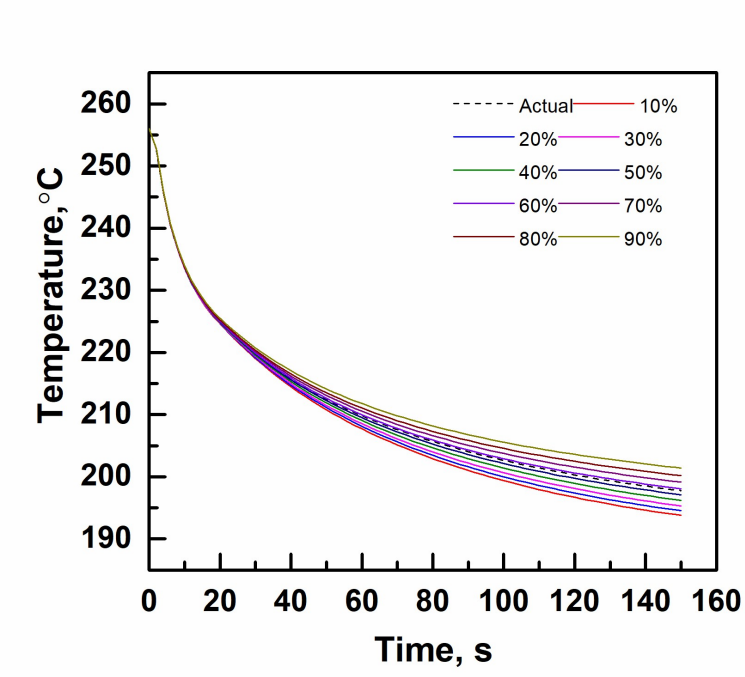

(b)

Figure 4.9 (a) Temperature distribution at T_1 for % change in values of a in h_i correlation. (b) Temperature distribution at T_1 for % change in values of b in h_i correlation.

Table 4.2 Estimated values of *a* and *b* using ANN-GA-LSM for different runs for exact temperature data.

Runs	*a* (18000)	absolute% error of *a*	*b* (0.47)	absolute% error of *b*	Time,s	Fitness value
1	18091.42	0.507	0.471	0.212	86.1	0.01743
2	18092.79	0.515	0.471	0.212	84.5	0.01743
3	18090.86	0.504	0.471	0.212	82.3	0.01743
Average	**18091.69**	**0.509**	**0.471**	**0.212**	**84.3**	**0.01743**

Table 4.3 Estimated values of *a* and *b* using ANN-GA-LSM for different runs for $\sigma = 0.01T_{max}$ temperature data.

Runs	*a* (18000)	absolute% error of *a*	*b* (0.47)	absolute% error of *b*	Time,s	Fitness value
1	19389.55	7.719	0.497	5.75	115.2	894.84
2	19376.83	7.649	0.497	5.75	105.45	894.84
3	19400.96	7.783	0.497	5.75	108.52	894.84
Average	**19389.113**	**7.717**	**0.497**	**5.75**	**109.72**	**894.84**

Table 4.4 Estimated values of *a* and *b* using ANN-GA-LSM for different runs for $\sigma = 0.02T_{max}$ temperature data.

Runs	*a* (18000)	absolute% error of *a*	*b* (0.47)	absolute% error of *b*	Time,s
1	11392.7	36.70	0.3	36.17	120.2
2	11392.7	36.70	0.3	36.17	99.5
3	11392.7	36.70	0.3	36.17	110.8
Average	**11392.7**	**36.70**	**0.3**	**36.17**	**110.17**

Choosing an appropriate value of h_i for the numerical simulation is most important decision because a random or guess value of h_i always results in different temperature distribution during the solidification. A common practice in industries is to use trial and error method to choose h_i. In order to show that, variation of temperature for small change of the unknown parameters at the sensor location T_1 is carried out where a change of 10% from the actual value of constants of the h_i correlation *a* and *b* are chosen and plotted in Figures 4.9a and 4.9b respectively.

Table 4.5 Estimated values of a and b using ANN-GA-LSM for different runs for $\sigma = 0.03T_{max}$ temperature data.

Runs	a (18000)	absolute% error of a	b (0.47)	absolute% error of b	Time,s
1	17005.28	5.526	0.3	36.17	104.3
2	17949.17	0.282	0.31	34.04	101.2
3	17584.88	2.306	0.307	34.68	107.5
Average	**17513.11**	**2.704**	**0.306**	**34.89**	**104.3**

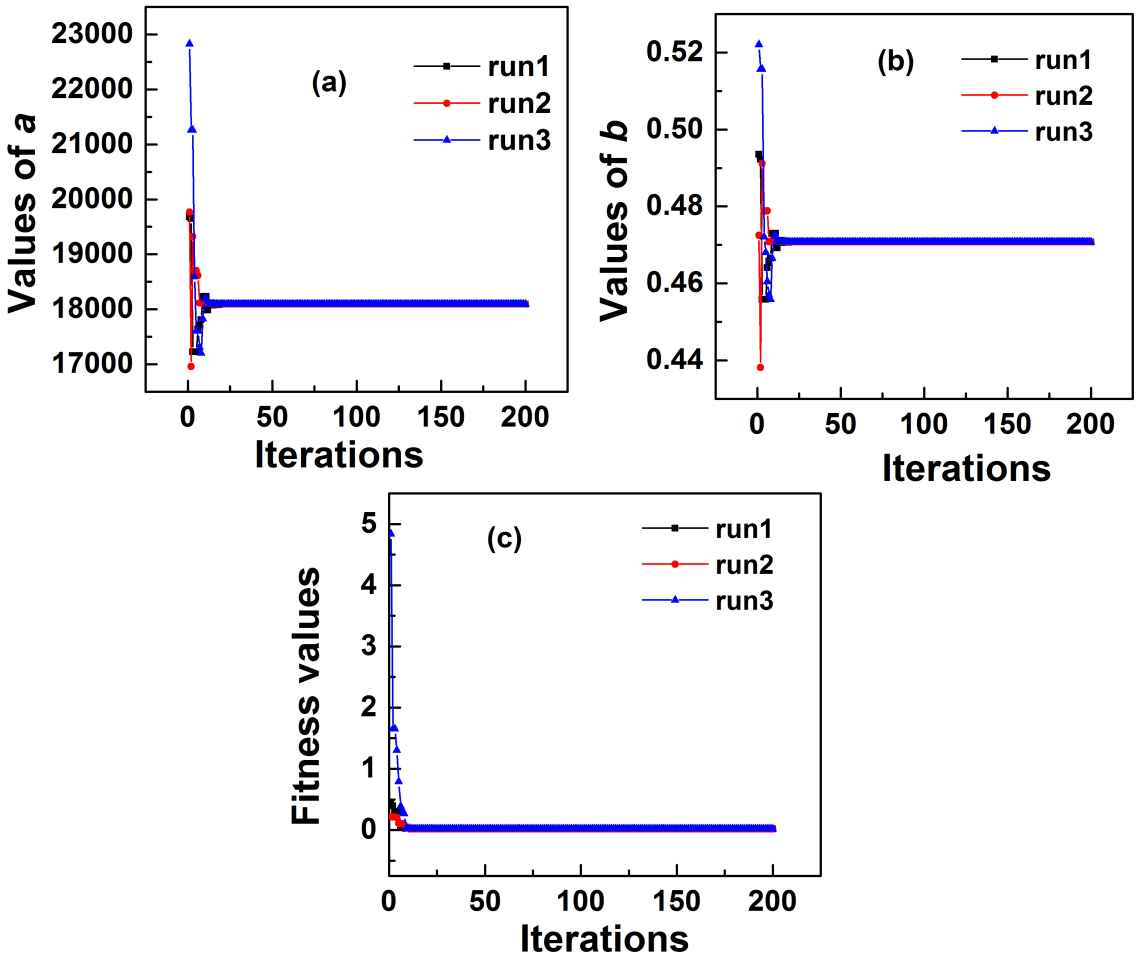

Figure 4.10 (a) Convergence of 'a' value (b) Convergence of 'b ' value (c) Convergence of fitness values for exact temperature data using ANN-GA-LSM.

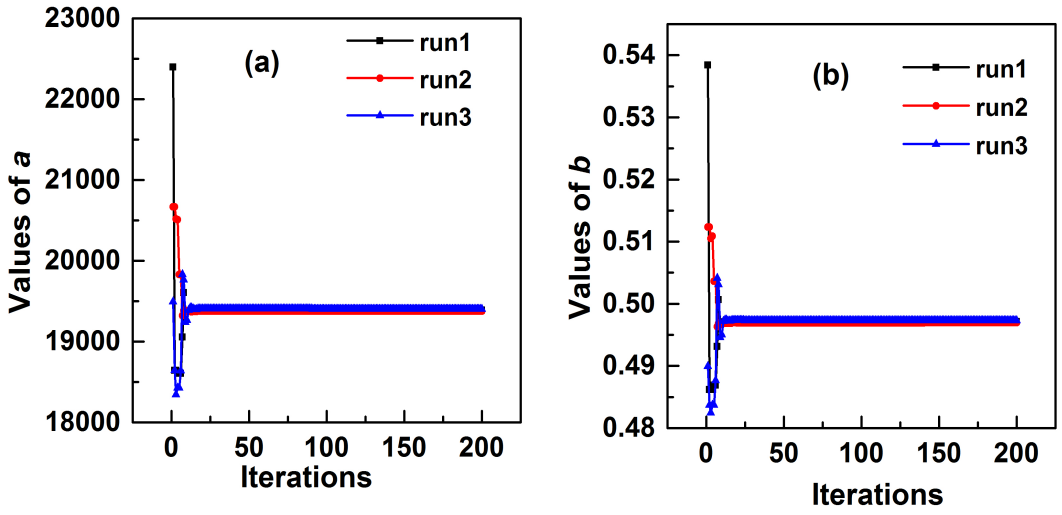

Figure 4.11 (a) Convergence of 'a' value (b) Convergence of 'b' value for σ=0.01T_{max} temperature data using ANN-GA-LSM.

Now the process of estimation of unknown parameters is carried out using GA. The input parameters for GA such as number of population=20, iterations=200, mutation rate=0.06 were initialized. The range of the values of a= [1000 30000] and b= [0.3 0.6] was selected based on the work of Santos et al. (2004), where a wealth of information is available for the solidification of Sn-Pb alloys. The inverse estimation was performed in 12GB RAM, INTEL i5 Core, 1.70 GHz computer. Three runs were carried out with the same initialized input parameters and the estimated values are collected and reported in Table 4.2. For the exact temperature data, ANN driven GA provides good estimates of a and b with LSM as objective function. The average value of a=18091.69 and b=0.471 was obtained with an absolute % error of a and b as 0.509 and 0.212 respectively. The minimum fitness value was found to be 0.01743. The ANN driven GA took around 83.4 seconds that shows a huge reduction in the computational cost compared to conventional model i.e., without ANN. Figures 4.10 (a) and (b) show the estimation of values of a and b using least square method for exact temperature data respectively. Figure 4.10 (c) provides the corresponding fitness values convergence for exact temperature data using LSM.

Table 4.6 Estimated values of *a* and *b* using ANN-GA-Bayesian framework for different runs for exact temperature data.

Runs	*a* (18000)	absolute% error of *a*	*b* (0.47)	absolute% error of *b*	Time,s	$-lnPPDF$
1	18001.41	0.0078	0.469	0.21	85.6	0.002275
2	18001.41	0.0078	0.469	0.21	88.74	0.002275
3	18002.41	0.0133	0.469	0.21	94.15	0.002275
Average	**18001.74**	**0.0096**	**0.469**	**0.21**	**89.49**	**0.002275**

Table 4.7 Estimated values of *a* and *b* using ANN-GA-Bayesian framework for different runs for $\sigma = 0.01T_{max}$ temperature data.

Runs	a (18000)	absolute% error of a	b (0.47)	absolute% error of b	ME	absolute% error of ME	Time,s	$-lnPPDF$
1	17984.31	0.0871	0.4708	0.1702	0.0101	1	83.32	67.54
2	17984.14	0.0881	0.4708	0.1702	0.0101	1	85.48	67.54
3	17983.69	0.0906	0.4708	0.1702	0.0101	1	85.48	67.54
Average	**17984.04**	**0.0886**	**0.4708**	**0.1702**	**0.0101**	**1**	**84.76**	**67.54**

Table 4.8 Estimated values of *a* and *b* using ANN-GA-Bayesian framework for different runs for $\sigma = 0.02T_{max}$ temperature data.

Runs	*a* (18000)	absolute% error of *a*	*b* (0.47)	absolute% error of *b*	ME	absolute% error of ME	Time,s	$-lnPPDF$
1	18019.42	0.107	0.468	0.425	0.0203	1.5	88.53	86.99
2	18019.43	0.107	0.468	0.425	0.0203	1.5	87.92	86.99
3	18019.41	0.107	0.468	0.425	0.0203	1.5	88.47	86.99
Average	**18019.42**	**0.107**	**0.468**	**0.425**	**0.0203**	**1.5**	**88.3**	**86.99**

Table 4.9 Estimated values of *a* and *b* using ANN-GA-Bayesian framework for different runs for $\sigma = 0.03T_{max}$ temperature data.

Runs	*a* (18000)	absolute% error of *a*	*b* (0.47)	absolute% error of *b*	ME	absolute% error of ME	Time,s	$-lnPPDF$
1	18036.02	0.2	0.468	0.425	0.0305	1.67	97.8	93
2	18036.05	0.2	0.468	0.425	0.0305	1.67	95.35	93
3	18036.05	0.2	0.468	0.425	0.0305	1.67	95.46	93
Average	**18036.04**	**0.2**	**0.468**	**0.425**	**0.0305**	**1.67**	**96.2**	**93**

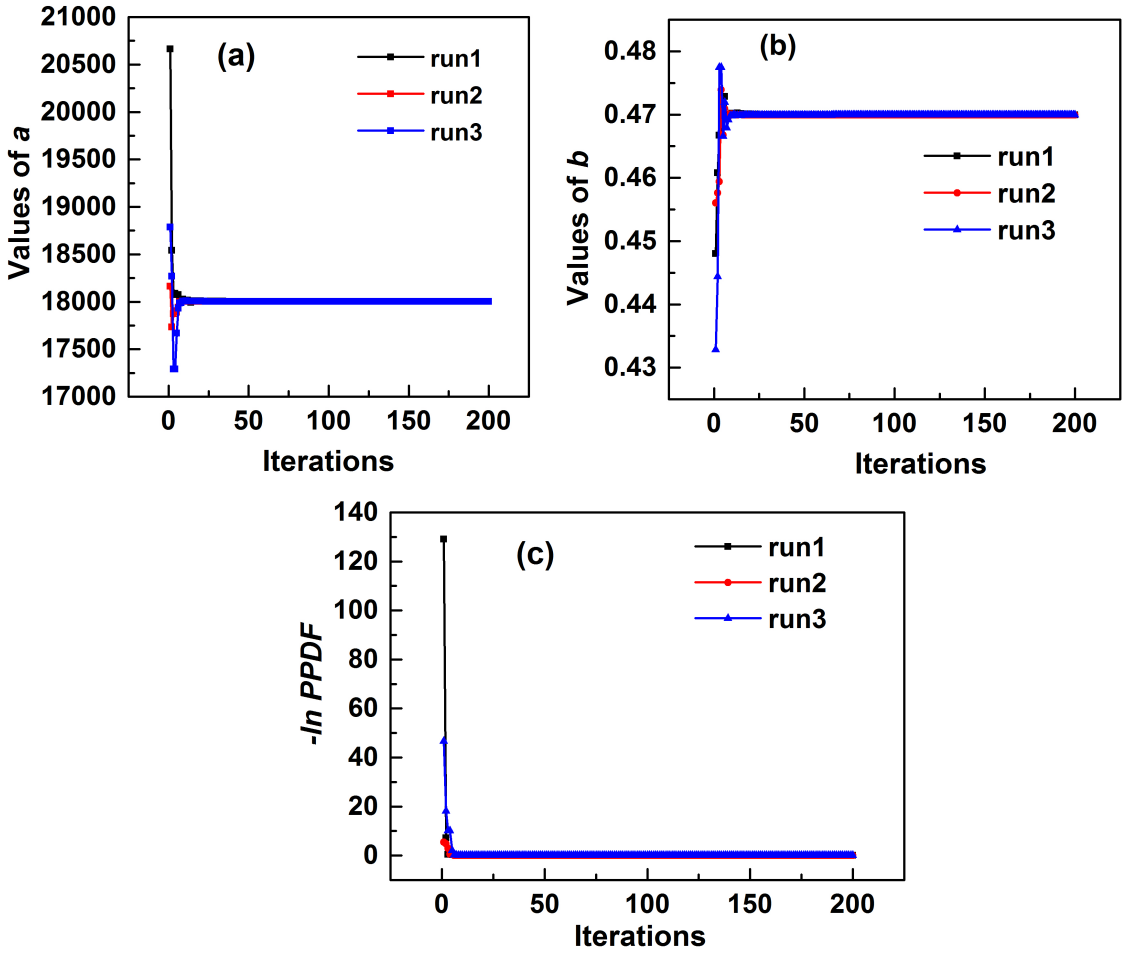

Figure 4.12 (a) Convergence of 'a 'value (b) Convergence of 'b 'value (c) Convergence of $-lnPPDF$ for exact temperature data using ANN-GA-Bayesian framework.

The estimation is now proceeded to a noisy temperature data of σ=0.01T_{max} and similarly three different runs were carried out and reported in Table 4.3. It was observed that the estimated values had a large deviation from the actual value with an absolute % error of 7.717 and 5.75 for the estimated a and b values respectively. The average fitness value was found to be 894.84. Figure 4.11 shows the convergence of a and b values for σ=0.01T_{max} temperature data respectively. Table 4.4 provides the details of the estimated unknown parameters for σ=0.02T_{max} noise data. The ANN-GA with LSM showed an unusual estimation with a very large absolute % error of 36. Hence, in order to check the accuracy of estimation for larger noisy data, a Gaussian noise of σ=0.03T_{max} is added for the exact temperature and the estimation was contin-

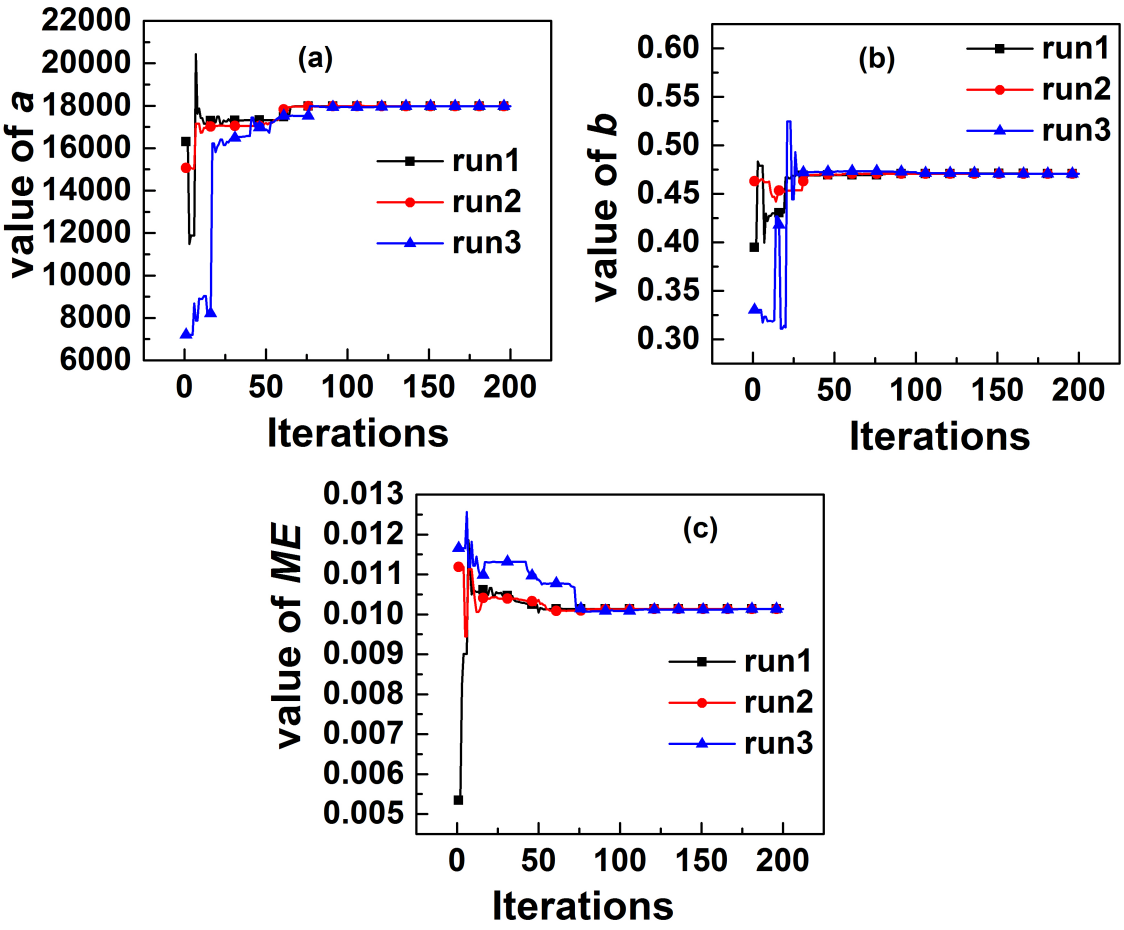

Figure 4.13 (a) Convergence of 'a 'value (b) Convergence of 'b 'value (c) Convergence of '*ME* 'value using ANN-GA-Bayesian framework for $\sigma = 0.01T_{max}$ noisy temperature data.

ued. It was observed that for high noisy data, a good estimation was achieved for the retrieval of a values with absolute % error of 2.704 where as for the value of b, there was again a huge deviation from the actual value 0.47 as mentioned in Table 4.5. The overall estimation with LSM using ANN trained inverse estimation was time saving but an accurate estimation was not achieved.

In order to overcome the disadvantage of LSM, the objective function was replaced by Bayesian framework. As mentioned in Equation (4.17), to estimate the unknown parameters, $-lnPPDF$ was calculated. Initially, for the exact temperature data, the prior information about the noise is not considered. In order to achieve this,

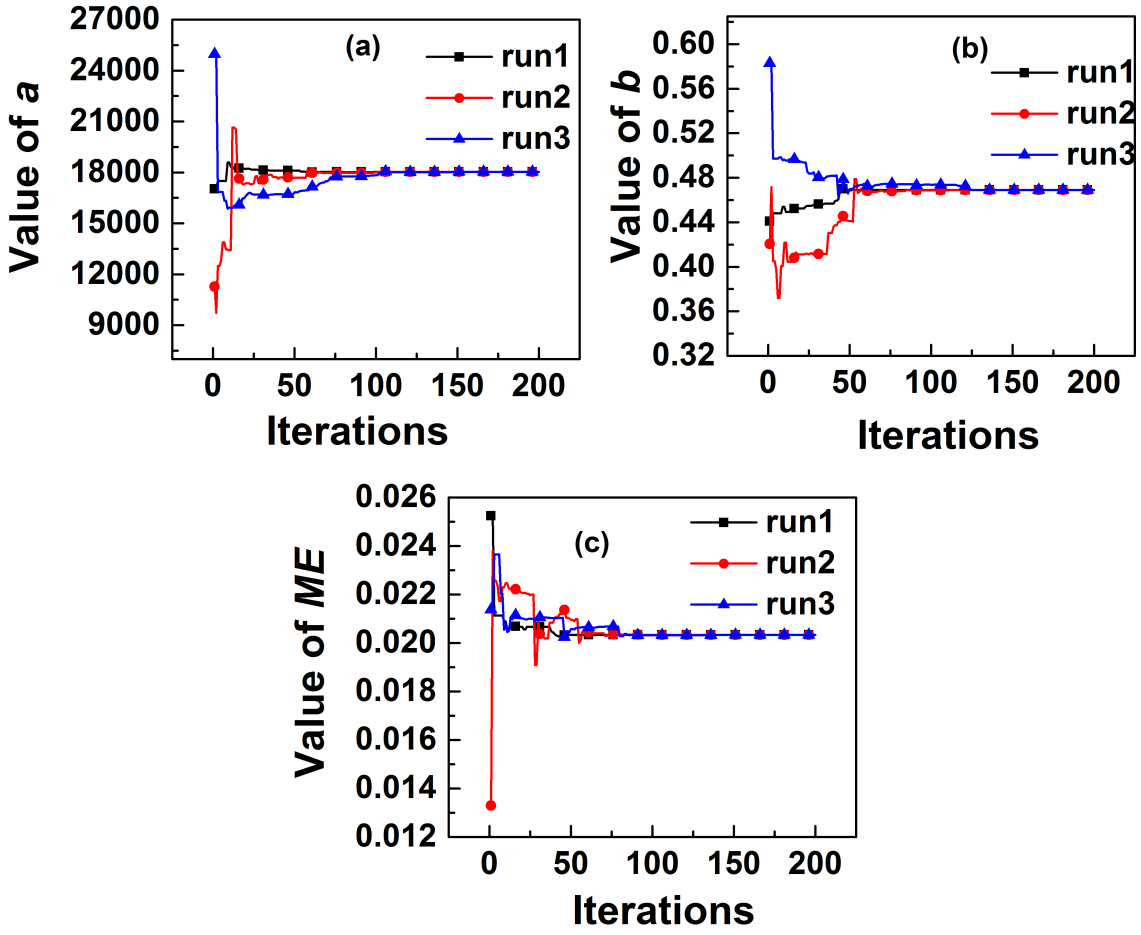

Figure 4.14 (a) Convergence of '*a* 'value (b) Convergence of '*b* 'value (c) Convergence of '*ME* 'value using ANN-GA-Bayesian framework for $\sigma = 0.02T_{max}$ noisy temperature data.

the range of values of *a*= [1000 30000], *b*= [0.3 0.6] was considered. Similar to the previous estimation, three runs with the same initial parameters using GA was carried out and the estimated values of *a* and *b* are reported in Table 4.6. Compared to LSM, ANN-GA-Bayesian framework the retrieved *a* and *b* values were very close to the actual value with absolute % error of 0.0096 and 0.21 respectively. The *-ln PPDF* value was 0.002275 which is found to be lesser compared to LSM. The convergence of *a* and *b* values and its fitness values are shown in Figure 4.12.

Further, the estimation is carried out for a noisy data of $\sigma = 0.01T_{max}$. The range of values of *a*= [1000 30000], *b*= [0.3 0.6] and modeling error, ME= [0 0.04]

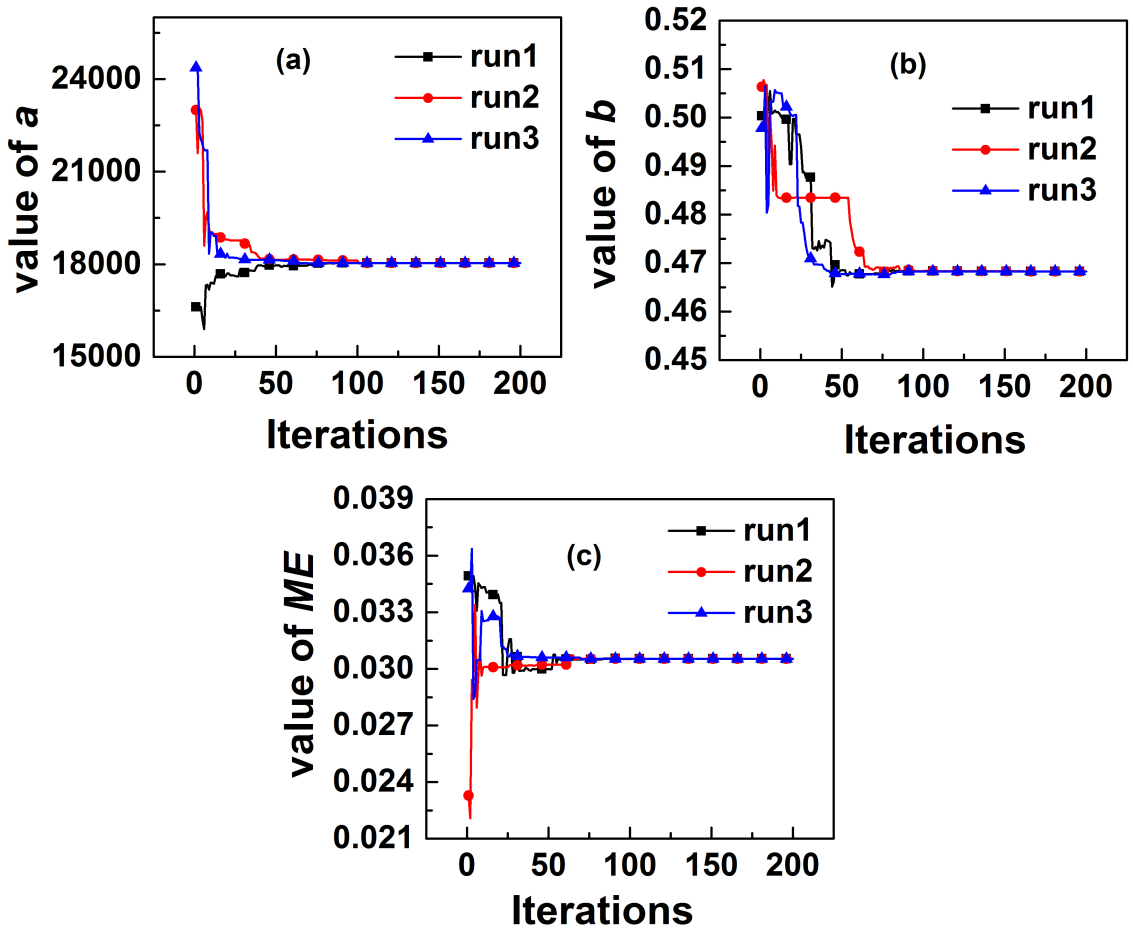

Figure 4.15 (a) Convergence of 'a 'value (b) Convergence of 'b 'value (c) Convergence of '*ME* 'value using ANN-GA-Bayesian framework for $\sigma = 0.03T_{max}$ noisy temperature data.

was chosen to solve using GA. The advantage of Bayesian framework over LSM can be observed here. The Bayesian framework not only retrieves very accurate values of a and b but also provides an opportunity to estimate the modeling error *(ME)* associated with the temperature measurements. As the Bayesian framework contains knowledge of priori information about the estimates, the method out-performs than the LSM which is evident from the reported Table 4.7. The retrieved values were having an error lesser than 2% compared to the actual values. The convergence of a, b and *ME* values are shown in the Figure 4.13.

As the experimental temperature measurements are more prone to errors, the

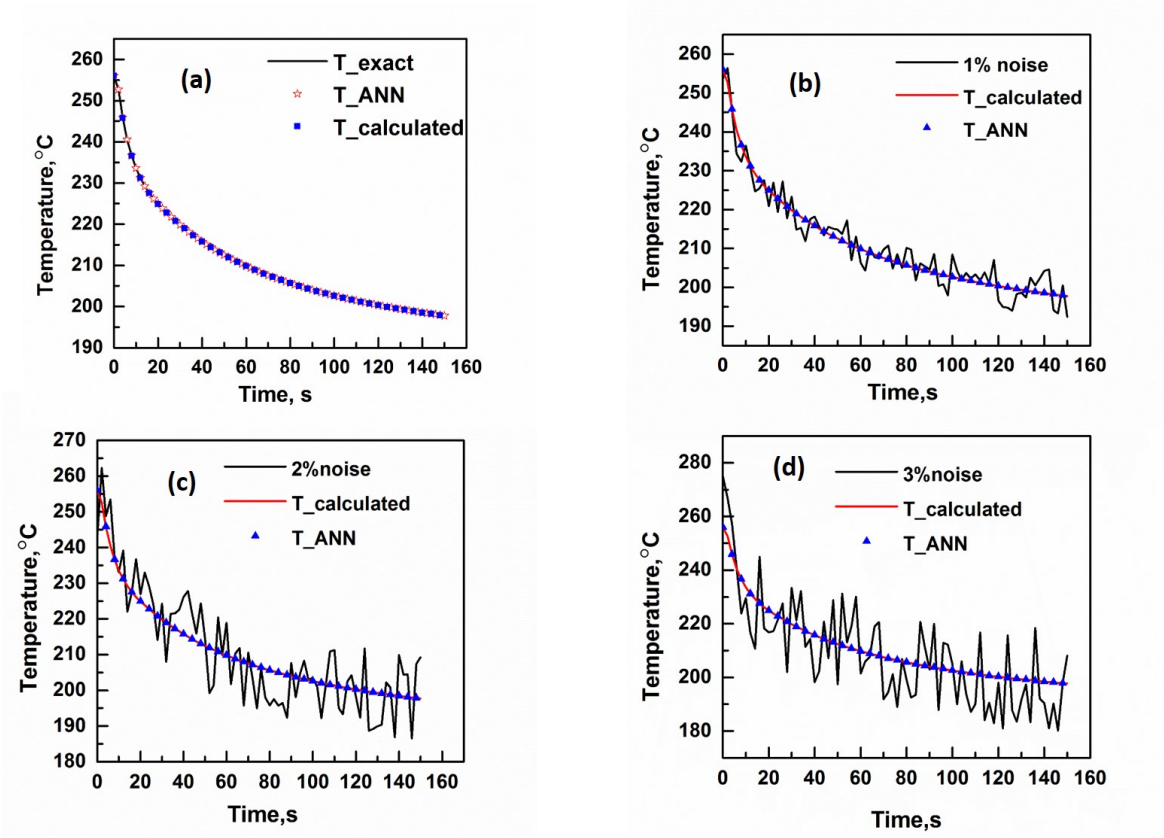

Figure 4.16 Comparison of temperature distribution obtained from the actual and retrieved values of a and b at T_1=20mm inside the mold cavity sensor. (a) For exact temperature. (b) For $\sigma = 0.01T_{max}$. (c) For $\sigma = 0.02T_{max}$. (d) For $\sigma = 0.03T_{max}$.

estimation is conducted for a noisy temperature data $\sigma = 0.02T_{max}$. The retrieved unknown parameters reported in Table 4.8 for the $\sigma = 0.02T_{max}$ noisy temperature data show a good agreement with the actual values. The convergence of the corresponding unknown parameters is shown in Figure 4.14. Similarly, the estimation was carried out for a noisy temperature of the $\sigma = 0.03T_{max}$ and as a result; GA in accordance with Bayesian found to be an effective method for solving high noisy data as noted from Table 4.9. The corresponding convergence of a, b and *ME* values are shown in Figure 4.15. The retrieved average values of a and b are used as an input for simulating forward model and ANN and the comparison of the obtained temperature distribution as shown in Figure 4.16 show the noise handling capability of the inverse method.

4.6 CONCLUSION

An ANN driven inverse estimation was attempted using GA. The forward model was solved to obtain the required temperature distribution for the solidification of Sn-5wt%Pb alloy. The major concern during inverse estimation of unknown parameters was the computational time. Therefore, a large data set, within the range of unknown parameters and corresponding temperatures was created by solving the forward model and an ANN model was developed to reduce the computational time, that acts as a fast forward model. Though the ANN-GA with LSM was found to be good for the noiseless temperature data, the methodology failed to produce satisfactory results for the noise added temperature data. Hence, the objective function was replaced with the Bayesian framework thereby exploring the a priori information of the unknown parameters. The ANN-GA with Bayesian framework established effective results with the overall average absolute error less than 2% , thus proves to be competent and potent tool for the present inverse problem.

4.7 CLOSURE

This chapter explored the use of GA as inverse method to estimate the constants of the IHTC correlation during solidification of casting. ANN as fast forward model helped to perform the estimation procedure quicker along with the Bayesian framework. In the next chapter, an attempt is made to retrieve multi-parameters using Bayesian framework along with GA and PSO algorithms during solidification of casting.

CHAPTER 5

INVERSE APPROACH USING BIO-INSPIRED ALGORITHM WITHIN BAYESIAN FRAMEWORK FOR THE ESTIMATION OF HEAT TRANSFER COEFFICIENTS DURING SOLIDIFICATION OF Al-4.5wt%Cu ALLOY

5.1 INTRODUCTION

The work presented in this chapter is the simultaneous estimation of interfacial heat transfer coefficient parameters, latent heat and modeling error during the solidification of Al-4.5wt%Cu alloy with the aid of Bayesian framework as an objective function that harmoniously match the mathematical model and measurements. A 1-D transient solidification problem is considered to be the mathematical model/forward model and numerically solved to obtain temperature distribution for the known boundary and initial conditions. Genetic algorithm (GA) and Particle Swarm Optimization (PSO) are used as an inverse approach and the estimation of unknown parameters is accomplished for both pure and noisy temperature data. The effect of number of temperature measurements on parameter estimation is also investigated in detail.

5.2 FORWARD MODEL

A one dimensional solidification problem is considered to solve the forward model that computes the temperature distribution inside the casting and chill. Figure 5.1 shows the schematic view of the problem. A mold cavity of 60mm and low carbon steel chill of 60mm is considered to cast the Al-4.5wt%Cu alloy. The temperature sensor T_1 is located inside the mold cavity at a distance of 20 mm from casting-chill interface and sensor T_2 at a distance of 3mm inside the steel chill from casting-chill interface to measure the temperatures (Santos et al. 2001). The domain is considered in such a way that the heat transfer from the casting to the chill is unidirectional. The mold cavity is insulated to restrict the heat transfer through walls and the placement of the chill acts as a heat extractor that allows the molten metal to solidify in the horizontal direction. When molten metal comes in contact with the chill, an air gap is formed at the casting-

chill interface. The heat transfer at this air gap depends on actual contact between surfaces of the chill and the casting. The air gap formed is very limited in size, as a result, the convection at the chill cast interface is neglected (Cheung et al. 2009). Also, the radiation effects at the air gap is neglected as it is found to be effective in case of high melting temperature alloys, example ferrous alloys (Prabhu and Griffiths 2001). Hence, the estimation of heat transfer coefficient during solidification of casting is adopted as inverse heat conduction problem (IHCP). Thus, the heat transfer across the casting-chill interface can be characterized by average interfacial heat transfer coefficient (h_i).

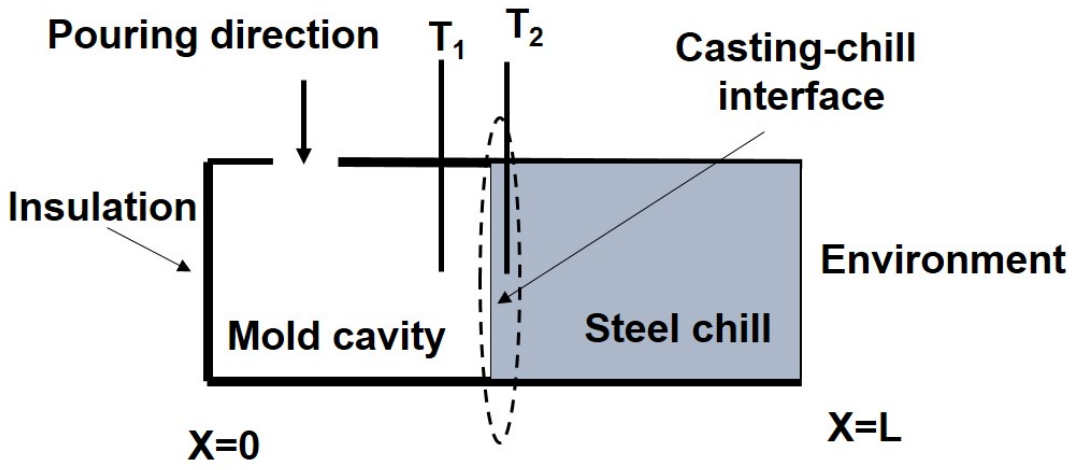

Figure 5.1 Schematic diagram of cast and chill arrangement with sensor locations.

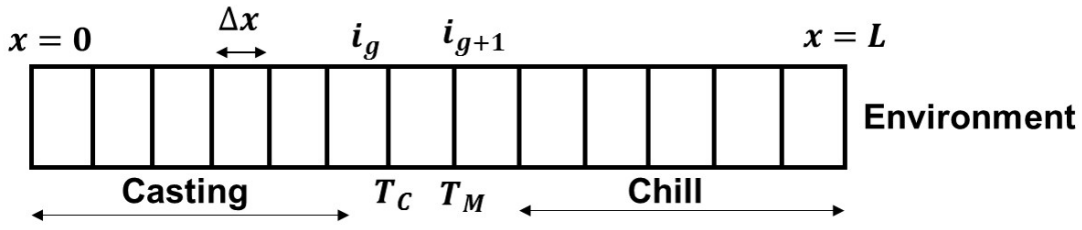

Figure 5.2 Discretization of the casting and chill system.

Figure 5.2 depicts the discretization of the solidification domain. The discretization of the casting-chill domain is considered from Kulkarni and Radhakrishna (2005). The average interfacial heat transfer coefficient h_i (W/(m^{2}K)) across the casting

Table 5.1 Thermophysical properties of the Al-4.5wt%Cu and steel material (Santos et al. 2001).

Properties	k_s	k_l	C_s	C_l	ρ_s	ρ_l	T_l	T_s	T_f	l
Al-4.5wt%Cu	193	85	1092	1059	2650	2480	645	548	660	381900
Steel	46		527		7860					

chill interface is given as,

$$h_i = \frac{q}{T_C - T_M} \tag{5.1}$$

where q is the average interfacial heat flux across the casting-chill interface in W/m^2 and T$_C$ is casting surface temperature, T$_M$ is chill surface temperature ($^\circ$C). The initial temperature of the casting and chill was taken as 700°C and 27°C, respectively. It is presumed that heat flux released by casting is equal to the heat flux gained by the chill. The h_i and h_a values are time dependent and assumed to vary as power law which is given in Equation (5.2),

$$h_i = at^{-b} \quad and \quad h_a = ct^d \tag{5.2}$$

To obtain the simulated temperatures, preselected values of h_i and h_a (Equation. (5.3)) from the literature are used (Santos et al. 2001).

$$h_i = 8650t^{-0.17} \quad and \quad h_a = 5.1t^{0.27} \tag{5.3}$$

The mathematical model represented in the Chapter section (4.2.1) along with the boundary conditions is evaluated to determine the temperature distribution in casting and chill using Explicit Finite Difference Method (FDM) (Kulkarni and Radhakrishna 2005). The prior information about h_i and h_a from Equations (5.3) is used to solve the forward model. The temperature dependent thermophysical properties considered are shown in Table 5.1[1]. The values of Δ *x*=1mm and Δ *t*=2ms for both the casting and chill were chosen satisfying Fourier number, f_0 <0.5. The exact temperatures at the mentioned sensor locations in the Figure 5.1 are added with Gaussian additive noise of $\sigma = 0.01T_{max}$, $\sigma = 0.02T_{max}$ and $\sigma = 0.03T_{max}$ as shown in Equation (4.15) to mimic the experimental temperatures.

[1]SI units: T-$^\circ$C, ρ-kg/m^3, *C*-J/(kgK), *k*-W/(mK), *l*-J/kg,suffix *l*-liquidus, *s*-solidus,*f*-fusion

5.3 SENSITIVITY ANALYSIS

A sensitivity analysis provides the information about the dependency of the unknown parameters with respective to each other. Sensitivity coefficient represents a deviation in the output for a small change in the input. Sensitivity coefficient in scaled form is defined by Equation (5.4) (Ozisik and Orlande 2000; Raudenskỳ et al. 1995)

$$J_{Pj} = P_j \frac{\partial T}{\partial P_j} = \frac{T(P_j + \epsilon P_j) - T(P_j - \epsilon P_j)}{2\epsilon P_j} \tag{5.4}$$

where P_j=1, 2, ...N is the number of unknown parameters, T is the temperature and ϵ is the value 1e-5 or 1e-6.

5.4 INVERSE ESTIMATION

The inverse estimation is carried out using Genetic Algorithm (GA) and Particle Swarm Optimization (PSO) methods. A detailed working procedure of GA and PSO is explained in Chapter 3.4 under sections 3.4.1 and 3.4.2. Bayesian framework as shown in Equation (5.5) is chosen as an objective function to exhibit the multi parameter estimation using GA and PSO.

$$\begin{aligned} -lnPPDF = \sum_{m=1}^{M}\sum_{i=1}^{N} \frac{[Y_{im} - T_{im}(h_i, l)]^2}{2(ME * T_{max})^2} + \frac{(a-\mu_a)^2}{2\sigma_a^2} + \frac{(b-\mu_b)^2}{2\sigma_b^2} \\ + \frac{(c-\mu_c)^2}{2\sigma_c^2} + \frac{(d-\mu_d)^2}{2\sigma_d^2} + \frac{(l-\mu_l)^2}{2\sigma_l^2} + \frac{(ME-\mu_{ME})^2}{2\sigma_{ME}^2} \end{aligned} \tag{5.5}$$

where h_i includes the constants of the correlation as unknown parameters (a, b, c, d) and l is latent heat, Y_{im} is the i^{th} observation from the m^{th} measurement, M and N are the number of measurements and observations, respectively. $T_{im}(h_i, l)$ is the simulated temperature obtained from the forward solution. a, b, c, d and l are the range of values generated by GA and PSO, μ_a=8650, μ_b=0.17, μ_c=5.1, μ_d=0.27, μ_l=381900. σ_a, σ_b, σ_c, σ_d and σ_l are taken as 0.01μ_a, 0.01μ_b, 0.01μ_c, 0.01μ_d and 0.01μ_l respectively.

The overview of the present work is represented as shown in Figure 5.3. A one dimensional transient solidification governing equations are solved for the known boundary conditions (forward model) to obtain the temperature distribution inside the casting and chill. The temperature distribution obtained by solving the forward model is now compared with the experimental temperatures. It is pertinent to mention here that,

the experiments are not performed in this work; hence, for the assumed value of input parameters the forward model is solved and the temperature data at a particular location is added with different level of noise in order to mimic experimental temperature data. The input parameters of the GA and PSO algorithms are initialized. In every iteration, a range of unknown parameter is initialized by GA and PSO and each value in the population will solve the forward model and corresponding calculated temperatures are compared with the simulated measurements at the mentioned locations. Based on the methodology of the algorithms, the *-lnPPDF* is minimized and the procedure is carried out till the convergence criteria is satisfied. The values of the unknown parameters for which the *-lnPPDF* is minimum are the estimated values of unknown parameters.

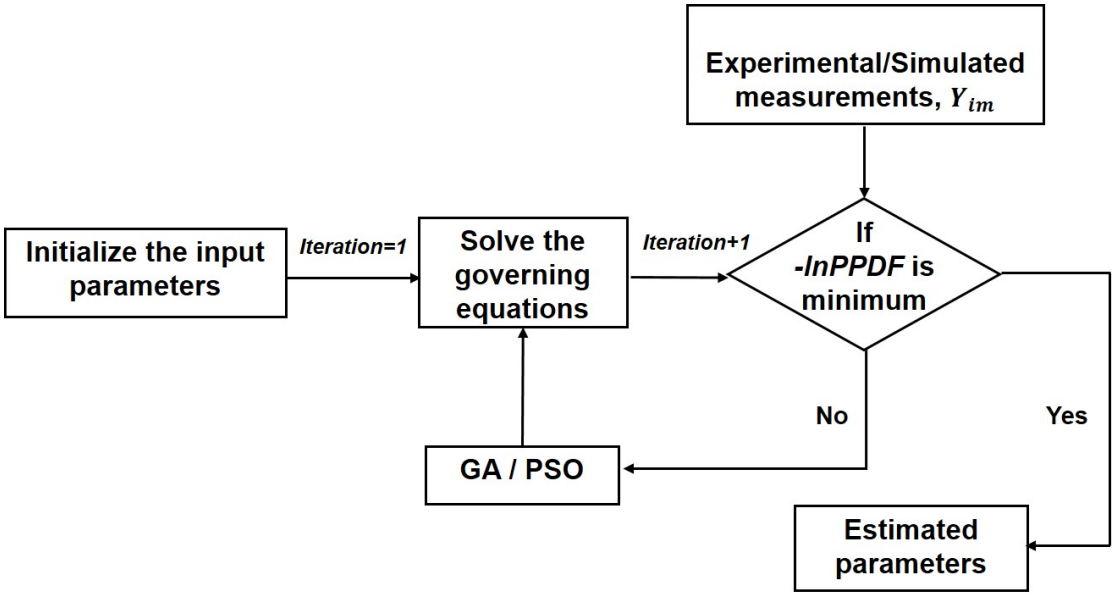

Figure 5.3 Overview of the present work for the multiparameter estimation with Bayesian framework using GA and PSO as inverse method.

5.5 RESULTS AND DISCUSSION

As discussed previously, a one dimensional solidification heat transfer problem is solved to obtain temperature distribution during solidification process. The available information about the values of h_i and h_a (Equation (5.3)) during horizontal directional solidification of Al-4.5wt%Cu alloy were used. The result of the forward model is compared with the work of Santos et al. (2001) for validation. The temperature curves obtained

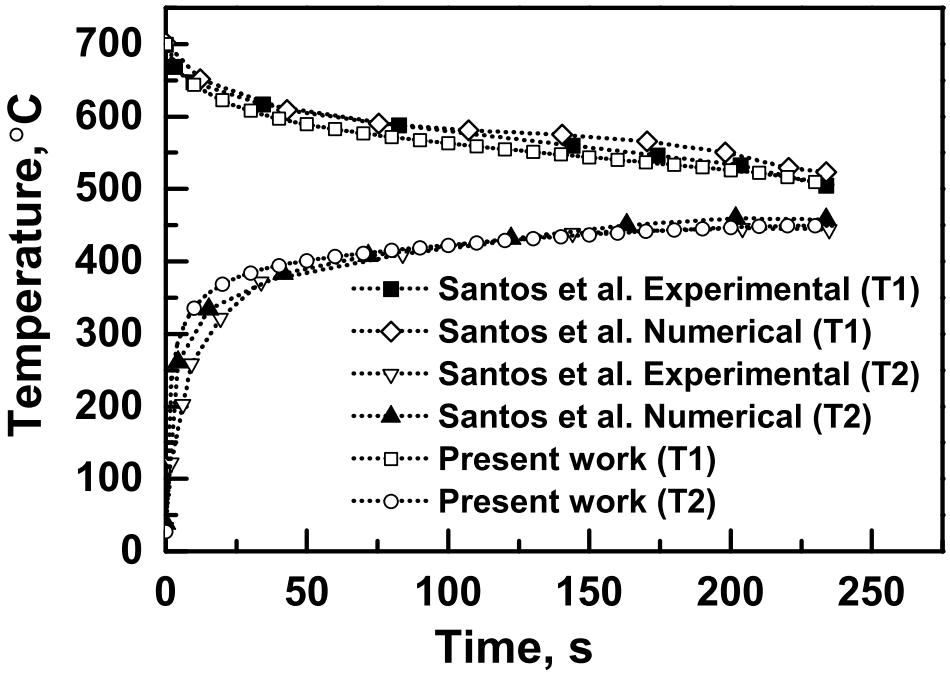

Figure 5.4 Temperature curves obtained from the temperature sensor located at a distance 20mm from the casting-chill interface inside the casting (T_1) and at a distance of 3mm from the casting-chill interface inside the chill (T_2) (Santos et al. 2001).

from the temperature sensor located at a distance of 20mm from the casting-chill interface inside the casting and at a distance of 3mm from the casting-chill interface inside the chill respectively are compared with the present mathematical model and a good agreement was observed as shown in the Figure 5.4. The molten metal starts solidifying at 660°C and ends at 548°C. The heat released during the solidification of casting is transferred to the chill and the temperature of the chill rises. The time duration till which the molten metal remains in contact with the chill depends on the metallostatic pressure and wettability of the molten metal. In the present study, a, b, c, d in h_i and h_a correlations and Latent heat (l) are the unknown parameters to be estimated. The dependency of the unknown parameters can be analyzed through scaled sensitivity values at one of the sensor locations T_2 which is shown in Figure 5.5. The values of scaled sensitivity for a, b and latent heat were found to be high compared to c and d hence they significantly affect the temperature distribution during solidification. The scaled

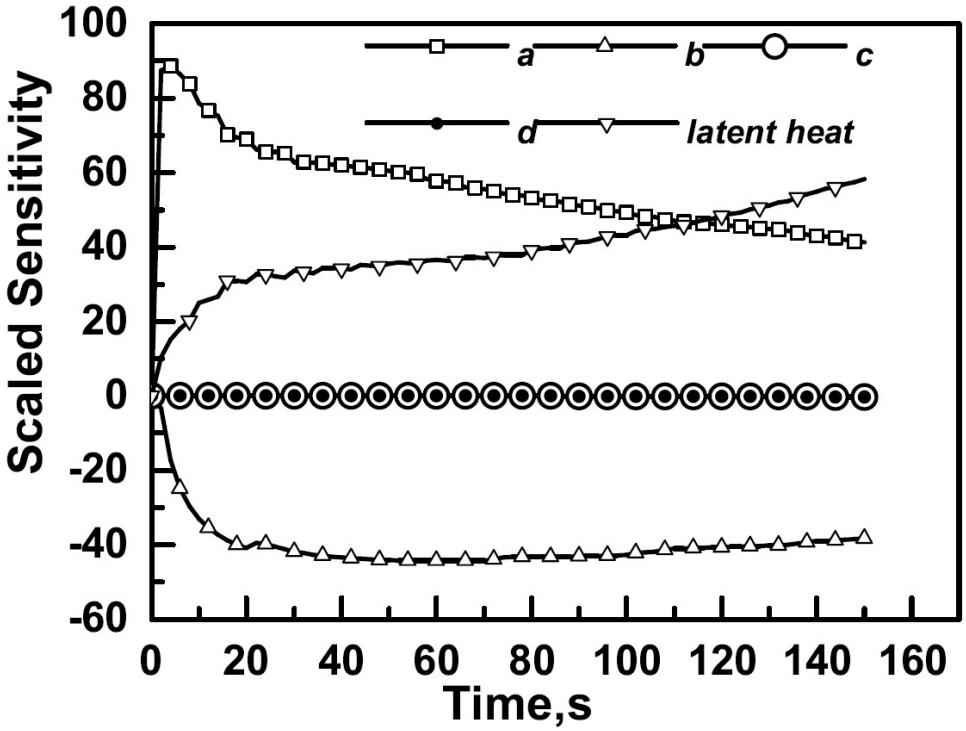

Figure 5.5 Scaled sensitivity values at temperature sensor located at a distance of 3mm from the casting-chill interface inside the chill (T_2).

sensitivity calculation of *c* and *d* is close to zero; therefore, the simultaneous estimation of all the unknown parameters is not possible without the Bayesian framework.

Upon performing the sensitivity study, GA and PSO are used as inverse methods with Bayesian framework as objective function, that helps to estimate the unknown parameters simultaneously with the beforehand available *a-priori* information. Generally, the selection of input parameters sometimes affect the solution as found in the literature. The increase in the number of population will increase the computational cost. In order to compare the performance of GA and PSO, in the present study, the input parameters of the GA are initially set as: number of population=50, number of generations=200, mutation rate =0.1. Słota (2008) analysed various combinations of GA input parameters and suggested that mutation rate of 0.1 was efficient. Generation gap is set as Ggap=1.

A generation gap of 1 represents that the entire population is replaced each generation. If the Ggap is chosen as some specific value, then few of the most fit in-

dividuals always propagate to successive generations. In the present work, no elitism was used. The real valued population was initialized and real valued mutation was performed using *mutbga* function in MATLAB (Chipperfield and Fleming 1995). Similarly for PSO, number of particles=50, number of generations=200, *w*=0.2, c_1=1, c_2=3 are initialized. The inverse estimation is accomplished using in-house codes developed using MATLAB and executed in computer with configuration of 64GB RAM, Intel xeon @2.40GHz. The values of *a*=[1000 25000], *b*=[0.01 0.6], *c*=[0.01 10], *d*=[0.01 0.6], *ME*=[0.001 0.06] and *l*=[100000 500000] are assumed. The range of values is selected from the correlation data available based on the work of Santos et al. (2001) for different compositions of Al-Cu alloys. In each iteration, GA and PSO generate random population within the specified range. Each value in the set of population represents the values of *a*, *b*, *c*, *d* and *l*. The forward model is executed for these population to obtain transient temperature distribution. Subsequently, the temperature obtained using forward model (at T_1 and T_2) is then compared with simulated measurements in the $-lnPPDF$ Equation (5.5). The inverse analysis is performed for the exact measurements and noise added measurements (σ=0.01T_{max}, σ=0.02T_{max} and σ=0.03T_{max}).

Initially the estimation procedure is carried out for exact temperatures. Three runs were performed with the same input parameters (number of population=50, number of generations=200) of GA and PSO and the retrieved unknown parameters along with the *-lnPPDF* values are plotted shown in 5.6. (The pre assumed values are mentioned in brackets in Tables 5.2-5.9). It can be seen that both GA and PSO estimated values are very close to the pre assumed values, refer Tables 5.2 and 5.3. With PSO, in every run the latent heat and *b* values were retrieved exact to the actual value and out of three runs, in two of the runs PSO estimated the values of *a* and *c* exact to the original values. The average $-lnPPDF$ values were found to be 1.85e-7 from GA and 2.31e-15 from PSO. As PSO method is simple to implement with few number of steps, it took less time i.e. 26142 s for the solution to converge compared to GA (29622 s) for exact temperature data. Figure 5.7 shows the retrieval of the constants of the heat transfer coefficient correlation, latent heat along with the modeling error for σ=0.01T_{max} noisy temperature data.

It is evident that the convergence of the values of *a*, *b*,*c*, *d* along with the la-

Table 5.2 Retrieved values of unknown parameters using GA with Bayesian framework for different runs for exact temperature data.

Runs	a (8650)	absolute% error of a	b (0.17)	absolute% error of b	c (5.1)	absolute % error of c	d (0.27)	absolute % error of d	Latent heat (381900)	absolute % error of Latent heat	-lnPPDF
1	8649.9	0.001	0.169	0.588	5.1	0	0.269	0.37	381900.65	0.0001	1.29e-7
2	8650.02	0.0002	0.17	0	5.09	0.19	0.27	0	381899.07	0.0002	2.15e-7
3	8650.04	0.0004	0.17	0	5.09	0.19	0.27	0	381899.74	0.00006	2.13e-7
Average	**8649.98**	**0.0002**	**0.169**	**0.588**	**5.09**	**0.19**	**0.269**	**0.37**	**381899.82**	**0.00004**	**1.85e-7**

Table 5.3 Retrieved values of unknown parameters using PSO with Bayesian framework for different runs for exact temperature data.

Runs	a (8650)	absolute% error of a	b (0.17)	absolute% error of b	c (5.1)	absolute % error of c	d (0.27)	absolute % error of d	Latent heat (381900)	absolute % error of Latent heat	-lnPPDF
1	8649.9	0.001	0.17	0	5.1	0	0.269	0.37	381900	0	2.89e-15
2	8650	0	0.17	0	5.09	0.19	0.27	0	381900	0	2.02e-15
3	8650	0	0.17	0	5.1	0	0.269	0.37	381900	0	2.02e-15
Average	**8649.96**	**0.0004**	**0.17**	**0**	**5.09**	**0.19**	**0.269**	**0.37**	**381900**	**0**	**2.31e-15**

Table 5.4 Retrieved values of unknown parameters using GA with Bayesian framework for different runs for $\sigma = 0.01T_{max}$ temperature data.

Runs	a (8650)	absolute% error of a	b (0.17)	absolute% error of b	c (5.1)	absolute % error of c	d (0.27)	absolute % error of d	ME (0.01)	absolute % error of ME	Latent heat (381900)	absolute % error of Latent heat	-lnPPDF
1	8628.4	0.249	0.169	0.588	5.1	0	0.27	0	0.0103	3	383630	0.45	171.46
2	8628.4	0.249	0.169	0.588	5.1	0	0.269	0.37	0.0103	3	383640	0.45	171.46
3	8628.3	0.25	0.169	0.588	5.1	0	0.27	0	0.0103	3	383641	0.45	171.46
Average	**8628.36**	**0.25**	**0.169**	**0.588**	**5.1**	**0**	**0.27**	**0**	**0.0103**	**3**	**383637**	**0.45**	**171.46**

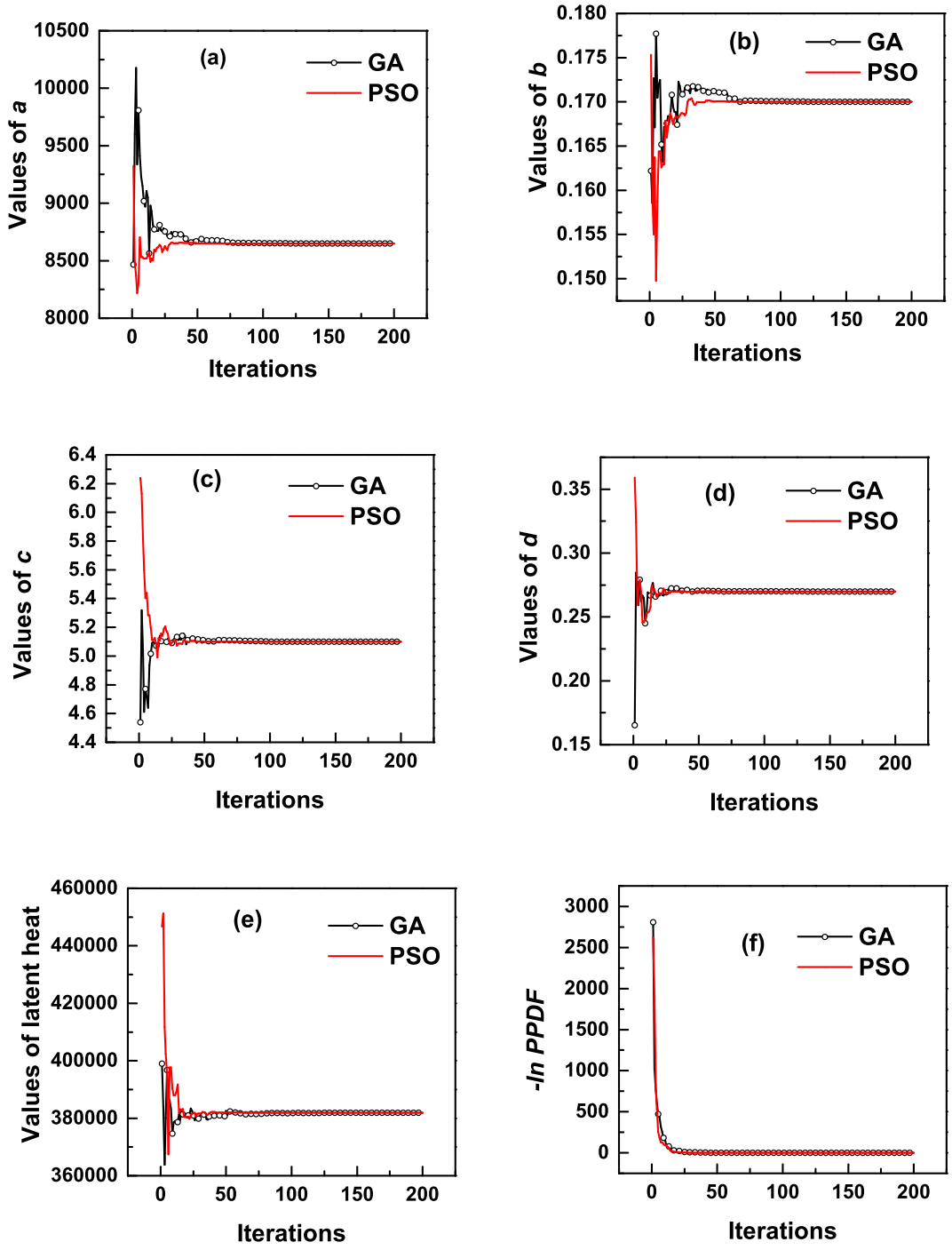

Figure 5.6 (a) Convergence of average values of 'a '(b) Convergence of average values of 'b '(c) Convergence of average values of 'c '(d) Convergence of average values of 'd'(e) Convergence of average values of $latent\ heat$ (f) Convergence of average values of $-lnPPDF$ using GA and PSO for exact temperature data.

Table 5.5 Retrieved values of unknown parameters using PSO with Bayesian framework for different runs for $\sigma = 0.01T_{max}$ temperature data.

Runs	a (8650)	absolute% error of a	b (0.17)	absolute% error of b	c (5.1)	absolute % error of c	d (0.27)	absolute % error of d	ME (0.01)	absolute % error of ME	Latent heat (381900)	absolute % error of Latent heat	-lnPPDF
1	8628.7	0.246	0.169	0.588	5.1	0	0.27	0	0.0103	3	383640	0.45	171.46
2	8628.5	0.248	0.169	0.588	5.1	0	0.27	0	0.0103	3	383630	0.45	171.46
3	8628.7	0.246	0.169	0.588	5.1	0	0.27	0	0.0103	3	383640	0.45	171.46
Average	**8628.6**	**0.247**	**0.169**	**0.588**	**5.1**	**0**	**0.27**	**0**	**0.0103**	**3**	**383636.7**	**0.45**	**171.46**

Table 5.6 Average retrieved values of unknown parameters using GA and PSO with Bayesian framework for different runs for $\sigma = 0.02T_{max}$ temperature data.

Average values	a (8650)	absolute% error of a	b (0.17)	absolute% error of b	c (5.1)	absolute % error of c	d (0.27)	absolute % error of d	ME (0.02)	absolute % error of ME	Latent heat (381900)	absolute % error of Latent heat	-lnPPDF
GA	8597.1	0.611	0.17	0	5.09	0.19	0.27	0	0.0205	2.5	381355	0.14	140.75
PSO	8596	0.625	0.17	0	5.1	0	0.27	0	0.0205	2.5	381407	0.129	140.75

Table 5.7 Average retrieved values of unknown parameters using GA and PSO with Bayesian framework for different runs for $\sigma = 0.03T_{max}$ temperature data.

Average values	a (8650)	absolute% error of a	b (0.17)	absolute% error of b	c (5.1)	absolute % error of c	d (0.27)	absolute % error of d	ME (0.03)	absolute % error of ME	Latent heat (381900)	absolute % error of Latent heat	-lnPPDF
GA	8643.4	0.076	0.169	0.588	5.1	0	0.27	0	0.0309	3	382349.7	0.117	163.04
PSO	8643	0.0809	0.169	0.588	5.1	0	0.27	0	0.0309	3	382347.7	0.1172	163.04

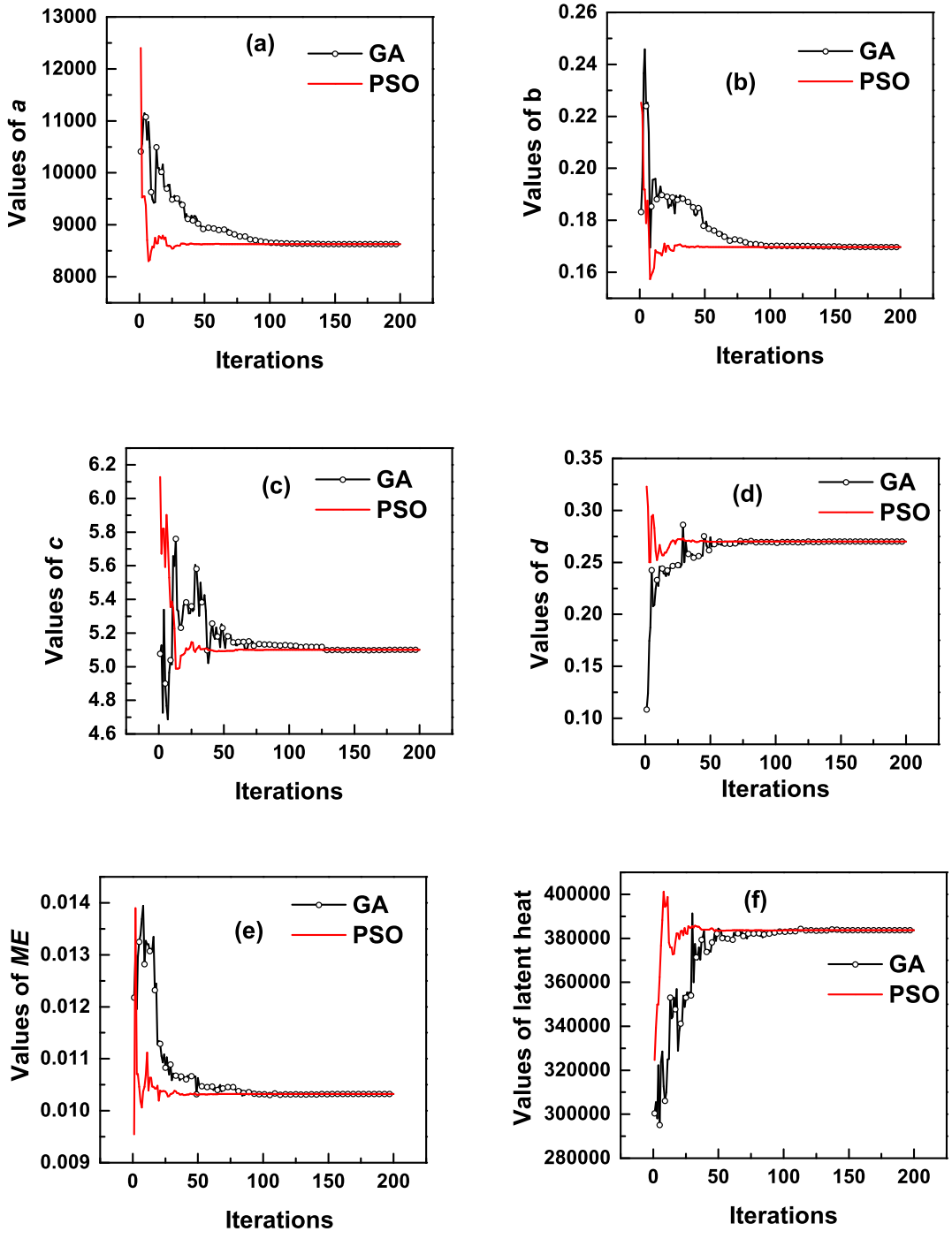

Figure 5.7 (a) Convergence of average values of 'a '(b) Convergence of average values of 'b '(c) Convergence of average values of 'c '(d) Convergence of average values of 'd '(e) Convergence of average values of 'ME '(f) Convergence of average values of $latent\ heat$ using GA and PSO for σ=0.01T_{max} noisy data.

Table 5.8 Average retrieved values of unknown parameters using GA and PSO with Bayesian framework for different runs for exact temperature data with five temperature sensors.

Average values	a (8650)	absolute% error of a	b (0.17)	absolute% error of b	c (5.1)	absolute % error of c	d (0.27)	absolute % error of d	Latent heat (381900)	absolute % error of Latent heat	-lnPPDF
GA	8649.93	0.0008	0.17	0	5.1	0	0.27	0	381900.33	0.00008	1.25e-6
PSO	8650	0	0.17	0	5.1	0	0.27	0	381900	0	5.01e-15

Table 5.9 Average retrieved values of unknown parameters using GA and PSO with Bayesian framework for different runs for $\sigma = 0.01T_{max}$ temperature data with five temperature sensors.

Average values	a (8650)	absolute% error of a	b (0.17)	absolute% error of b	c (5.1)	absolute % error of c	d (0.27)	absolute % error of d	ME (0.01)	absolute % error of ME	Latent heat (381900)	absolute % error of Latent heat	-lnPPDF
GA	8677.2	0.313	0.169	0.588	5.1	0	0.269	0.37	0.0106	6	379860.2	0.534	389.27
PSO	8676.6	0.30	0.17	0	5.1	0	0.27	0	0.0106	6	379931.83	0.515	389.269

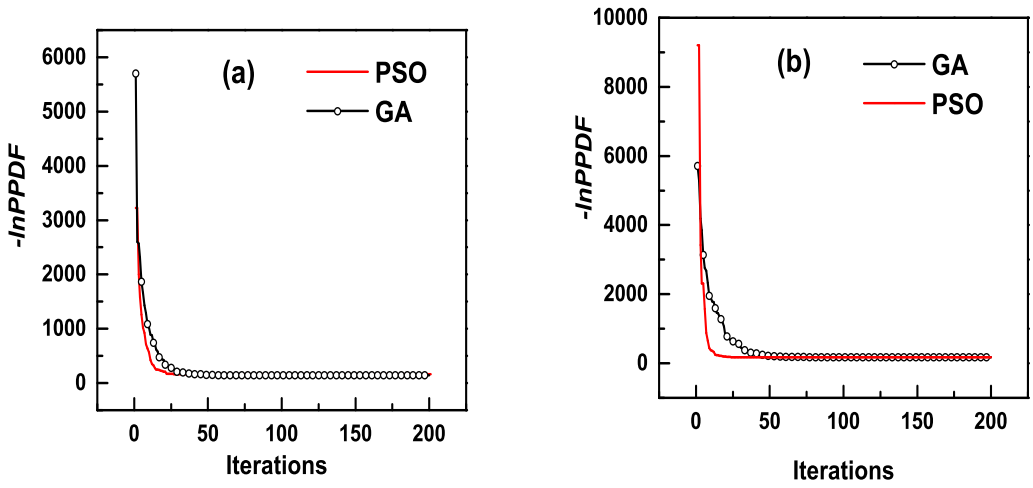

Figure 5.8 (a) Convergence of average values of $-lnPPDF$ for σ=0.01T_{max} (b) Convergence of average values of $-lnPPDF$ for σ=0.02T_{max} noisy temperature data.

tent heat and ME was faster by using PSO and also produced smooth results compared to GA. Figure 5.8(a) shows faster convergence of the $-lnPPDF$ for PSO than GA and it was observed that GA converging to a value of 171.46 at 163 iteration where as PSO converges to the same value at 65 iteration. This convergence capability is based on the principle of search mechanism where PSO drives the population towards the global optimum quickly compared to GA. Corresponding estimated values by GA and PSO for σ=0.01T_{max} noisy data can be found from Tables 5.4 and 5.5. The retrieved values of latent heat showed a slight variation from the original value with absolute % error of 0.45 using GA and PSO respectively. The estimation shows the main feature of the Bayesian framework where fitness functions like Least squares, Tikhonov regularization are not essentially drafted to provide the information about the error estimates which has statistical exposition.

As the experimental temperatures are subjected to more errors, the noise level of the temperature is increased to σ=0.02T_{max} and the average retrieved values of the unknown parameters are reported in Table 5.6. The estimated average values of a by PSO was 8596 and by GA was 8597.1 with absolute % error of 0.625 and 0.611 respectively. The estimated average value of latent heat by PSO was 381407 and by GA was 381355 with absolute % error of 0.129 and 0.14 respectively. Figures 5.8(b) and 5.9

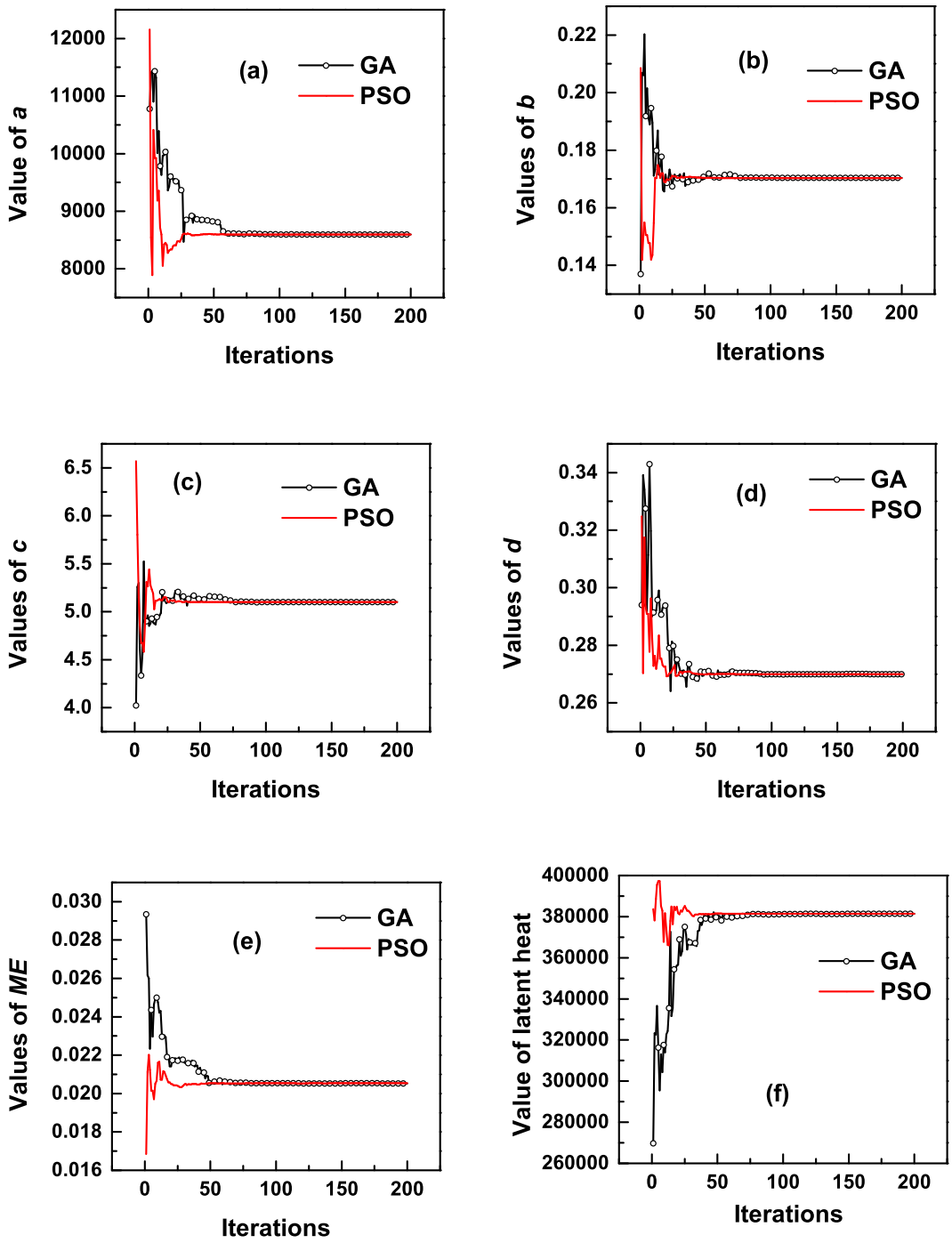

Figure 5.9 (a) Convergence of average values of 'a '(b) Convergence of average values of 'b '(c) Convergence of average values of 'c '(d) Convergence of average values of 'd '(e) Convergence of average values of 'ME '(f) Convergence of average values of $latent\ heat$ using GA and PSO for σ=0.02T_{max} noisy data.

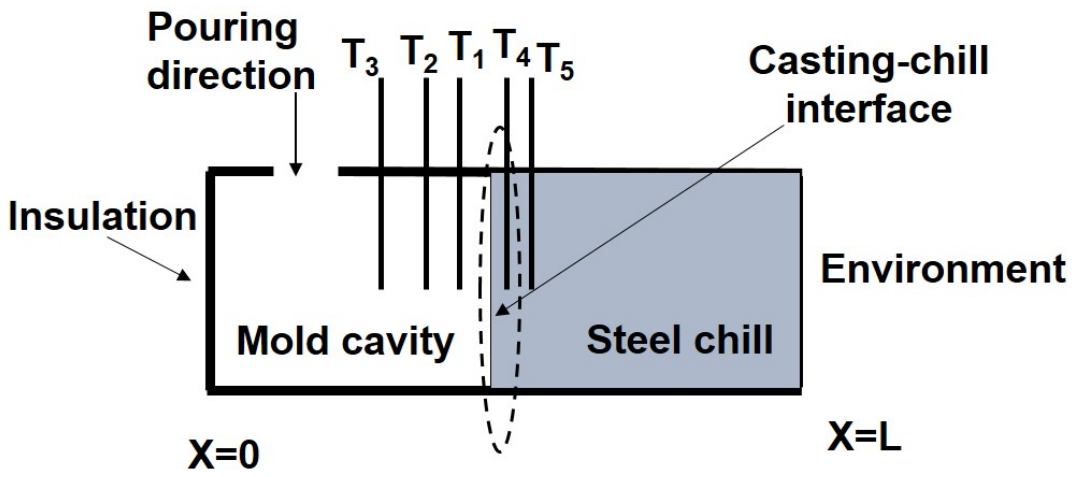

Figure 5.10 Schematic diagram of cast and chill arrangement with five temperature sensor locations.

again show the quick convergence of $-lnPPDF$ and the unknown parameters respectively. The average computational time taken by GA and PSO was 29513 s and 26718 s respectively for σ=0.02T_{max} temperature data. Further the estimation is carried out for σ=0.03T_{max} and the benefit of the proposed methodology in handling the noise during inverse estimation can be observed in Table 5.7. The average computational time taken by GA and PSO was found to be 29366 s and 26232 s respectively for σ=0.03T_{max} temperature data. The convergence of estimation of unknown parameters from PSO for noisy data showed within 80 iterations where as for GA it was found to be more than 100 iterations.

In addition, the effect of number of sensors are also investigated. Five temperature sensors in which three of them placed at the distance of 5mm, 10mm and 20mm from the casting-chill interface inside the mold cavity and other two at the distance of 3mm and 6mm from the casting-chill interface inside the steel chill were chosen as shown in Fig.5.10 and the temperature distributions at the mentioned locations were collected. The inverse analysis using GA and PSO is conducted for both exact and σ=0.01T_{max} noise data. The retrieval of unknown parameters using 5 sensors with exact temperatures is demonstrated in Table 5.8. It was found that GA and PSO estimated the unknown parameters close to the actual values for exact temperatures compared to

Table 5.2 and 5.3. Using, PSO, the estimation achieved was accurate and took less time to converge to the solution compared to GA. The average time taken by GA and PSO was 29278 and 26319 s respectively. Table 5.9 shows the retrieved values of the unknown parameters and the estimated average values of *a* by GA was 8677.2 and by PSO was 8676.6 with absolute % error of 0.313 and 0.3 respectively. PSO retrieved *b*, *c* and *d* values exactly to the original values. Further, the retrieved values of latent heat by GA was 379860.2 and by PSO was 379931.83 respectively. It was also observed that the absolute % error for ME was higher with five sensors compared to the results using two sensors (refer Tables 5.4 and 5.5). This may be because of the fact that, higher the number of temperature sensors, higher is the noise associated in the temperatures. It has been observed that the average retrieved values of unknown parameters with two temperature sensors for σ=0.01T_{max} noise were close to the actual values compared to the average values of unknown parameters obtained using five temperature sensors. Hence, it sufficient enough to have two temperature sensors for the present analysis. The results substantiate the use of GA and PSO within Bayesian framework to obtain better estimates of the unknown parameters and hence proving an effective tool in the field of solidification inverse problem.

5.6 CONCLUSIONS

An inverse heat conduction problem was identified to estimate the interfacial heat transfer coefficient and mold environment heat transfer coefficient. During the process of estimation of interfacial heat transfer coefficients, it has been identified that the Bayesian framework provides a window where the constants involved in the interfacial heat transfer coefficients along with the modeling error and latent heat of the casting can also be simultaneously estimated with subjective priors. The use of Bayesian framework alleviates the problem of ill-conditioning of the present inverse problem. The popular Genetic algorithm and Particle Swarm Optimization were used as the inverse approach for the estimation of the unknown parameters based on the simulated measurements. Later, the robustness of the proposed methodology was tested using noisy temperature data. The following are the key findings of the present work:

1. The observations from scaled sensitivity revealed that the parameters *a*, *b* and latent heat of the alloy were more sensitive and thus affecting temperature disti-

bution significantly; hence, estimation was crucial. The scaled sensitivity values of a, b and $latent\ heat$ are showing a trend where they can be simultaneously estimated but the scaled sensitivity values of c and d which are close to zero cannot be retrieved with the temperature measurements unless there is some *a-priori* information about those parameters. Hence, this entails and reinforces the use of Bayesian framework.

2. The results from the PSO algorithm converged quickly with less computational time compared to GA for both exact and added noisy temperature data. It was also found that, there was no significant effect of noisy measurements on the computational time during the process of estimation.

3. The investigation on effect of number of sensors revealed that the average retrieved values of unknown parameters were close to the actual data for both two and five number of sensors hence, it would be sufficient to have two temperature sensors for the present analysis.

4. The methodology adopted provides adequate information about the error associated with the real time temperature measurements and thus buttresses the use of present methodology for further studies on uncertainties of the parameters involved in the mathematical model.

5.7 CLOSURE

In this chapter an explication of potential of Bayesian framework along with GA and PSO as inverse method for multi-parameter estimation was addressed. In the next chapter, a comparison of a hybrid PSO along with conventional GA and PSO algorithms for a conjugate heat transfer experiments is discussed.

CHAPTER 6

3D COUPLED CONDUCTION-CONVECTION PROBLEM USING IN-HOUSE HEAT TRANSFER EXPERIMENTS IN CONJUNCTION WITH HYBRID INVERSE APPROACH

6.1 INTRODUCTION

The first class of problem explained the 1-D inverse heat conduction problem for solidification of casting where retrieval of more information was focused with less available simulated measurements. Various multi-parameters like constants of the heat transfer correlation, latent heat and modeling error were simultaneously estimated using GA and PSO in conjunction with Bayesian framework. In this chapter, the challenges associated in integrating the complex forward model that involves Navier Stokes equation and energy equations is highlighted. After exploring the ability of GA and PSO for 1-D heat conduction problem, the use of hybrid evolutionary algorithm that overcomes the disadvantages of GA and PSO is studied. The demonstration of hybrid robust evolutionary algorithm for the inverse solution for an effective and quick estimation of heat flux and heat transfer coefficient during conjugate fin heat transfer problem is performed.

Many a times, the information about the boundary heat flux is obtained only through inverse approach by locating the thermocouple or temperature sensor in accessible boundary. Most of the work reported in literature for the estimation of unknown parameters is based on heat conduction model. Inverse approach using conjugate heat transfer is found inadequate in literature as discussed in the Chapter 2 under section 2.5. Therefore, a 3D conjugate heat transfer model is solved without model reduction for the estimation of heat flux and heat transfer coefficient from the measured temperatures. The application of the evolutionary algorithms to obtain accurate results from simulated measurements is performed. Efficacy of the hybrid algorithm is established using real time measurements.

6.2 EXPERIMENTAL PROCEDURE

In-house experimental setup has been developed to facilitate the free convection heat transfer from the fin. The layout of the experimental setup is shown in Figure 6.1. The detailed connections involved in the experiments are represented in Figure 6.2. The mild steel fin with dimensions 150x250x6 mm^3 is placed centrally on to an aluminium base of dimensions 150x250x8 mm^3 as shown in Figure 6.3 (Gnanasekaran and Balaji 2011).

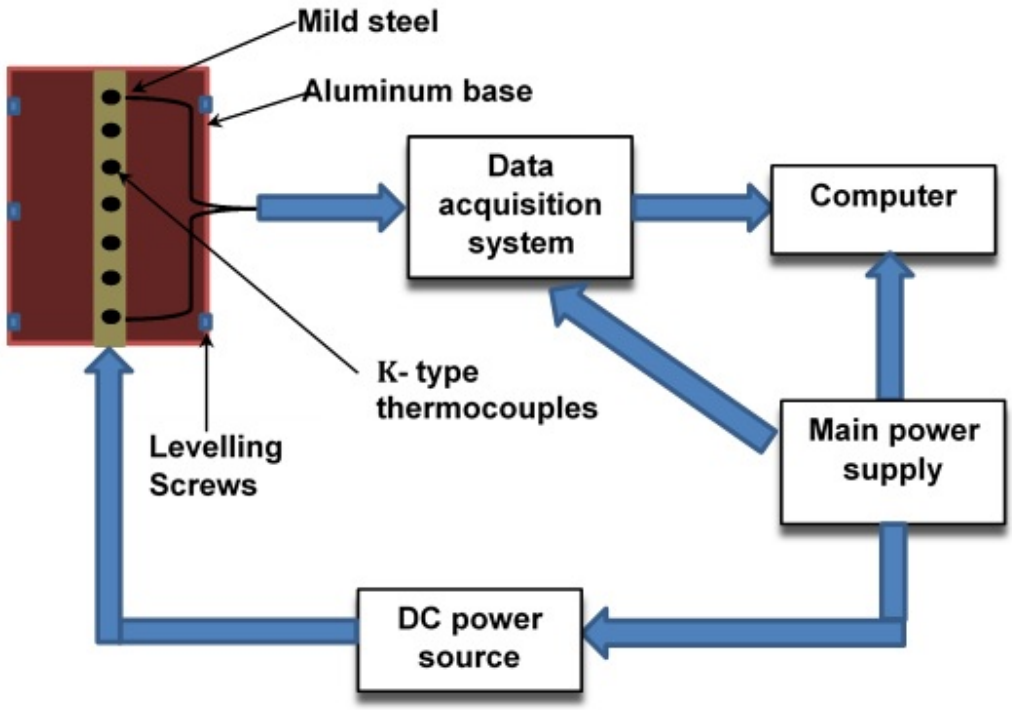

Figure 6.1 Layout of the experimental setup.

A nichrome wire wound over a mica sheet shown in Figure 6.4a is used as the heater having the dimensions of the aluminium plate but the thickness is 1.4mm. The sides of the aluminium base plate and bottom of the heater are insulated with glass wool to prevent heat loss. The aluminium plate is placed in such a way that the longer side is perpendicular to the ground and the longer side of the fin is parallel to the longer side of the base. Several layers of glass wool are placed beneath the heater and sides of the base plate to minimise heat loss. The backside portion of the heater is insulated

and a thermocouple is placed on the insulation surface. Complete contact between the heater and the base plate was ensured by tightening the screws in the frame as shown in the Figure 6.4b, which helped in pushing the base plate against the heater. The size of the heater is same as the size of the base plate. The fin setup is placed in an enclosed chamber so as to avoid natural disturbances. Holes of 3mm diameter are drilled for a depth of 20mm along the measuring length of the fin and the base plate. Calibrated K-type sheathed thermocouples are used to measure the temperature of the fin and the base plate. The thermocouples are calibrated with the standard thermostatic bath supplied by Thermo Scientific, with the range of -60°C to 200°C and with accuracy of 0.01°C. The heater, placed below the base plate, is powered by a DC power source that can supply constant power to the setup. Different trials of experiments are conducted by varying the range of power input to the heater. The temperature recorded using thermocouple is accessed with the help of data acquisition system equipped with the Labview software supplied by the National Instruments. The DAQ used in the present work consists of 16 channels with the model no: NI 9213. Temperature is recorded for every 10s during

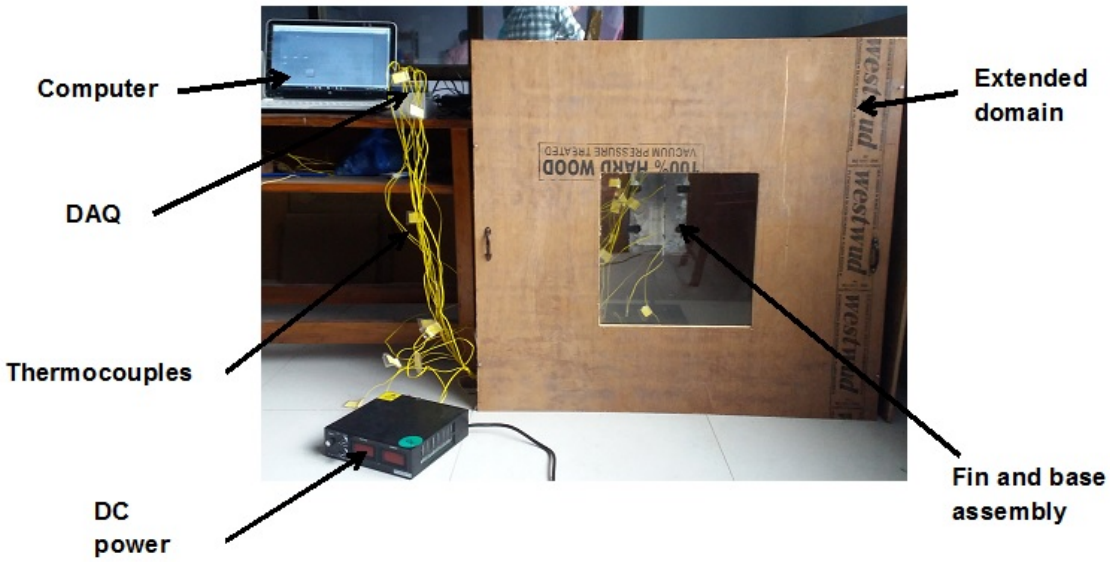

Figure 6.2 Photographic representation of the experimental setup.

the experiments; however, only steady state measurements are taken into account for the purpose of estimation. A typical natural convection fin experiments requires 5-6 hours to reach steady state. The steady state is confirmed when the change in temperature is

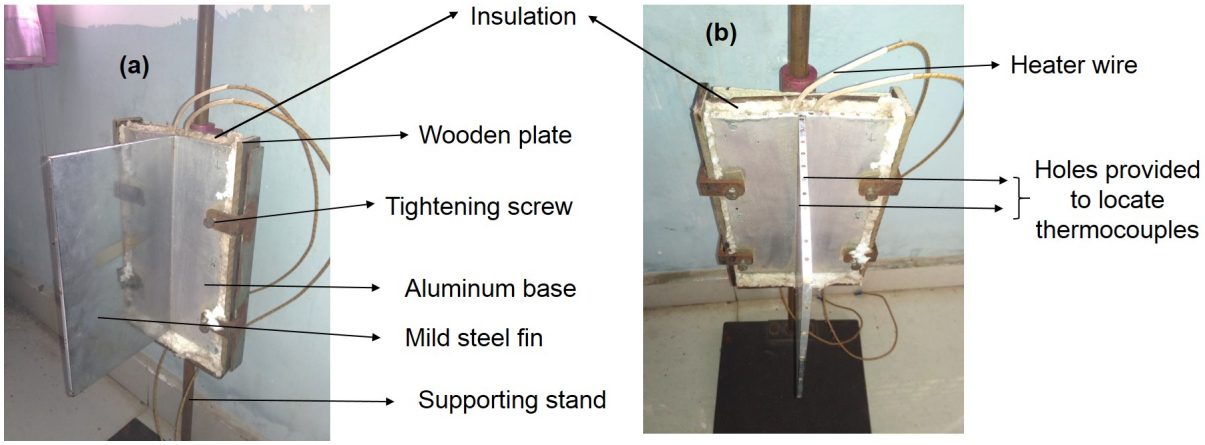

Figure 6.3 Photographic view of vertical fin setup.

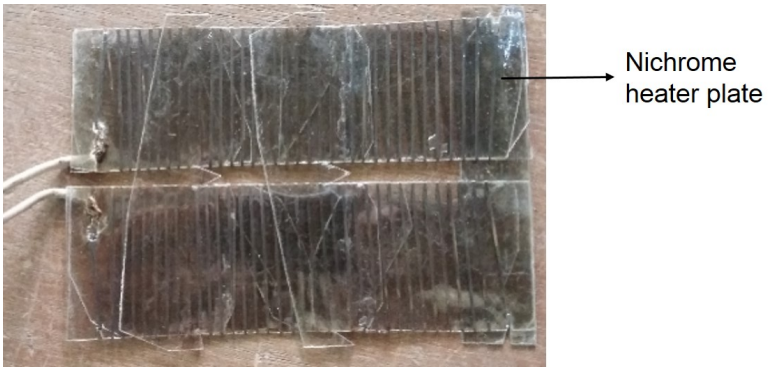

(a)

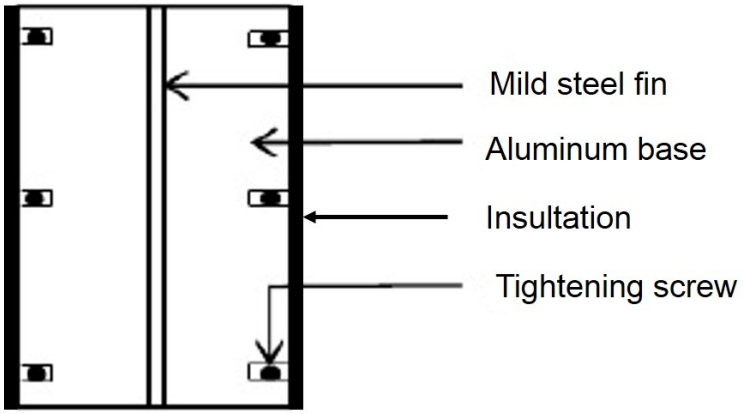

(b)

Figure 6.4 (a) Nichrome heater plate (b) Front view of the vertical fin setup.

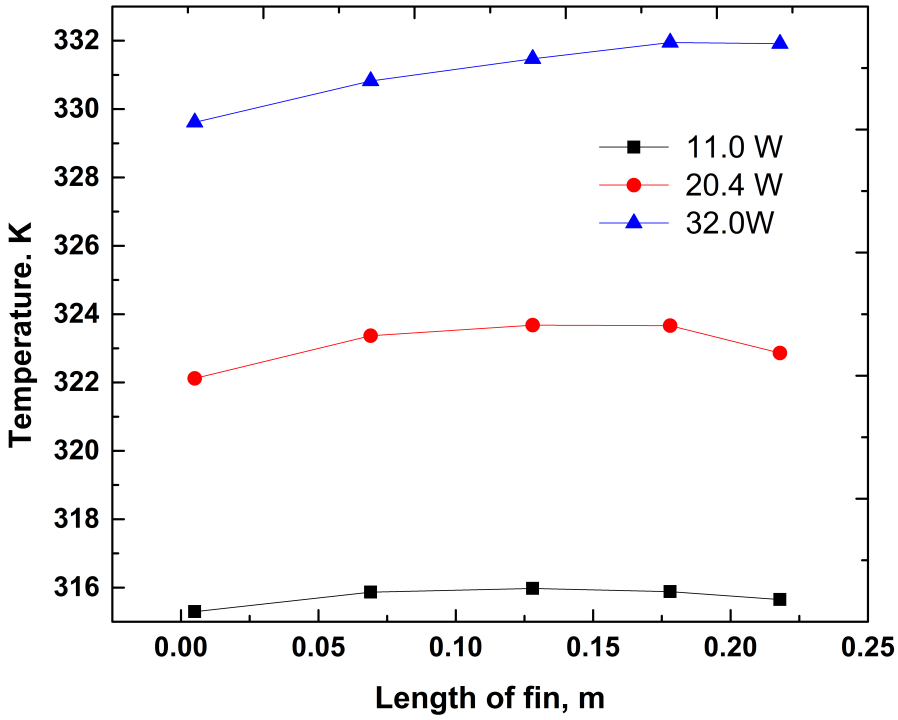

Figure 6.5 Measured temperature along the length of fin.

0.1 °C for a time duration of 10min. Experiments are conducted for different heat flux values of 305, 544, 853 and 1232 W/m^2 and corresponding temperature distribution along the vertical fin is recorded from beginning of the experiment till the end in the system with the help of DAQ. A typical experimental plot for three different power inputs is shown in Figure 6.5.

6.2.1 Uncertainty analysis

The uncertainty due to the voltage and the current in DC power source is presented below. The heat is supplied to the experimental setup using DC power source. The uncertainty of the power source should be known beforehand since the uncertainty of the voltage and current have some effect on the final estimates of heat flux and heat transfer coefficient. Table 6.1 shows the uncertainty associated with the instruments.

Table 6.1 Instruments and uncertainty.

Instrument	Uncertainty
DC power source	$\pm 0.2\%$
Digital multimeter	$\pm 1.6\%$

For a typical power of 32W, the uncertainty in the power is given by,

$$P = V \times I \tag{6.1}$$

$$\pm \sqrt{(\frac{\partial P}{\partial V}\sigma_V)^2 + (\frac{\partial P}{\partial I}\sigma_I)^2} \tag{6.2}$$

$$\pm \sqrt{(0.64 \times 0.002)^2 + (50 \times 0.016)^2} \tag{6.3}$$

$$= \pm 0.64W \quad or \quad 2\% \tag{6.4}$$

Where *P* is Power in W, *V* is voltage and *I* is current in amphere.

6.3 FORWARD PROBLEM

6.3.1 Numerical Simulations

The numerical model consists of a fin and base assembly placed inside an extended domain. The setup has an aluminium base with dimensions of 250x150x8mm^3 and steel fin with dimensions of 250x150x6 mm^3. Figure 6.6 shows the numerical model representing physics of the actual model. An extended domain is modelled to study the effects of convection and also to obtain velocity of the fluid. A domain independence study has been carried out for the given geometry by varying the dimensions of the extended domain. Finally, the dimension of the extended domain was considered to be 975x995x930 mm^3 in x, y, z direction, respectively. The properties of the materials used in this study are provided in Table 6.2. The fluid medium considered in the extended domain is air and is considered to be of constant thermo-physical properties except for the density so as to model natural convection. Boussinesq approximation is incorporated to treat density as a constant in the momentum and the continuity equations but it varies with temperature in the energy equation. The present numerical study is modelled as a three dimensional conjugate heat transfer problem. The domain is modelled with ANSYS 14.5 design modeler and meshed using ANSYS meshing tool.

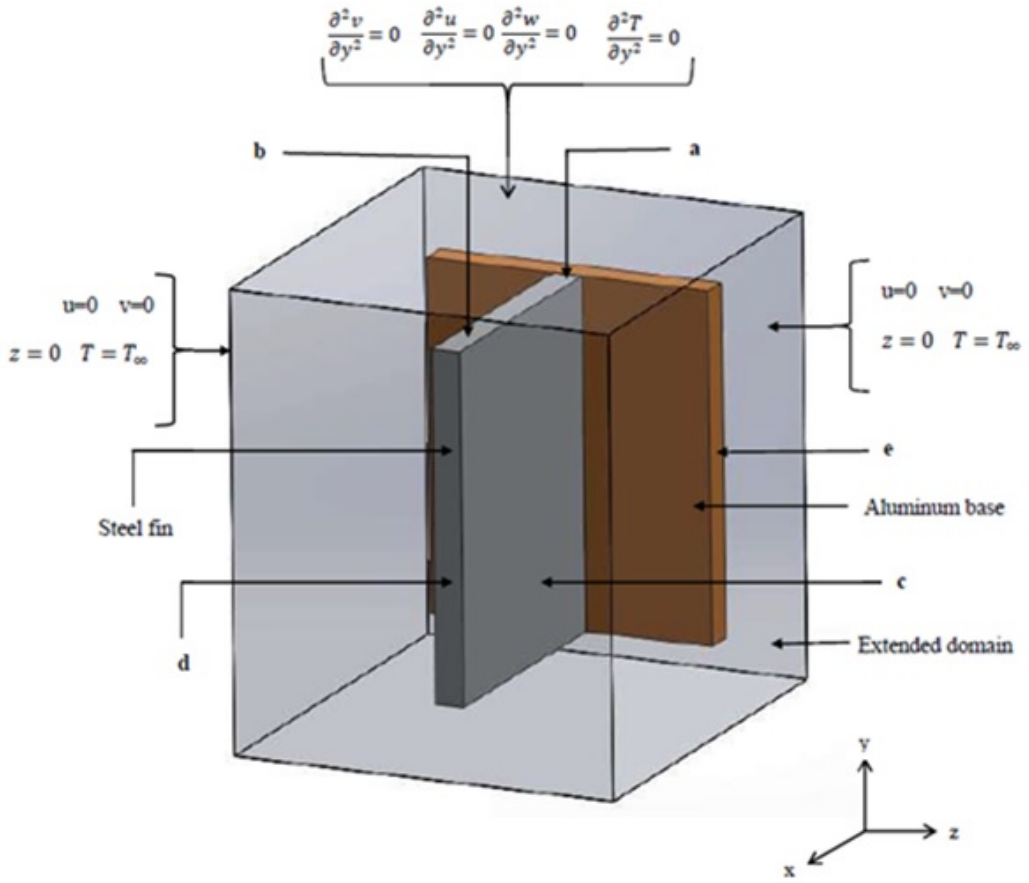

Figure 6.6 Numerical model of fin and base setup with extended domain considered for simulation.

The governing equations of the present study are given as

Continuity

$$\nabla.\overrightarrow{\mathrm{V}} = 0 \tag{6.5}$$

X-momentum equation

$$\overrightarrow{\mathrm{V}}.\nabla u = -\frac{1}{\rho}\frac{\partial p}{\partial x} + \vartheta\nabla^2 u \tag{6.6}$$

Y-momentum equation

$$\overrightarrow{\mathrm{V}}.\nabla v = -\frac{1}{\rho}\frac{\partial p}{\partial y} + \vartheta\nabla^2 v + g\beta.\Delta T \tag{6.7}$$

Z-momentum equation

$$\overrightarrow{\mathrm{V}}.\nabla w = -\frac{1}{\rho}\frac{\partial p}{\partial z} + \vartheta\nabla^2 w \tag{6.8}$$

Table 6.2 Properties of materials.

Properties	**Mild Steel**	**Aluminum**
Density (kg/m^3)	8030	2719
Specific heat (J/kgK)	502.48	871
Thermal conductivity (W/mK)	46	202.4

Energy equation (for fluid)

$$\overrightarrow{\mathrm{V}}.\nabla T = \alpha \nabla^2 T \tag{6.9}$$

Energy equation (for fin and aluminium base)

$$\nabla^2 T = 0 \tag{6.10}$$

Figure 6.6 depicts the boundary conditions of the present problem. At the inlet, the following boundary conditions are imposed,

$$u = 0, v = 0, z = 0, T = T_\infty \tag{6.11}$$

At the outlet of the domain the following boundary condition is used,

$$\frac{\partial^2 u}{\partial y^2} = 0, \frac{\partial^2 v}{\partial y^2} = 0, \frac{\partial^2 z}{\partial y^2} = 0, \frac{\partial^2 T}{\partial y^2} = 0, \tag{6.12}$$

The x-face of the domain is subjected to,

$$u = 0, v = 0, z = 0, \frac{\partial T}{\partial x} = 0 \tag{6.13}$$

Also z-face of the domain is subjected to,

$$u = 0, v = 0, z = 0, \frac{\partial T}{\partial z} = 0 \tag{6.14}$$

Region 'a 'is a solid-solid interface and the transfer of energy at this region is through conduction, where the wall of the fin and the aluminum base are treated as coupled wall.

$$k_{Al}\frac{\partial T}{\partial n} = k_{ms}\frac{\partial T}{\partial n} \quad \text{and} \quad T_{Aluminum} = T_{Mildsteel} \tag{6.15}$$

At regions 'b ', 'c 'and 'd 'the boundary condition imposed is solid-liquid interface, so the energy transfer between the fin faces to the air in the extended domain is by convection.

$$k_{ms}\frac{\partial T}{\partial n} = k_f\frac{\partial T}{\partial n} \quad \text{and} \quad T_{Mildsteel} = T_{fluid} \tag{6.16}$$

At region where the top surface of the aluminum base is in contact with fluid. The following boundary condition is specified.

$$k_{Al}\frac{\partial T}{\partial n} = k_f\frac{\partial T}{\partial n} \quad \text{and} \quad T_{Aluminum} = T_{fluid} \tag{6.17}$$

where k_{Al} is the thermal conductivity of the aluminum, k_{ms} is the thermal conductivity of the mild steel, k_f is the thermal conductivity of the fluid.
The base of the aluminium is subjected to constant heat flux,

$$q_0 = -k\frac{\partial T}{\partial x} \tag{6.18}$$

At region 'e 'i.e. along the sides of the base insulated boundary condition is applied.

$$\frac{\partial T}{\partial z} = 0 \tag{6.19}$$

No slip condition is applied along all solid walls. All these regions are treated as interfaces. It is pertinent to mention here that Equations (6.5-6.10) are solved for an assumed heat flux (refer Equation (6.18)) and known boundary conditions to obtain the temperature distribution. Finite volume method is used as the numerical method to solve the partial differential equations. Commercial software, ANSYS FLUENT was used to accomplish this task. The solution procedure included the use of Semi Implicit Pressure Linked Equation (SIMPLE) algorithm. Second order upwind scheme was used and the convergence criterion of 10^{-6} was fixed for the energy and the momentum equations.
One of the findings of the present work is the estimation of heat transfer coefficient mentioned in region ‘c’ where the side of the mild steel plate is dissipating heat by convection to the ambient by natural convection; hence, the forward model is solved based on the boundary condition given in Equation (6.20) which replaces the Equation (6.16),

$$-k_{ms}\frac{\partial T}{\partial n} = h\Delta T \tag{6.20}$$

In the inverse estimation, the heat flux mentioned in Equation (6.18) and the heat transfer coefficient in Equation (6.20) are estimated for the known temperature distribution obtained from in-house experiments.

6.4 GRID INDEPENDENCE STUDY

Grid independence study is shown in Figure 6.7. A 3-D numerical model for fin heat transfer was developed and meshed using ANSYS package. Structured mesh was used for the entire domain. For the heat flux input of 1200 W/m^2, simulation was carried out for the selected domain with 117438 nodes and the temperature at the location of 0.13m on the mild steel plate along the y- direction as shown in Figure 6.3 was recorded. This

Table 6.3 Grid independence study.

Location, m		**Nodes**	
(x,y,z)	117438	463116	756516
(0.14,0.005,0.075)	355.696	347.740	347.697
(0.14,0.07,0.075)	356.100	348.557	348.645
(0.14,0.013,0.075)	356.620	349.374	349.475
(0.14,0.018,0.075)	356.936	349.878	349.995
(0.14,0.022,0.075)	357.069	350.101	350.225

was followed by reducing the mesh size which resulted in the increase of the nodes. The mesh size was reduced at the regions of interest such as the solid-solid and solid-liquid interface layers. The next set of nodes obtained was 463116 and the simulation was carried out for the same value of heat flux. Once again the temperature was recorded. Further the node number was increased to 756516 nodes and the temperature for the same value of heat flux is recorded at the same height of the plate. It was observed that the difference in temperature decreased as the nodes were increased. The difference in temperature between 463116 and 756516 was not very significant as shown in Table 6.3. Hence, 463116 nodes were used for further simulations as increase in the number of nodes would also increase the computational time. Numerical simulations are carried out in a 32core 64GB RAM workstation and the average time taken for obtaining a single forward solution was 30-45 mins. The results obtained from the simulations are validated with measured data as shown in Figure 6.8.

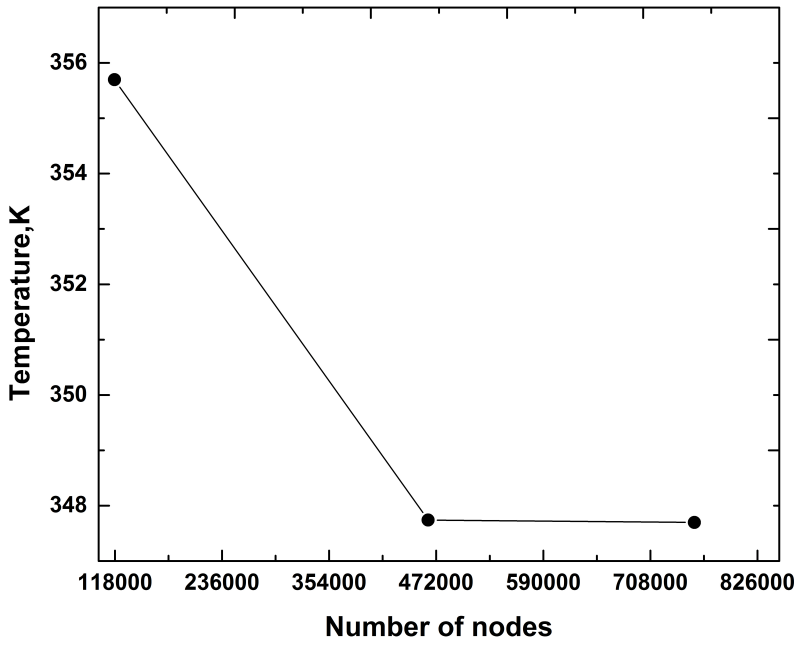

Figure 6.7 Grid Independence study.

6.5 FAST FORWARD MODEL

6.5.1 Artificial neural network

ANN is based on neural computing similar to the biological nervous system. It creates a relation between the input and the output based on some weighted function. The structure of the ANN includes three layers; The first layer through which data is fed in to the network is the input layer and the results are obtained from the output layer. In between the input and the output layer is the hidden layer where training the network is accomplished (Deng and Hwang 2006; Zhang et al. 2010). As discussed earlier, solving the forward model using ANSYS FLUENT to obtain the temperature distribution for the assumed heat flux is time consuming. An ANN is proposed in this work as a fast forward model which is created using large data set containing different values of heat fluxes and corresponding temperature distributions which are obtained from Computational Fluid Dynamics (CFD) solutions.

The neurons in the hidden layer are decided based on the neuron independence study. Each interconnection between the neurons is associated with weight. The

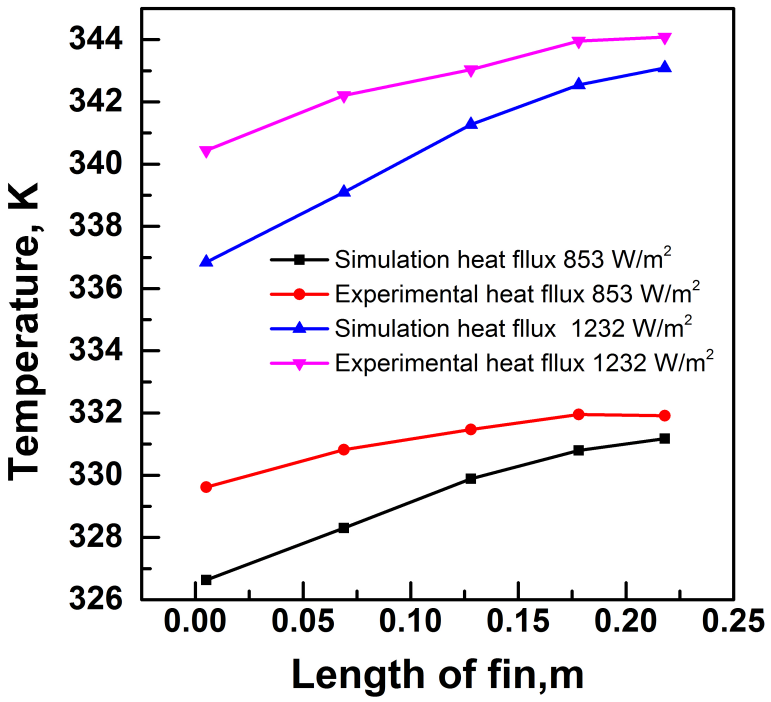

Figure 6.8 Comparison of simulated and measured temperatures for different heat flux values.

strength of the connections between the neurons is determined by these weights. The back propagation algorithm is used in the present work to upgrade the weights. Using certain training algorithms the weights connecting neurons in the different layers is adjusted according to the training set. This process is called training the network. Learning the connection between the input and the output layers based on the corresponding input-output pairs is the main feature of ANN. During network training, 75% of the data is considered for training and remaining 25% is kept aside for testing. Sometimes, training the network is time consuming depending on the number of unknowns and data, but after establishing the network, the output is considerably faster than the CFD computations. In the present case, the maximum time taken for training the network was 2 hours that involved neuron independence study, testing and validation between the input and the target data. Heat flux values and temperatures are chosen as input and output respectively. Network is trained for different number of neurons and corresponding R^2 values are recorded. Table 6.4 shows the neuron independence study and it is observed that 6 neurons are sufficient for the purpose of training as the value of

$R^2 \approx 1$. The point to be noted here is, within the range of heat flux values specified to train the ANN model, in the process of inverse estimation of heat flux and heat transfer coefficient, the ANN model will also provide the output for a given input which was not a part of the training sets.

Table 6.4 Neuron independence study.

Sl.No.	Neurons	MRE	R^2
1	6	0.00041	0.99999
2	12	0.01391	0.99940
3	19	0.00986	0.99982
4	27	0.02058	0.99940

6.6 SENSITIVITY STUDY

The sensitivity approach has an important role in the estimation of unknown parameters. The solution to the sensitivity problem is defined as the directional derivative of the temperature corresponding to the perturbation of the unknown parameters. For example, the effect of change in the heat flux or the heat transfer coefficient results in change in temperature of the fin which is the study of sensitivity. The sensitivity coefficient is expressed as (Ozisik and Orlande 2000),

$$J_{ij} = \frac{\partial T_i}{\partial P_j} = \frac{T_i(P_1 \ldots, P_j + \Delta P_j \ldots, P_N) - T_i(P_1 \ldots, P_j \ldots, P_N)}{\Delta P_j} \tag{6.21}$$

where J_{ij} is the sensitivity coefficient, T_i is the i^{th} estimated temperature, P_j is the j^{th} unknown parameter, ΔP_j is the change in the unknown parameter. When the magnitude of J_{ij} is small, it indicates that large changes in P_j results in small changes in T_i. In such case, the estimation of unknown parameters is exceedingly difficult, and the methods like gradient based technique are seldom used as an inverse approach because of its inability to estimate the required parameter. Sometimes, the gradient based method gets entrapped in the local minima or maxima. It is always desirable to obtain a large magnitude for J_{ij} so that accurate estimation of the unknown parameters is possible. Small magnitude of J_{ij} necessitates the use of prior information about the unknown parameters in the inverse approach. Sensitivity coefficients expressed in the form of matrix is termed as Jacobian matrix. The determinant of the Jacobian matrix i.e $|\ J_{ij}^T\ J_{ij}|$ defines

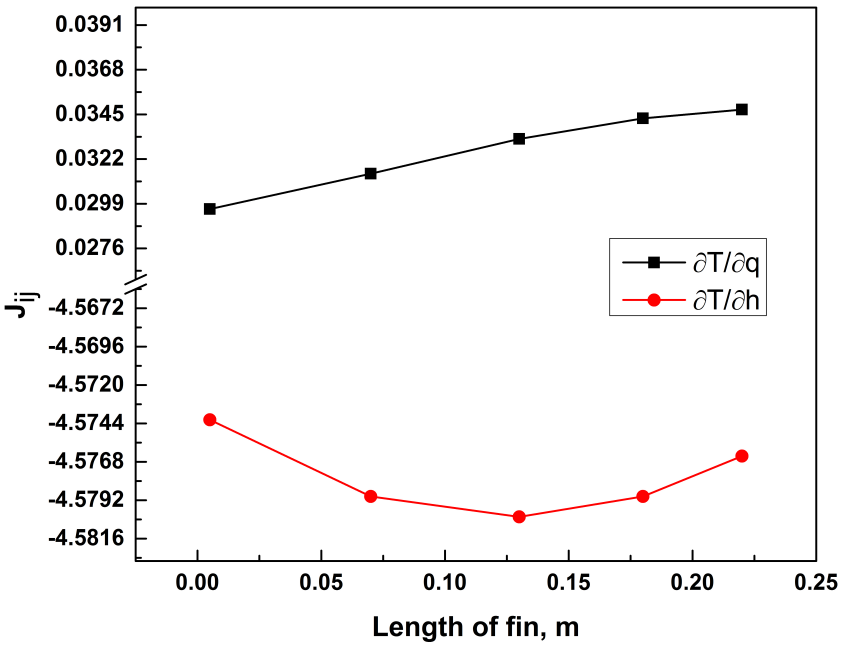

Figure 6.9 Sensitivity coefficient plot.

the condition of the problem. When $| J_{ij}^T J_{ij}| \approx 0$, the problem is then ill-conditioned. The sensitivity analysis for the heat flux and the heat transfer coefficient is shown in Figure 6.9. The magnitude of the sensitivity coefficient of heat flux is found to be less and positive, while the other sensitivity coefficient is negative. The sensitivity coefficient of the heat flux and the heat transfer coefficient show linear dependency, therfore the simultaneous estimation of the heat flux and the heat transfer coefficient is more difficult without a priori information since the magnitude of the sensitivity coefficient of the heat flux is close to zero and hence no information can be obtained from it. Needless to say, the heat transfer coefficient and the heat flux are estimated independently using GA, PSO, PSO-BFGS for the proposed inverse conjugate heat transfer problem without the use of *a priori* information.

6.7 INVERSE METHODS

A detailed explanation of inverse methods is provided in Chapter 3.4. In the present work, GA, PSO and PSO-BFGS are used as inverse methods. To improvise the existing conventional evolutionary algorithm, a hybrid algorithm is proposed to demonstrate its

effective use in estimation of unknown parameters. In comparison with the existing metaheuristic algorithms, hybridizing PSO algorithm with other deterministic method is easy as PSO contains lesser parameters to solve the optimum solution and also several studies show that hybrid GA give poor results than hybrid PSO for the estimation of parameters in heat transfer problem. Besides that hybrid PSO also achieves better search capabilities to produce better solutions compared to hybrid GA (Vakili and Gadala 2009; Lee et al. 2008). For nonlinear optimization, the use of Broyden Fletcher Goldfarb Shanno (BFGS) method is very efficient as its performance is found to be more accurate compared to other optimization algorithms.

6.8 OVERVIEW OF THE PRESENT WORK

In the present paper GA, PSO and PSO-BFGS are used as the inverse algorithms with the common objective of minimizing the error between the measured and the simulated temperatures. Least squares method is chosen as the fitness function expressed in Equation (6.22).

$$S(q \; or \; h) = \sum_{m=1}^{M} \sum_{i=1}^{N} [Y_{im} - T_{ANN}(q \; or \; h)]^2 \tag{6.22}$$

where $q \; or \; h$ is the unknown parameter. Y_{im} is the i^{th} observation from the m^{th} measurement; *M* and *N* are the number of measurements and observations, respectively. $T_{ANN}(q \; or \; h)$ is the simulated temperature obtained from the fast forward model.

For the forward problem, the temperature distribution was obtained by considering the heat flux as the input. For inverse approach, heat flux and heat transfer coefficient are to be determined from the known temperature information. Figure 6.10 represents the overview of the present work. CFD simulations are performed for various values of heat flux and corresponding heat transfer coefficient (*h*) and temperature data (T_{sim}) are collected. As the CFD simulations are time consuming, a neural network is trained between the available heat flux/ heat transfer coefficient and corresponding temperature data obtained from CFD simulations. The trained ANN model predicts the temperatures (T_{ANN}) for any given value of heat flux/ heat transfer coefficient input. A range of heat flux/ heat transfer coefficient is initialized by GA/PSO/PSO-BFGS optimization algorithms. Every value in the range is passed to ANN model and temperatures are predicted which are then compared with the observed temperatures to find

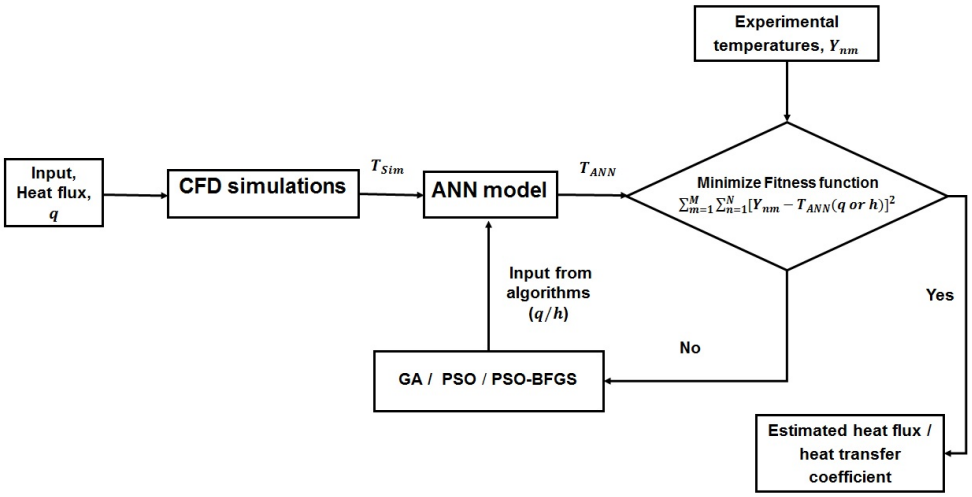

Figure 6.10 Overview of the present work.

the fitness values using Equation (6.22). Based on the methodology of the mentioned optimization algorithms, the fitness function is minimized and the procedure is carried out till the criterion is satisfied. The value of the heat flux and heat transfer coefficient for which the fitness function is minimum, would be the estimated value.

6.9 RESULTS AND DISCUSSION

6.9.1 Solution from forward model

With the known thermo-physical properties and appropriate boundary conditions, the governing equations are solved to obtain the temperature distribution for different values of heat flux as input. The temperature distribution along the height of the fin is shown in Figure 6.11. It can be observed that along the length of the fin there is a gradual increase in the temperature indicating that the heat transfer from the fin surface to ambient as y$\rightarrow$ L is decreasing because the cold air from the bottom receives more heat and raises upstream due to the difference in density. The temperature contour for the heat flux value of 1600 W/m^2 is shown in the Figure 6.12. Heat transfer by natural convection takes place as shown in the Figure 6.13 along the y-direction i.e, along the length of the mild steel plate. The analysis was carried out assuming Boussinesq approximation. The density difference causes the flow of the air as observed. Hence, the

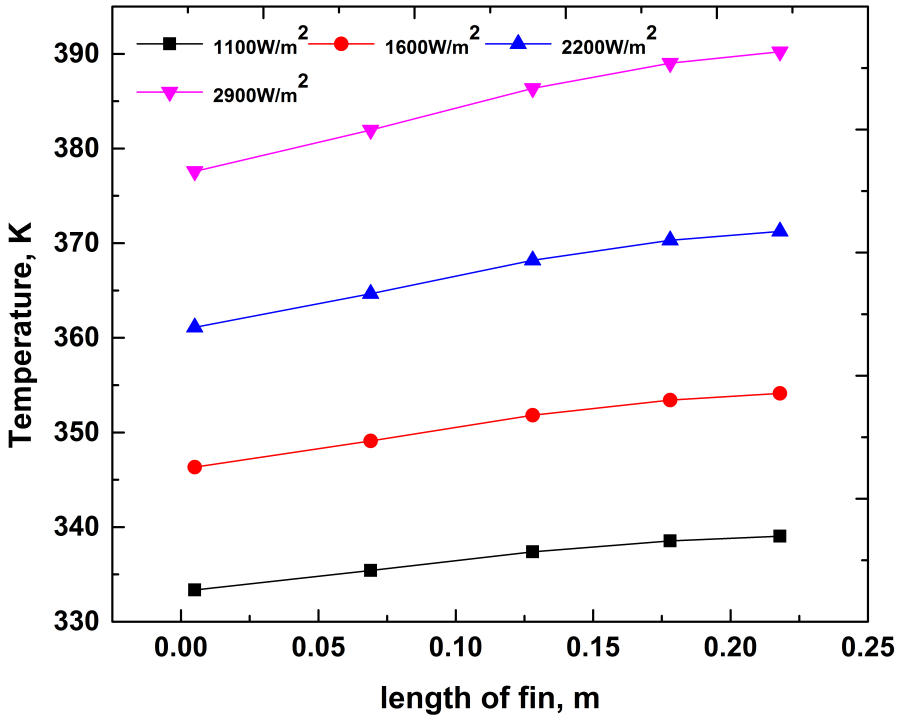

Figure 6.11 Simulated temperature distribution along the length of the fin.

velocity is maximum at the top end which is evident from the Figure 6.13.

6.9.2 Forward solution based on Fast Forward model

The use of iterative based method in the inverse approach leads to cumbersome task due to evaluation of the forward model each time for every new value of the parameters generated during the inverse process. In order to overcome this, the CFD simulations are performed for different values of heat fluxes and the corresponding temperature distributions are noted down. To solve the forward model by CFD simulation, the computational time required is 30-45 minutes depending upon the convergence. A neural network is now trained between the heat flux values and respective temperature data. The network not only reduces the computational time drastically but also provides the temperature distribution for any given heat flux within the range of heat flux used for training the network. The trained neural network produces temperature distribution in less than 5 seconds for a given heat flux (within specified range). From Table 6.5, it can

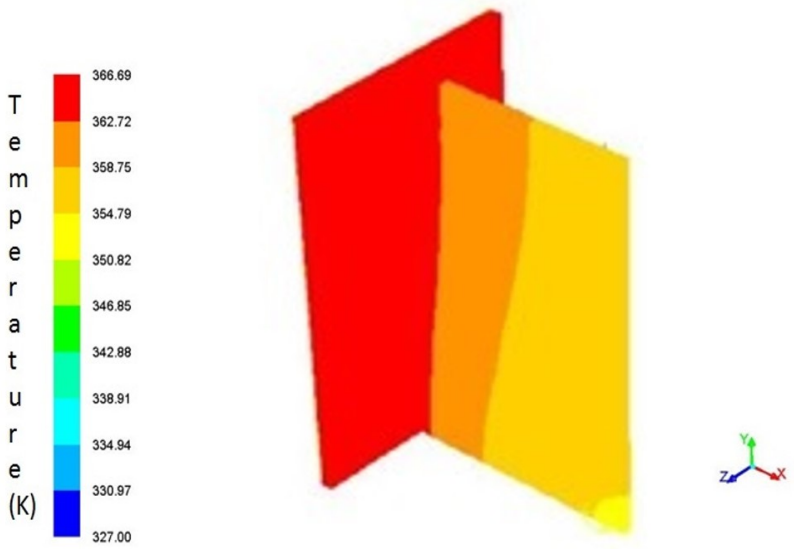

Figure 6.12 Temperature contour for the heat flux of 1600 W/m^2.

be seen that ANN temperatures are in good agreement with CFD temperatures. Therefore, for the estimation of the unknown heat flux and the heat transfer coefficient using the inverse method, ANN replaces the CFD solutions as a fast forward model.

Table 6.5 The comparison between ANN and CFD simulations.

	1100W/m^2		1600W/m^2		2200W/m^2	
Distance from base (m)	T_{Sim} (K)	T_{ANN} (K)	T_{Sim} (K)	T_{ANN} (K)	T_{Sim} (K)	T_{ANN} (K)
Base	363.43	363.43	389.49	389.52	419.77	419.78
0.005	333.36	333.35	346.33	346.32	361.10	361.09
0.178	338.54	338.53	353.42	353.42	370.30	370.30

6.10 ESTIMATION OF HEAT FLUX

As mentioned earlier, the inverse conjugate fin heat transfer problem is solved using GA, PSO and PSO-BFGS as optimization algorithms. The inverse estimation along with the neural network method is accomplished using in-house codes developed in

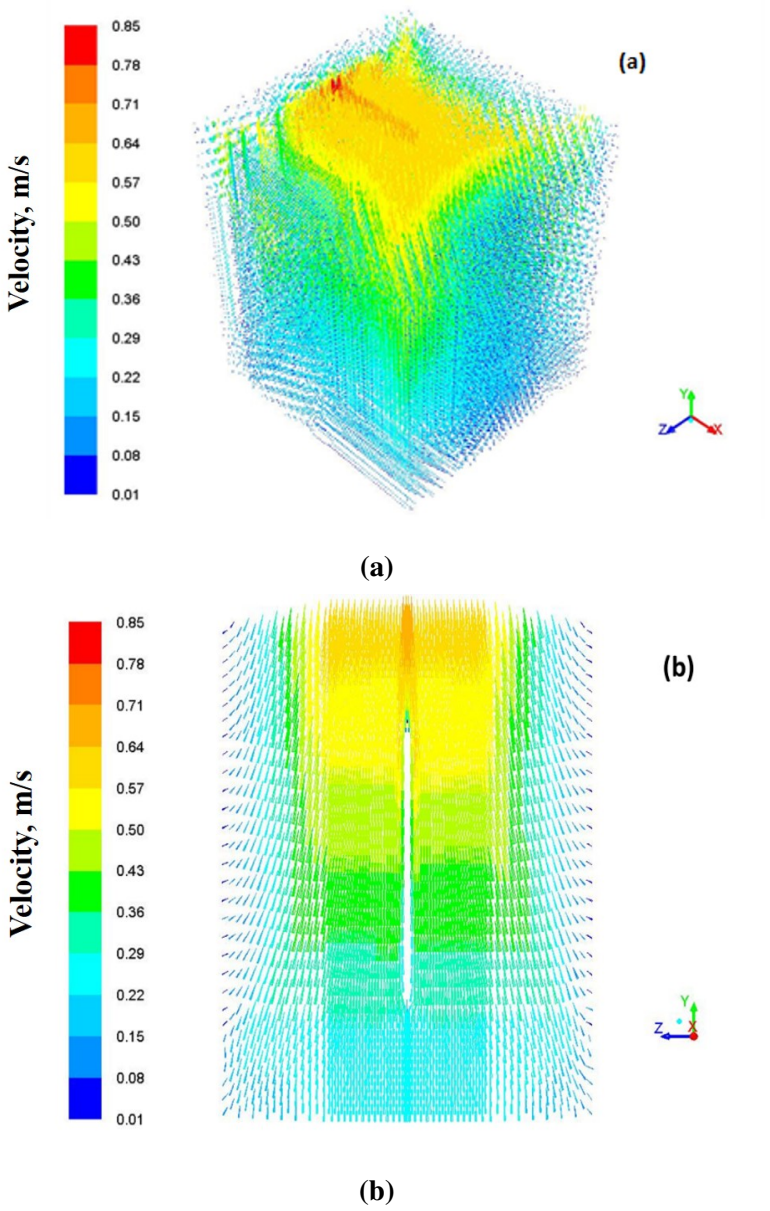

Figure 6.13 (a) Velocity streamlines for heat flux of 1600 W/m^2 and (b) velocity vector plot in y-z plane for the heat flux of 1600 W/m^2.

MATLAB. The estimation is attempted using simulated measurements, for this, the heat flux value is chosen in the range between 305 W/m^2 and 3300 W/m^2. Figure 6.14a and 6.14b show the heat flux and fitness values obtained using GA, PSO and PSO-BFGS as inverse methods for the heat flux 700 W/m^2 respectively. The estimation is achieved using all the mentioned algorithms with the same initialization parameters for several trials and three such runs are reported in Table 6.6. For GA, the number of iterations

is set to 50. The mutation rate, chromosomes number and gene number are assigned to be 0.1, 12 and 8 respectively. Every chromosome represents heat flux values for which the array of temperatures are obtained from neural network. This array of temperatures is used in Equation (6.22) to calculate the error between the measured and simulated temperatures. From Table 6.7 it can be observed that the computational time was

Table 6.6 Estimated values for the actual heat flux of 700 W/m^2 using GA, PSO and PSO-BFGS.

Runs	GA heat flux (W/m^2)	Time,s	PSO heat flux (W/m^2)	Time,s	PSO-BFGS heat flux (W/m^2)	Time,s
1	699.95	8.19	700	11.14	700	20.9
2	699.95	8.29	700	12.56	700	15.15
3	699.95	8.21	700	11.08	700	18.02

Table 6.7 Effect of chromosome number in estimating actual heat flux of 700 W/m^2 using GA.

Chromosomes	GA heat flux (W/m^2)	Time,s	Fitness value
8	699.95	8.19	4.08e-05
30	699.95	33.49	4.08e-05
60	699.95	62.38	4.08e-05

found to increase with increasing chromosomes and this is due to the evaluation of more number of inputs during the calculation of fitness function. When the number of genes is assumed to be 8, the heat flux estimated by GA is 704.33 W/ m^2 whereas, the retrieved value of heat flux now becomes very close to the actual value of heat flux for 12 genes which is evident from Table 6.8. Hence, the number of genes is fixed as 12 for further analysis. The effect of change in the mutation rate was found to be insignificant.

For the same range of initial guesses, the estimation of actual heat flux is carried out using PSO algorithm. In the beginning, the position and velocities are randomly

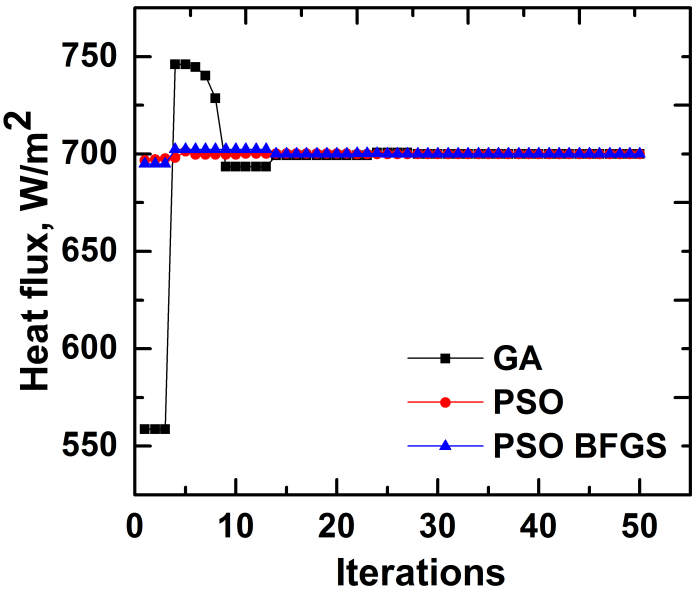

(a)

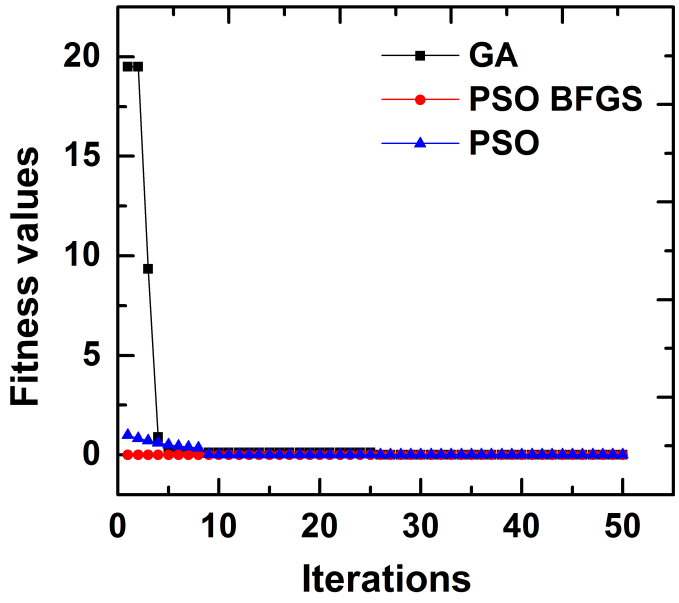

(b)

Figure 6.14 (a) Estimation of heat flux using GA, PSO and PSO-BFGS, (b) Fitness values for the estimation of heat flux of 700 W/m^2 using GA, PSO and PSO-BFGS.

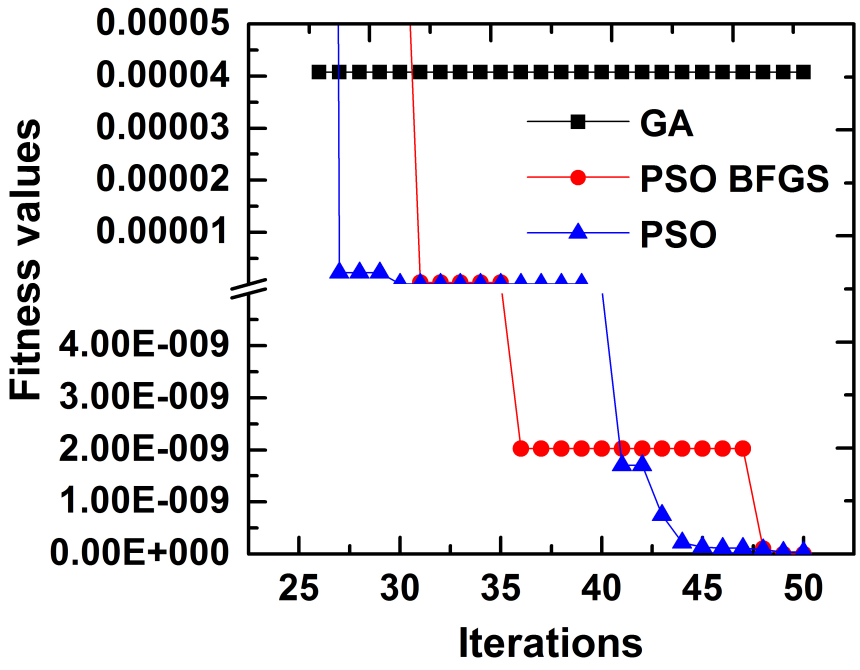

Figure 6.15 Enlarged view of fitness values for 700 W/m^2 heat flux.

Table 6.8 Effect of gene number in estimating actual heat flux of 700 W/m^2 using GA.

genes	GA heat flux (W/m^2)	Time,s	Fitness value
8	704.33	8.05	0.2536
12	699.95	8.19	4.08e-05

generated. In order to evaluate the fitness function, the input parameters are initialized. In the present case, the particles represent a range of heat flux values. In each iteration the particle's previous best and the global best are updated. The values of c_1 and c_2 are set to 1.43 and 1.43 respectively. After evaluation of fitness function, the personal best and global best values are updated appropriately. In the next iteration, the updated velocities and positions of each particle are considered. A modification for the present PSO algorithm is employed by using BFGS to improve the inverse solution. This hybrid strategy follows the initialization of heat flux values similar to PSO algorithm, but the algorithm makes use of hessian matrix to improve the solution. The value of γ i.e., step size and the direction is calculated using line search method (Nocedal and Wright

Table 6.9 Effect of particles numbers on the estimation of actual heat flux 700 W/m^2.

Particles	PSO heat flux (W/m^2)	PSO Time,s	Fitness values	PSO-BFGS heat flux (W/m^2)	PSO-BFGS Time,s	Fitness values
10	700	11.14	3.85e-11	700	20.9	1.3e-13
30	700	29.65	9.25e-11	700	31.26	7.66e-10
60	700	60.32	10.05e-12	700	61.95	5.07e-11

2006; Rao 2009) to find out the unknown parameter. The computational time required for the estimation of heat flux using PSO-BFGS algorithm was observed to be more compared to the other two algorithms because it needs to find out appropriate value of γ to predict the increment of the next parameter. Like GA, the increase in the number of particles increases the computational cost (Vakili and Gadala 2009) as reported in Table 6.9. The enlarged view of Figure 6.14b is shown in Figure 6.15. The convergence rate of the fitness function for PSO and PSO BFGS was found to be faster than GA. For the actual heat flux value of 700 W/m^2, GA estimates a value of 699.95 W/m^2 with a fitness value of 4.07575e-5 whereas PSO and PSO-BFGS algorithm estimates 700 W/m^2 with fitness values 3.84829e-11 and 1.30006e-13 respectively.

Now the process of estimation of unknown heat flux is carried out for the experimental temperatures. Figure 6.16a illustrates the retrieval of experimental heat flux. As the experimental temperatures are prone to errors, it is very difficult and also quite challenging to retrieve the unknown heat flux. It is evident that the PSO-BFGS was able to find a closer estimate compared to the other two algorithms. It can also be observed that PSO accomplishes the estimation quicker than GA but no improvement in the solution was found with further iterations. Table 6.10 represents the estimated values of unknown heat flux for experimental heat flux of 853 W/m^2 using GA, PSO and PSO-BFGS respectively. The plot for the fitness values is shown in Figure 6.16b. From Table 6.11, it can be well judged that the PSO-BFGS algorithm show good performance in retrieving the unknown heat flux very near to the actual value with a fitness value of 9.87e-7 compared to GA and PSO whose fitness values are found to be 1.27e-4 and 5.37e-13, respectively. The computational time taken by PSO-BFGS was nearly equal to GA where as for PSO it was observed to be considerably less. The estimation is

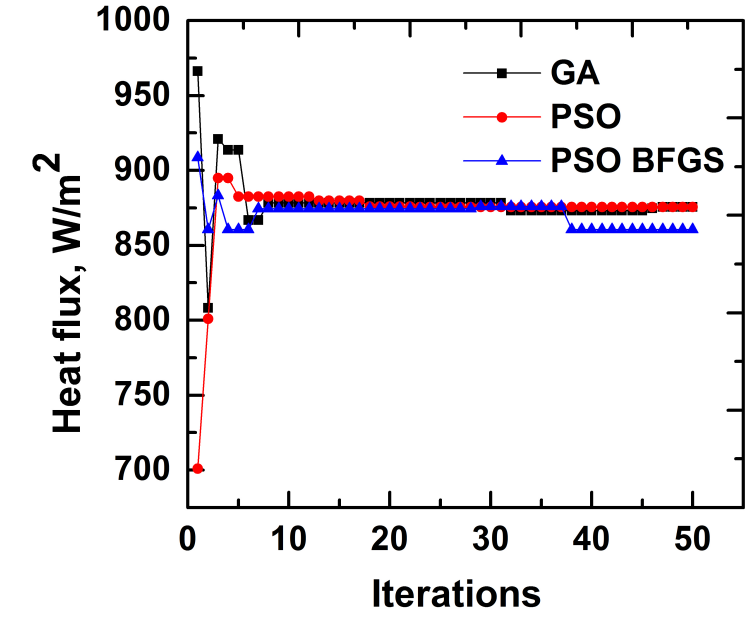

(a)

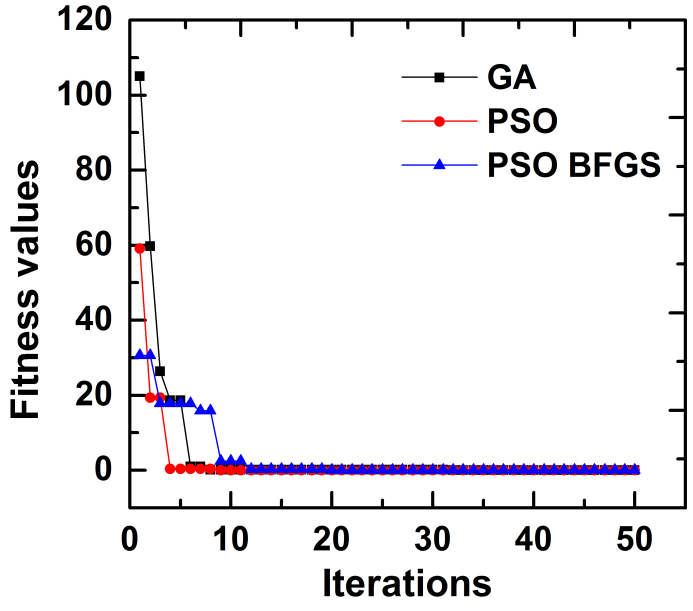

(b)

Figure 6.16 (a) Retrieved heat flux using GA, PSO and PSO-BFGS from the measured temperatures performed for the experimental heat flux of 853 W/m^2 and (b) best fitness values for the experimental heat flux of 853 W/m^{2}using GA, PSO and PSO-BFGS.

carried out for one more experimental heat flux of 1232 W/m ^{2} and the results are tabulated in Table 6.12. The error percentages in the estimation of experimental heat fluxes of 853 W/m^2 and 1232W/m^2 are found to be 0.86 and 0.44 respectively. The heat flux estimated from the experimental temperature is now fed in to the forward model to obtain the temperature distribution. The agreement between the experimental temperature and ANN temperature is found to be good and is shown in Figure 6.17a in terms of parity plot. The dotted lines show the range of deviation of the temperature between the experimental and trained value of the temperature.

6.11 ESTIMATION OF HEAT TRANSFER COEFFICIENT

From the previous section, it can be seen that the evolutionary methods are well suited for the estimation of heat flux for the experimental temperatures. In this section, the input to the forward model is the heat transfer coefficient and the output is the temperature distribution. The agreement between the average temperature from simulated values and the neural network is shown in Figure 6.17b. The range for the heat transfer coefficient is considered between 2.378W/m^{2}K and 5.581W/m^{2}K . Figure 6.18a shows

Table 6.10 Heat flux values estimated for the experimental heat flux of 853 W/m^2.

Runs	GA heat flux (W/m^2)	GA Time,s	PSO heat flux (W/m^2)	PSO Time,s	PSO-BFGS heat flux (W/m^2)	PSO-BFGS Time,s
1	875.43	12.62	875.58	9.39	860.41	11.75
2	875.43	12.36	875.58	9.85	860.41	13.06
3	875.43	13.68	875.58	10.15	860.41	12.65

Table 6.11 Comparison of retrieved heat flux and fitness values for experimental heat flux of 853 W/m^2.

Algorithms	Retrieved heat flux (W/m^2)	Fitness values	Time,s	% error
GA	875.43	1.27e-4	12.62	2.63
PSO	875.59	5.37e-13	9.39	2.64
PSO-BFGS	860.41	9.87e-7	11.75	0.86

Table 6.12 Comparison of retrieved heat flux and fitness values for experimental heat flux of 1232 W/m^2.

Algorithms	Retrieved heat flux (W/m^2)	Fitness values	Time,s	% error
GA	1257.1	1.87e-4	6.86	2.03
PSO	1258.1	1.69e-14	9.67	2.11
PSO-BFGS	1237.5	5.22e-10	10.84	0.44

Table 6.13 Retrieval of actual heat transfer coefficient value of 4.121 W/m^{2}K using GA, PSO and PSO-BFGS algorithms.

Runs	GA, h (W/m^{2}K)	GA Time, s	PSO, h (W/m^{2}K)	PSO Time, s	PSO-BFGS, h (W/m^{2}K)	PSO-BFGS Time, s
1	4.121	13.54	4.121	14.59	4.121	15.42
2	4.119	13.32	4.121	14.84	4.121	14.32
3	4.121	13.41	4.121	14.93	4.121	14.06

Table 6.14 Retrieval of heat transfer coefficient from experimental temperature using GA, PSO and PSO-BFGS algorithms.

Actual, h (W/m^{2}K)	GA, h (W/m^{2}K)	GA Time, s	PSO, h (W/m^{2}K)	PSO Time, s	PSO-BFGS, h (W/m^{2}K)	PSO-BFGS Time, s
3.782	3.81	11.57	3.81	17.1	3.786	24.64
4.283	4.318	8.21	4.316	11.54	4.293	15.28

the retrieval of actual value of 4.121W/m^{2}K for simulated temperature data using GA, PSO and PSO BFGS algorithms. From Table 6.13, it can be observed that PSO and PSO-BFGS algorithms produce best estimates but GA was found to have instability in retrieving the same value for different runs. The computational time taken by GA was found to be less compared to other two algorithms. Figure 6.18b shows the convergence of the fitness values for the estimation of actual heat transfer coefficient of 4.121 W/m^{2}K. The fitness values at the end of 50 iterations are found to be 7.67e-4, 2.86e-8 and 2.104e-12 for GA, PSO and PSO-BFGS respectively.

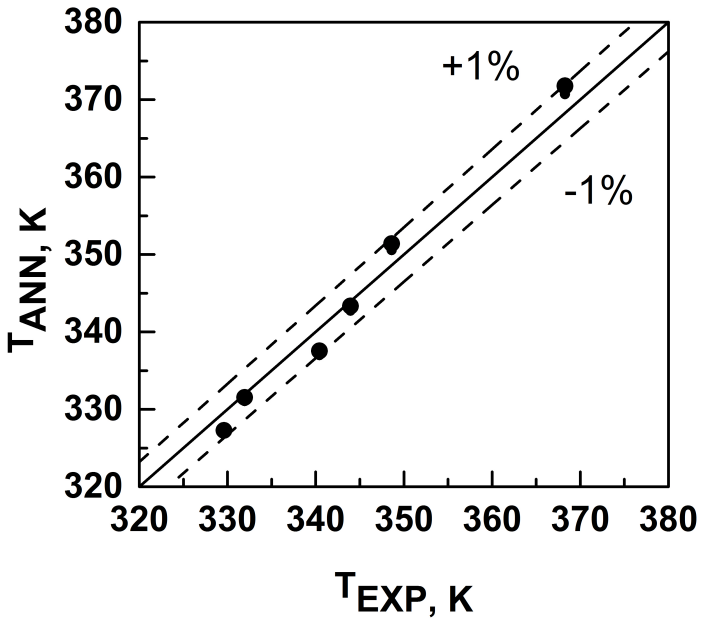

(a)

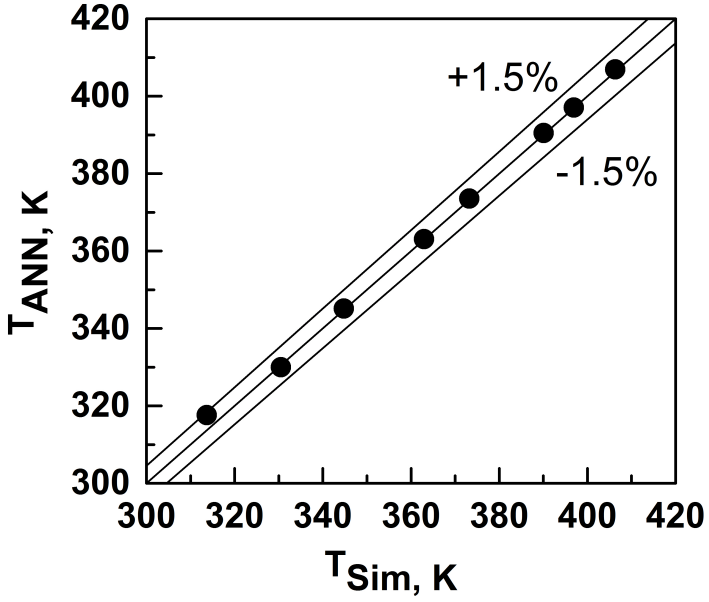

(b)

Figure 6.17 (a) Parity plot for between the experimental and simulated temperature from the estimated heat flux and (b) parity plot between the temperatures obtained using ANN and numerical simulations.

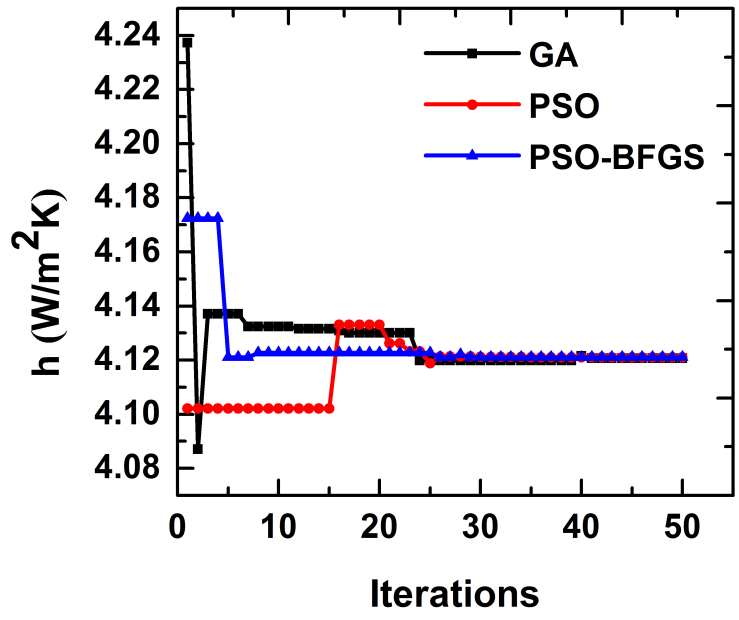

(a)

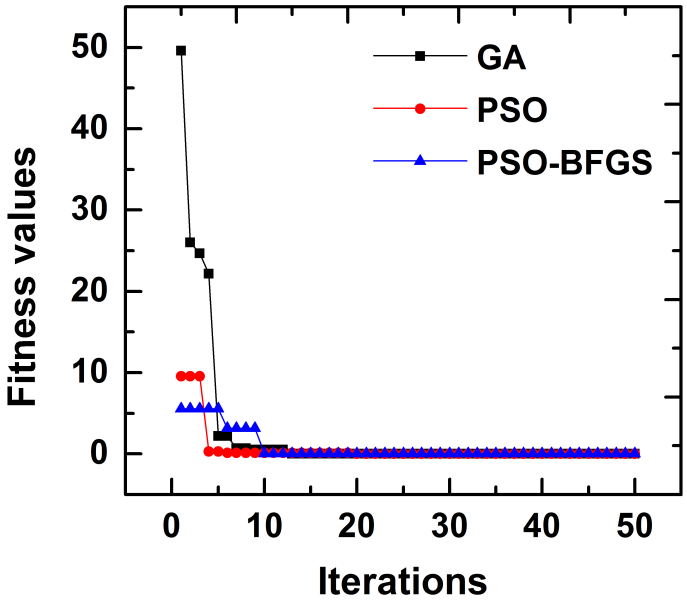

(b)

Figure 6.18 (a) Retrieval of actual *h* value of 4.121 W/m^{2}K using GA, PSO and PSO-BFGS algorithms respectively. (b) Fitness values of GA, PSO and PSO-BFGS algorithms for the actual *h* value of 4.121W/m^{2}K.

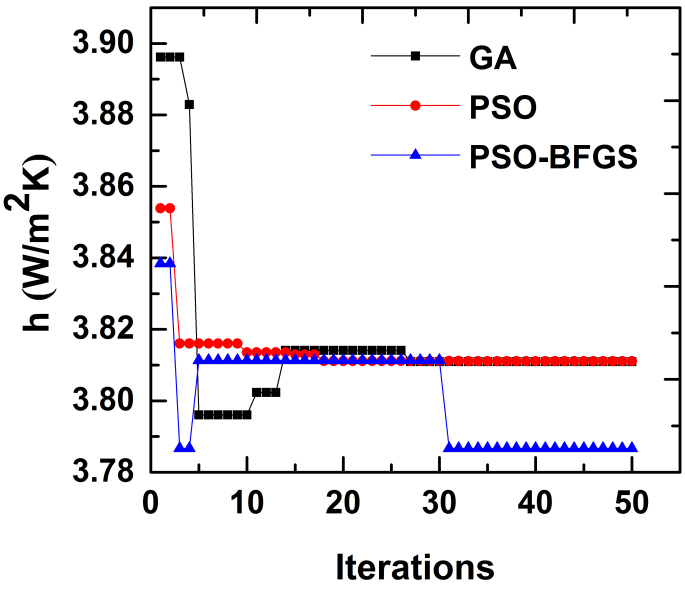

(a)

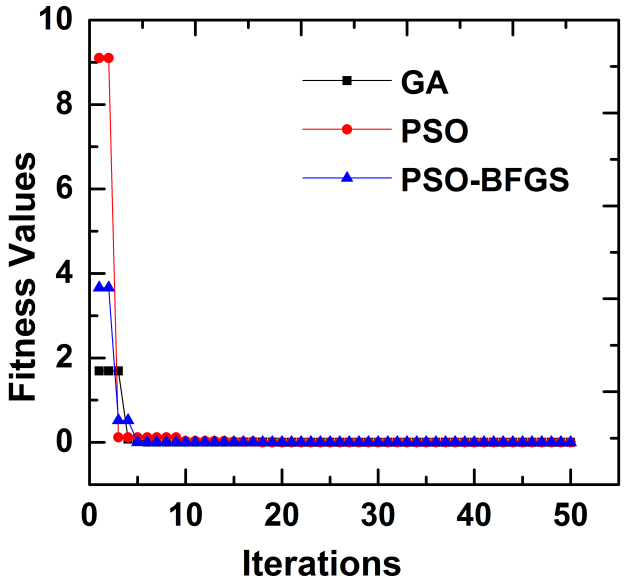

(b)

Figure 6.19 (a) Retrieval of actual experimental heat transfer coefficient of 3.78 W/m^{2}K using GA, PSO and PSO-BFGS algorithms respectively. (b) Fitness values of GA, PSO and PSO-BFGS algorithms for the actual heat transfer coefficient of 3.78W/m^{2}K.

After estimating the heat transfer coefficient values for the simulated measurements, the estimation is extended to the experimental temperature to prove the efficacy of all the algorithms. From Figure 6.19a, it is seen that the PSO-BFGS again provides closer findings compared to the other two algorithms. For different runs the estimated values of heat transfer coefficient against the actual value are reported in Table 6.14. Computational time was found to be more for PSO-BFGS due to evaluation of BFGS method, but the value retrieved was noticed to be 3.786 W/m^{2}K with an error of 0.105%. The retrieved values from GA and PSO are 3.81 W/m^{2}K with an error of 0.74%. The convergence of the fitness value plot is shown in Figure 6.19b.

6.12 CONCLUSION

In this work the solution of an inverse problem has been presented for a three dimensional conjugate heat transfer problem. The forward problem was solved using ANSYS-FLUENT software. The objective of the inverse problem was to estimate the unknown heat flux and the heat transfer coefficient from the measured temperatures. To accomplish this, a simple inexpensive natural convection fin setup was fabricated and several steady state experiments have been performed to obtain the temperature distribution of the fin. The forward problem based on CFD solutions was then replaced by Artificial Neural Network in order to expedite the computational process. The inverse estimation was accomplished using GA, PSO and PSO-BFGS algorithms. Sensitivity coefficient analysis was also examined for the unknown parameters. The estimation using simulated measurements showed good results from the inverse approaches. In addition, the proposed approach was also applied to the actual measurement data obtained from in-house experiments. It was concluded that PSO-BFGS, a new hybrid optimization algorithm, can effectively be used to solve the inverse conjugate heat transfer problems with more accurate results. BFGS algorithm helps the hybrid algorithm to overcome the disadvantage of PSO and GA in handling noisy data. For simulated measurements, all the three algorithms were found to be effective; whereas, PSO-BFGS demonstrated to be a good choice for the estimation of heat flux and heat transfer coefficient with absolute %error less than 1 and 0.25 respectively compared to PSO and GA for the experimental data. Hence, the use of the evolutionary algorithms in combination with ANN was found to be a formidable approach in the estimation of the unknown param-

eters. Thus, the above hybridization of forward and inverse solutions in the field of inverse estimation opens up new vistas for solving more complex conjugate problems in heat transfer.

6.13 CLOSURE

This chapter reported the estimation of heat and heat transfer coefficients associated during 3D conjugate fin heat transfer problem. The estimation obtained from PSO-BFGS algorithm along with ANN showed that it can be well utilized for solving complex conjugate heat transfer problems.

CHAPTER 7

CONCLUSIONS

The present work is concentrated towards the exploration of inverse methods for the estimation of multiple parameters associated with solidification of casting and conjugate fin heat transfer problems. Estimating the parameters at the surface which is subjected to high temperature becomes crucial when direct estimation is non-feasible. **Chapter 1** described the introduction to the inverse problems, basic concepts of solidification of casting and conjugate fin heat transfer. **Chapter 2** briefly described the literature review on various inverse methods for heat transfer problems; especially, application of evolutionary algorithms and neural network for the estimation of heat transfer parameters which led to define the objective of the present work. **Chapter 3** explained the forward model, numerical simulations, neural networks as fast forward model considered in the inverse problem and procedure of GA, PSO and PSO-BFGS algorithms.

Chapter 4 explained the solution of first class of problem considered in the present work. The IHTC estimation at the casting-chill interface during solidification of Sn-5wt%Pb alloy was chosen and solved using the available prior information about the IHTC from the literature. The temperatures from the numerical simulations using an explicit FDM scheme and corresponding inputs are trained using ANN. The major concern with the inverse estimation was computational time, hence a GA-ANN approach was attempted. Bayesian approach was implemented where the error associated with the temperature measurements can be incorporated. Both GA-ANN-least squares and GA-ANN-Bayesian showed accurate estimation for exact temperature data but for the noisy measurements GA-ANN-Bayesian approach retrieved accurate estimation with an absolute % error of *a*, *b* and *ME* as 0.0886, 0.172 and 1 for σ=0.01T_{max}; 0.107, 0.425 and 1.5 for σ=0.02T_{max} ; 0.2, 0.425 and 1.67 for σ=0.03T_{max} respectively. The conventional estimation using genetic algorithm would take 8-9 hours for the estimation but the use of ANN produced the results with an average of less than 125 seconds. This approach furnished an advantage over the other inverse methods as the prior knowledge

of the parameters to be estimated can be inserted in the Bayesian framework which could result in achieving effective retrievals.

The state of the art research of **Chapter 5** was the use of Bayesian framework combined with GA and PSO in order to estimate the constants involved in the heat transfer coefficients, latent heat and quantification of uncertainties in the form of standard deviation during solidification of Al-4.5wt%Cu alloy. The goal of accomplishing several unknown parameters simultaneously from single simulated experiment was successfully attempted. The Bayesian framework regularizes the inverse solution with help of informative priors. Scaled sensitivity analysis of the unknown parameters has been highlighted to express the effect of unknown parameters with temperature sensor locations and to find out the feasibility of the estimation process. The values of scaled sensitivity for a, b and latent heat were found to be high compared to c and d hence they significantly affect the temperature distribution during solidification. A range of a=[1000 25000], b=[0.01 0.6], c=[0.01 10], d=[0.01 0.6], ME=[0.001 0.06] and latent heat=[100000 500000] initialized for GA and PSO. The convergence of the *-lnPPDF* was faster for PSO than GA and it was observed that GA converging to a value of 171.46 at 163 iteration where as PSO converges to the same value at 65 iteration. The methodology was successfully implemented for both exact and noisy data and also the Study of effect of number sensors was also carried out. For five sensors, the retrieved values of the unknown parameters and the estimated average values of a by GA was 8677.2 and by PSO was 8676.6 with absolute % error of 0.313 and 0.3 respectively. PSO retrieved b, c and d values exactly to the original values. Further, the retrieved values of latent heat by GA was 379860.2 and by PSO was 379931.83 respectively which was found be comparatively higher to that of two sensors as increase in the number of sensors would increase noise associated in the temperatures.

Developing new techniques for the parameter estimation will always provide a choice to solve heat transfer problems. In **Chapter 6**, a 3D conjugate steady state fin heat transfer problem was considered and a numerical model was developed using ANSYS Fluent to obtain the temperatures distribution in fin. Each simulation took 30-45 mins for the convergence hence, a neural network was trained between the range of heat fluxes and corresponding temperatures which produced the output less than

5 seconds, used replaced by CFD simulations. In-house natural convection fin heat transfer experiments were also conducted for various heat fluxes and the estimation was performed for experimental temperatures. GA, PSO and PSO-BFGS algorithms exhibited good results for simulated temperatures. During the estimation of heat flux from measurements, PSO-BGFS provided the results with an average % error of 0.86 and 0.44 for 853 W/m^2 and 1232 W/m^2 respectively. The retrieval of heat transfer coefficient was also attempted for both simulated and experimental temperatures. PSO-BFGS estimated the heat transfer coefficient with an average %error 0.105 and 0.233 for 3.782W/m^{2}K and 4.283W/m^{2}K respectively. A new hybrid PSO-BFGS algorithm was developed and the efficacy was compared with conventional GA and PSO algorithms. The estimation using PSO-BFGS observed to be a preferred choice for the estimation of heat flux and heat transfer coefficient with absolute % error less than 1 and 0.25 respectively for the experimental data.

7.1 LIMITATIONS OF THE PRESENT WORK

1. The use of evolutionary algorithms become a time-consuming process of estimation when compared to gradient-based methods as it requires a range of input parameters to be solved to obtain the values of the fitness function in every iteration.

2. Though ANN is found to be an effective approach as a reduced model, for the multi-parameter problems, training of ANN also requires more time.

3. This approach is more suitable for heat transfer problems with prior information.

4. To choose an effective algorithm for the estimation, one has to perform several runs to optimize the algorithm parameters.

5. The trained ANN represents a reduced model for a particular case of a problem. If the dimensions of the domain are changed, the network has to be trained again to use it as fast forward model.

7.2 FUTURE SCOPE

The overall work presented in the thesis thus provides a new approach in the inverse parameter estimation for various heat transfer problems.

1. Consideration of radiation effects along with conduction at mold metal interface for the estimation of IHTC during solidification of casting.

2. Application of fin designed molds to enhance heat transfer during solidification of casting and optimization of number of fins on mold to maximize the heat transfer.

3. The estimation of heat flux and heat transfer coefficients can be further extended for transient conjugate heat transfer.

4. Exploring various hybrid techniques and comparing the performances with the existing methods.

REFERENCES

Arunkumar, S Rao, K.S. and Kumar, T.S.P. (2008). "Spatial variation of heat flux at the metal–mold interface due to mold filling effects in gravity die-casting." Int. J. Heat. Mass. Transfer.. 51(11-12), 2676–2685.

Aweda, J.O. and Adeyemi, M.B. (2009). "Experimental determination of heat transfer coefficients during squeeze casting of aluminium." J. Mater. Process. Technol.. 209(3), 1477–1483.

Azimifar, A. and Payan, S. (2017). "Optimization of characteristics of an array of thin fins using PSO algorithm in confined cavities heated from a side with free convection." Appl. Therm. Eng.. 110, 1371–1388.

Balaji, C. and Padhi, T. (2010). "A new ANN driven MCMC method for multi-parameter estimation in two-dimensional conduction with heat generation." Int. J. Heat Mass Transfer. 53(23-24), 5440–5455.

Balaji, C., Reddy, B.K. and Herwig, H. (2013). "Incorporating engineering intuition for parameter estimation in thermal sciences." Heat. Mass. Transfer. 49(12), 1771–1785.

Beck, J.V. (1970). "Nonlinear estimation applied to the nonlinear inverse heat conduction problem." Int. J. Heat Mass Transfer. 13(4), 703–716.

Chanda, S., Balaji, C., Venkateshan, S.P. and Yenni, G.R. (2017). "Estimation of principal thermal conductivities of layered honeycomb composites using ANN–GA based inverse technique." Int. J. Therm. Sci.. 111, 423–436.

Chen, H., Cao, D., Wang, G., Wan, S. and Li, Y. (2016). "Fuzzy estimation for unknown boundary shape of fluid-solid conjugate heat transfer problem." Int. J. Therm. Sci.. 106, 112–121.

Chen, W.L., Yang, Y.C. and Lee, H.L. (2007). "Inverse problem in determining convection heat transfer coefficient of an annular fin." Energy Convers. Manage.. 48(4), 1081–1088.

Cheung, N., Ferreira, I.L., Pariona, M.M., Quaresma, J.M. and Garcia, A. (2009). "Melt characteristics and solidification growth direction with respect to gravity affecting the interfacial heat transfer coefficient of chill castings." Mater. Des.. 30(9), 3592–3601.

Chipperfield, A.J. and Fleming, P.J. (1995). "The MATLAB Genetic Algorithm Toolbox." IET Conference Proceedings. 10–10(1).

Colaco, M.J. and Orlande, H.R.B. (2001). "Inverse forced convection problem of simultaneous estimation of two boundary heat fluxes in irregularly shaped channels." Numer. Heat Transfer, Part A. 39(7), 737–760.

Colaço, M.J., Orlande, H.R.B. and Dulikravich, G.S. (2006). "Inverse and optimization problems in heat transfer." J. Braz. Soc. Mech. Sci. Eng.. 28(1), 1–24.

Davey, K. (1993). "An analytical solution for the unidirectional solidification problem." Appl. Math. Modell.. 17(12), 658–663.

Deng, S. and Hwang, Y. (2006). "Applying neural networks to the solution of forward and inverse heat conduction problems." Int. J. Heat. Mass. Transfer.. 49(25-26), 4732–4750.

Ding, P. and Sun, D. (2015). "Resolution of unknown heat source inverse heat conduction problems using particle swarm optimization." Numer. Heat Transfer, Part B. 68(2), 158–168.

Dousti, P., Ranjbar, A.A., Famouri, M. and Ghaderi, A. (2012). "An inverse problem in estimation of interfacial heat transfer coefficient during two-dimensional solidification of Al 5% Wt-Si based on PSO." Int. J. Numer. Methods Heat Fluid Flow. 22(4), 473–490.

Eberhart, R. and Kennedy, J. (1995). "A new optimizer using particle swarm theory." "Proc., Int.Symp.on Micro Machine and Human Science.", . 39–43. Ieee.

Farahani, S.D. and Kowsary, F. (2017). "Experimental estimation of convective heat transfer coefficient from pulsating semi-confined impingement air slot jet by using inverse method." Heat Mass Transfer. 53(9), 2853–2866.

Ghadimi, B., Kowsary, F. and Khorami, M. (2015). “Heat flux on-line estimation in a locomotive brake disc using artificial neural networks.” Int. J. Therm. Sci.. 90, 203–213.

Gnanasekaran, N. and Balaji, C. (2011). “A Bayesian approach for the simultaneous estimation of surface heat transfer coefficient and thermal conductivity from steady state experiments on fins.” Int. J. Heat Mass Transfer. 54(13-14), 3060–3068.

Goldberg, D.E. and Holland, J.H. (1988). “Genetic algorithms and machine learning.” Mach. Learn.. 3(2), 95–99.

Gossard, D. and Lartigue, B. (2013). “Three-dimensional conjugate heat transfer in partitioned enclosures: determination of geometrical and thermal properties by an inverse method.” Appl. Therm. Eng.. 54(2), 549–558.

Hadamard, J. (2003). Lectures on Cauchy’s problem in linear partial differential equations. Courier Corporation.

Harsha, K. and Gnanasekaran, N. (2018). “A Bayesian inference approach: estimation of heat flux from fin for perturbed temperature data.” Sadhana Acad.. 43(4), 62.

Harsha, K., Vishweshwara, P.S., Gnanasekaran, N. and Balaji, C. (2018). “A combined ANN-GA and experimental based technique for the estimation of the unknown heat flux for a conjugate heat transfer problem.” Heat. Mass. Transfer. 54(11), 3185–3197.

Hetmaniok, E., Słota, D. and Zielonka, A. (2013). “Experimental verification of immune recruitment mechanism and clonal selection algorithm applied for solving the inverse problems of pure metal solidification.” Int. Commun. Heat Mass Transfer. 47, 7–14.

Ho, K. and Pehlke, R.D. (1985). “Metal-mold interfacial heat transfer.” Metall. Trans. B. 16(3), 585–594.

Huang, C.H. and Tsai, Y.L. (2005). “A transient 3-D inverse problem in imaging the time-dependent local heat transfer coefficients for plate fin.” Appl. Therm. Eng.. 25(14-15), 2478–2495.

Incropera, F.P., Lavine, A.S., Bergman, T.L. and DeWitt, D.P. (2007). Fundamentals of heat and mass transfer. Wiley.

Knupp, D.C., Naveira-Cotta, C.P., Orlande, H.R.B. and Cotta, R.M. (2013). "Experimental identification of thermophysical properties in heterogeneous materials with integral transformation of temperature measurements from infrared thermography." Exp. Heat Transfer. 26(1), 1–25.

Kulkarni, S.N. and Radhakrishna, K. (2005). "Evaluation of metal–mould interfacial heat transfer during the solidification of aluminium–4.5% copper alloy castings cast in CO2–sand moulds." Mater. Sci. Poland.. 23(3), 821–838.

Lee, H.L., Chang, W.J., Chen, W.L. and Yang, Y.C. (2012). "Inverse heat transfer analysis of a functionally graded fin to estimate time-dependent base heat flux and temperature distributions." Energy Convers. Manage.. 57, 1–7.

Lee, K.H. (2019). "Application of repulsive particle swarm optimization for inverse heat conduction problem–Parameter estimations of unknown plane heat source." Int. J. Heat Mass Transfer. 137, 268–279.

Lee, K.H., Baek, S.W. and Kim, K.W. (2008). "Inverse radiation analysis using repulsive particle swarm optimization algorithm." Int. J. Heat Mass Transfer. 51(11-12), 2772–2783.

Li, H., Lei, J. and Liu, Q. (2012). "An inversion approach for the inverse heat conduction problems." Int. J. Heat Mass Transfer. 55(15-16), 4442–4452.

Li, S., Tan, M., Tsang, I.W. and Kwok, J.T.Y. (2011). "A hybrid PSO-BFGS strategy for global optimization of multimodal functions." IEEE Trans. Syst. Man Cybern. Part B Cybern.. 41(4), 1003–1014.

Liu, F.B. (2012). "An application of particle swarm optimization to identify the temperature-dependent heat capacity." Heat Mass Transfer. 48(1), 99–107.

Lugon, J.J. and Silva, N.A.J. (2011). "Solution of porous media inverse drying problems using a combination of stochastic and deterministic methods." J. Braz. Soc. Mech. Sci. Eng.. 33(4), 400–407.

Lugon, J.J., Silva, N.A.J. and Santana, C.C. (2009). “A hybrid approach with artificial neural networks, Levenberg–Marquardt and simulated annealing methods for the solution of gas–liquid adsorption inverse problems.” Inverse Prob. Sci. Eng.. 17(1), 85–96.

Majchrzak, E., Mochnacki, B. and Suchy, J.S. (2008). “Identification of substitute thermal capacity of solidifying alloy.” J. Theor. Appl. Mech.. 46(2), 257–268.

Mejias, M.M., Orlande, H.R.B. and Ozisik, M.N. (1999). “A comparison of different parameter estimation techniques for the identification of thermal conductivity components of orthotropic solids.” “Third International Conference on Inverse Problems in Engineering, Port Ludlow, WA, June,” . 13–18. Citeseer.

Mota, C.A.A., Orlande, H.R.B., De Carvalho, M.O.M., Kolehmainen, V. and Kaipio, J.P. (2010). “Bayesian estimation of temperature-dependent thermophysical properties and transient boundary heat flux.” Heat Transfer Eng.. 31(7), 570–580.

Najafi, H. and Woodbury, K.A. (2015). “Online heat flux estimation using artificial neural network as a digital filter approach.” Int. J. Heat Mass Transfer. 91, 808–817.

Nishida, Y., Droste, W. and Engler, S. (1986). “The air-gap formation process at the casting-mold interface and the heat transfer mechanism through the gap.” Metall. Trans. B. 17(4), 833–844.

Nocedal, J. and Wright, S. (2006). “Numerical optimization: Springer science & business media.” New York.

Orlande, H.R., Dulikravich, G.S., Neumayer, M., Watzenig, D. and Colaço, M.J. (2014). “Accelerated Bayesian inference for the estimation of spatially varying heat flux in a heat conduction problem.” Numer. Heat Transfer, Part A. 65(1), 1–25.

Ousegui, A., Marcos, B. and Havet, M. (2019). “Inverse method to estimate air flow rate during free cooling using PCM-air heat exchanger.” Appl. Therm. Eng.. 146, 432–439.

Ozisik, M.N. and Orlande, H.R.B. (2000). Inverse heat transfer: fundamentals and applications. Taylor and Francis, LLC.

Plevris, V. and Papadrakakis, M. (2011). “A hybrid particle swarm—gradient algorithm for global structural optimization.” Comput.-Aided Civ. Infrastruct. Eng.. 26(1), 48–68.

Prabhu, K.N. and Griffiths, W.D. (2001). “Metal/mould interfacial heat transfer during solidification of cast iron in sand moulds.” Int. J. Cast Met. Res.. 14(3), 147–155.

Rajaraman, R. and Velraj, R. (2008). “Comparison of interfacial heat transfer coefficient estimated by two different techniques during solidification of cylindrical aluminum alloy casting.” Heat. Mass. Transfer. 44(9), 1025–1034.

Ranjbar, A.A., Ghaderi, A., Dousti, P. and Famouri, M. (2010). “A transient two-dimentional inverse estimation of the metal-mold heat transfer coefficient during squeeze casting of AL-4.5 wt% CU.” Int. J. Eng. Trans.. 23, 274–286.

Rao, S.S. (2009). Engineering optimization: theory and practice. John Wiley & Sons.

Raudenskỳ, M., Woodbury, K.A., Kral, J. and Brezina, T. (1995). “Genetic algorithm in solution of inverse heat conduction problems.” Numer. Heat. Transfer. B—Fund.. 28(3), 293–306.

Razzaghi, H., Kowsary, F. and Ashjaee, M. (2019). “Derivation and application of the adjoint method for estimation of both spatially and temporally varying convective heat transfer coefficient.” Appl. Therm. Eng.. 154, 63–75.

Reddy, B.K., Gnanasekaran, N. and Balaji, C. (2012). “Estimation of thermo-physical and transport properties with Bayesian inference using transient liquid crystal thermography experiments.” “J. Phys. Conf. Ser.”, . 012082. IOP Publishing.

Rojczyk, M., Orlande, H.R., Colaço, M.J., Szczygieł, I., Nowak, A.J., Białecki, R.A. and Ostrowski, Z. (2017). “Inverse heat transfer problems: an application to bioheat transfer.” Comput. Assisted Methods Eng. Sci.. 22(4), 365–383.

Rosenbrock, H. (1960). “An automatic method for finding the greatest or least value of a function.” Comput J.. 3(3), 175–184.

Sahin, H.M., Kocatepe, K., Kayıkcı, R. and Akar, N. (2006). "Determination of unidirectional heat transfer coefficient during unsteady-state solidification at metal casting–chill interface." Energy Convers. Manage.. 47(1), 19–34.

Santos, C.A., Quaresma, J.M.V. and Garcia, A. (2001). "Determination of transient interfacial heat transfer coefficients in chill mold castings." J. Alloys Compd.. 319(1-2), 174–186.

Santos, C.A., Siqueira, C.A., Garcia, A., Quaresma, J.M. and Spim, J.A. (2004). "Metal–mold heat transfer coefficients during horizontal and vertical Unsteady-State solidification of Al–Cu and Sn–Pb Alloys." Inverse Prob. Sci. Eng.. 12(3), 279–296.

Słota, D. (2008). "Solving the inverse Stefan design problem using genetic algorithms." Inverse Prob. Sci. Eng.. 16(7), 829–846.

Soeiro, F., Soares, P.O., Campos Velho, H. and Silva Neto, A. (2004). "Using neural networks to obtain initial estimates for the solution of inverse heat transfer problems." "Inverse Problems, Design an Optimization Symposium," . 358–363.

Stefanescu, D.M. (2015). Science and engineering of casting solidification. Springer.

Sui, D.S. and Cui, Z.S. (2008). "Regularized determination of interfacial heat transfer coefficient during ZL102 solidification process." Trans. Nonferrous. Met. Soc. China.. 18(2), 399–404.

Sun, H.C. and Chao, L.S. (2006). "Analysis of Interfacial Heat Transfer Coefficient of Green Sand Mold Casting for Aluminum and Tin-Lead Alloys by Using a Lump Capacitance Method." J. Heat Transfer. 129(4), 595–600.

Tabrizi, B.A. and Jaluria, Y. (2018). "An optimization strategy for the inverse solution of a convection heat transfer problem." Int. J. Heat Mass Transfer. 124, 1147–1155.

Udayraj, Mulani, K., Talukdar, P., Das, A. and Alagirusamy, R. (2015). "Performance analysis and feasibility study of ant colony optimization, particle swarm optimization and cuckoo search algorithms for inverse heat transfer problems." Int. J. Heat. Mass. Transfer.. 89, 359–378.

Vakili, M., Khosrojerdi, S., Aghajannezhad, P. and Yahyaei, M. (2017). “A hybrid artificial neural network-genetic algorithm modeling approach for viscosity estimation of graphene nanoplatelets nanofluid using experimental data.” Int. Commun. Heat Mass Transfer. 82, 40–48.

Vakili, S. and Gadala, M.S. (2009). “Effectiveness and efficiency of particle swarm optimization technique in inverse heat conduction analysis.” Numer. Heat Transfer, Part B. 56(2), 119–141.

Vasileiou, A., Vosniakos, G.C. and Pantelis, D. (2017). “On the feasibility of determining the heat transfer coefficient in casting simulations by genetic algorithms.” Procedia Manufacturing. 11, 509–516.

Vasileiou, A.N., Vosniakos, G.C. and Pantelis, D.I. (2015). “Determination of local heat transfer coefficients in precision castings by genetic optimisation aided by numerical simulation.” Proc. Inst. Mech. Eng. Part C: J. Mech.. 229(4), 735–750.

Victoire, T.A.A. and Jeyakumar, A.E. (2004). “Hybrid PSO–SQP for economic dispatch with valve-point effect.” Electr. Power Syst. Res.. 71(1), 51–59.

Voller, V.R. and Swaminathan, C.R. (1991). “General Source-Based Method for Solidification Phase Change.” Numer. Heat Transfer, Part B. 19(2), 175–189.

Wang, G.G., Hossein Gandomi, A., Yang, X.S. and Hossein Alavi, A. (2014). “A novel improved accelerated particle swarm optimization algorithm for global numerical optimization.” Eng. Computation.. 31(7), 1198–1220.

Wang, J. and Zabaras, N. (2004). “A Bayesian inference approach to the inverse heat conduction problem.” Int. J. Heat Mass Transfer. 47(17-18), 3927–3941.

Wang, X., Li, H. and Li, Z. (2018). “Estimation of interfacial heat transfer coefficient in inverse heat conduction problems based on artificial fish swarm algorithm.” Heat Mass Transfer. 54(10), 3151–3162.

Wang, X., Wang, Z., Liu, Y., Du, F., Yao, M. and Zhang, X. (2016). “A particle swarm approach for optimization of secondary cooling process in slab continuous casting.” Int. J. Heat Mass Transfer. 93, 250–256.

Wankhade, P.A., Kundu, B. and Das, R. (2018). “Establishment of non-Fourier heat conduction model for an accurate transient thermal response in wet fins.” Int. J. Heat Mass Transfer. 126, 911–923.

Wood, R.L. (1996). “Genetic algorithm behaviour in the solution of an inverse thermal field problem.” Eng. Comput.. 13(5), 38–56.

Yadav, R., Balaji, C. and Venkateshan, S. (2019). “Inverse estimation of number and location of discrete heaters in radiant furnaces using artificial neural networks and genetic algorithm.” J. Quant. Spectrosc. Radiat. Transfer. 226, 127–137.

Yan, L., Yang, F. and Fu, C. (2009). “A Bayesian inference approach to identify a Robin coefficient in one-dimensional parabolic problems.” J. Comput. Appl. Math.. 231(2), 840–850.

Zeng, Y., Wang, H., Zhang, S., Cai, Y. and Li, E. (2019). “A novel adaptive approximate Bayesian computation method for inverse heat conduction problem.” Int. J. Heat Mass Transfer. 134, 185–197.

Zhang, B., Qi, H., Sun, S.C., Ruan, L.M. and Tan, H.P. (2015). “Solving inverse problems of radiative heat transfer and phase change in semitransparent medium by using Improved Quantum Particle Swarm Optimization.” Int. J. Heat Mass Transfer. 85, 300–310.

Zhang, L. and Li, L. (2013). “Determination of heat transfer coefficients at metal/chill interface in the casting solidification process.” Heat. Mass. Transfer. 49(8), 1071–1080.

Zhang, L., Li, L., Ju, H. and Zhu, B. (2010). “Inverse identification of interfacial heat transfer coefficient between the casting and metal mold using neural network.” Energy Convers. Manage. 51(10), 1898–1904.

LIST OF JOURNALS

1. **Vishweshwara, P.S.**, Gnanasekaran, N. and Arun, M., 2019. Simultaneous estimation of unknown parameters using a-priori knowledge for the estimation of interfacial heat transfer coefficient during solidification of Sn–5wt%Pb alloy—an ANN-driven Bayesian approach. Sadhana, 44(4), pp.100, [SCIE indexed], https://doi.org/10.1007/s12046-019-1076-2
2. **Vishweshwara, P.S.**, Gnanasekaran, N. and Arun, M., 2020. Inverse Approach Using Bio-Inspired Algorithm Within Bayesian Framework for the Estimation of Heat Transfer Coefficients During Solidification of Casting. Journal of Heat Transfer, 142(1), pp.1-11, [ASME], https://doi.org/10.1115/1.4045134
3. **Vishweshwara, P.S.**, Harsha Kumar, M.K., Gnanasekaran, N. and Arun. M., 2019. 3D coupled conduction-convection problem using in-house heat transfer experiments in conjunction with hybrid inverse approach, Engineering Computations, 36 (9), pp.3180-3207, [SCIE indexed], https://doi.org/10.1108/EC-11-2018-0496

LIST OF BOOK CHAPTERS

1. **Vishweshwara, P.S.**, Gnanasekaran, N. and Arun, M., 2019. Inverse Estimation of Interfacial Heat Transfer Coefficient During the Solidification of Sn-5wt% Pb Alloy Using Evolutionary Algorithm. In Advances in Materials and Metallurgy, pp. 227-237, Springer, Singapore.
   https://doi.org/10.1007/978-981-13-1780-4_23

2. **Vishweshwara, P.S.**, Gnanasekaran, N. and Arun, M., 2019. Estimation of Interfacial Heat Transfer Coefficient for Horizontal Directional Solidification of Sn-5 wt% Pb Alloy Using Genetic Algorithm as Inverse Method. In Soft Computing for Problem Solving, pp. 447-459, Springer, Singapore.
   https://doi.org/10.1007/978-981-13-1592-3_35

LIST OF CONFERENCES

1. **Vishweshwara P S**, Gnanasekaran N and Arun M 2019, "A Novel Framework for the estimation of interfacial heat transfer coefficient using BAT algorithm during solidification of metal casting ", 12th International Conference on Thermal Engineering: Theory and Applications (ICTEA-2019), February 23-26, 2019 , PDP University, Gandhinagar, India.

2. **Vishweshwara P S**, Gnanasekaran N and Arun M, 2018, “Inverse estimation of interfacial heat transfer coefficient during the solidification of Sn-5wt%Pb alloy using evolutionary algorithm”, International Conference on Engineering Materials, Metallurgy and Manufacturing-2018 (ICEMMM-2018), SSN College of Engineering, Chennai, Feb 15-16, 2018, IEEE conference.

3. **Vishweshwara P S**, Gnanasekaran N and Arun M,2017,“Estimation of interfacial heat transfer coefficient for horizontal directional solidification of sn-5wt%pb alloy using genetic algorithm as inverse method”, Soft Computing for Problem Solving - SocProS 2017, 23-24 December, 2017, Indian Institute of Technology, Bhubaneswar.

4. **Vishweshwara P S**, Gnanasekaran N, Arun M,2016,“Determination of Metal Mold Interfacial Heat Transfer Coefficient During Solidification of Casting: A Review”, The 4th International Conference on Advances in Materials and Materials Processing, iCAMMP-iv, 5-7 November, 2016, Indian Institute of Technology Kharagpur, India.

BIODATA

VISHWESHWARA P S

Department of Mechanical Engineering

National Institute of Technology Karnataka Surathkal,

Mangalore- 575025, India.

Email id: vishweshwara.ps@gmail.com

EDUCATION

2012–2014 M.Tech, Thermal Power Engineering, Bapuji Institute of Engineering and Technology, Davanagere, Karnataka, India. (First class with Distinction, 72.79%).

2008-2012 B.E, Mechanical Engineering, Bapuji Institute of Engineering and Technology, Davanagere, Karnataka, India. (First class, 67.74%).

2006-2008 12th, Nutana P.U college, Davanagere, Karnataka, India. (First class, 81.83%).

2003-2006 10th std, B.E.A High school, Davanagere, Karnataka. (Distinction, 88.32%).

PROFESSIONAL EXPERIENCE

Project Trainee: Project entitled "Prediction of NOx emission in primary zone of anAnnular Combustor using Zeldovich Mechanism" at Gas Turbine Research Establish-ment (GTRE, DRDO), CV Raman Nagar, Bangalore during 2013-2014 for 10 months.

COMPUTER SKILLS

MATLAB, COMSOL, Excel, MS Word, Latex

AWARDS AND RECOGNITION

1. Best paper award, "Inverse estimation of interfacial heat transfer coefficient during solidification of Sn5%wt Pb alloy using evolutionary algorithm", International conference on engineering materials, metallurgy and manufacturing -2018, SSN college of Engineering, Chennai, India, Feb 15-16,2018.

2. Best paper award, “Surrogate forward model using Artificial Neural Networks in conjunction with Bayesian computations for 3D conduction convection heat transfer problem”, Soft Computing in Problem Solving (SocProS)-2019 conference, Vellore Institute of Technology, Tamil Nadu, India, Dec 17-19, 2018.

3. Best Student Award by Indian Society for Technical Education (ISTE) in 2012.

PROFESSIONAL TRAINING

1. Five day GIAN course on Inverse Heat Transfer delivered by Prof. Helicio B Orlande, Brazil at NITK Surathkal in 2016.

2. Five day GIAN course on Transfer Function Based on Green’s Function Method to solve inverse heat conduction problem (IHCP): Manufacturing process Application delivered by Prof. Gilmar, Brazil at NITK, Surathkal in 2016.

3. Five day GIAN course on Advanced Casting and Solidification of Light Alloys for Transportation delivered by Prof. Ravi Ravindran, Canada at IIT Madras in 2016.

4. Two day workshop on Evolutionary computing and biologically inspired algorithms using MATLAB at PSG college of Technology, Coimbatore in 2016.

5. One day workshop on on Statistical learning at PSG college of Technology, Coimbatore in 2016.

6. Three Day National Workshop on Intelligent Optimization Techniques for Engineering Problems, at NITK Surathkal, 2019.

PROFESSIONAL AND VOLUNTEER ACTIVITIES

1. Delivered talk on Use of Evolutionary Algorithms in Heat Transfer Analysis at P.E.S. Institute of Technology and Management, Shimoga, Karnataka, India in July 2018.

2. Volunteer in TEQIP-III one week workshop on Inverse Problems and Applications, July 9-13, 2018 at NITK.

3. Volunteer in Expert lecture on Why is my paper not getting accepted? Prof. C Balaji, IIT Madras, 2018 at NITK.

4. Volunteer for TEQIP-III one week workshop on Frontiers in Design, Manufacturing and Energy Sustainability, September 3-7, 2018 at NITK.

5. Conducted one day happiness activities in orphanage, Mangalore, India, 2018.

6. Indian Society for Technical Education (ISTE) Students Chairman for the year 2011-12 in Bapuji Institute of Engineering and Technology, Davanagere.

I certify that the foregoing information is correct and complete to the best of my knowledge and belief and nothing has been concealed / distorted.

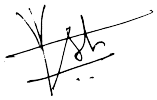

VISHWESHWARA P S

NITK, SURATHKAL